UNIVERSIDADE DE LISBOA
FACULDADE DE CIÊNCIAS
DEPARTAMENTO DE ENGENHARIA GEOGRÁFICA, GEOFÍSICA E ENERGIA

Interaction of salt-fresh water using airborne TEM methods

Joana Alves Ribeiro

Mestrado em Ciências Geofísicas

Especialização em Geofísica Interna

2010

UNIVERSIDADE DE LISBOA
FACULDADE DE CIÊNCIAS
DEPARTAMENTO DE ENGENHARIA GEOGRÁFICA, GEOFÍSICA E ENERGIA

Interaction of salt-fresh water using airborne TEM methods

Joana Alves Ribeiro

Fernando Santos (Faculdade de Ciências – Universidade de Lisboa)

Esben Auken (Departamento de Ciências da Terra – Universidade de Aarhus)

Mestrado em Ciências Geofísicas

Especialização em Geofísica Interna

2009

Abstract

It is in everyone interest to have a certain pessimist thinking about the climate changes in the future and its possible consequences. The European CLIWAT project (CLImate change and Ground WATer) focus on the climate change in the North Sea Region and its consequences on the groundwater system and how it would affect the water supply.

Airborne TEM (Time domain Electromagnetic Method) is known for its ease of covering large areas in a short period of time as well as its sensitivity to changes in geology such as type of rock, porosity, grain size, fracture and clay content. The SkyTEM system is developed by the HGG Group (Aarhus University, Denmark) for groundwater investigations which makes this method suitable for the study of the North of the Province of Friesland and the Island of Terschelling (Netherlands).

One of the main concerns on the Terschelling Island is the sustainability of drinkable water, were only 36% is explored on a local well and the remaining 64% comes from a pipeline from the mainland. Geophysical interpretation of the SkyTEM data reinsures existence of two fresh water lenses on the Western side of the island and on the region of Hoorn. The SkyTEM results are in coherence with different data sets of other methods such as CPT's, VES, CVES and Ground TEM. It also identified the thin clay layers, which is an important finding since it has an important role on the protection of groundwater due to its impermeability properties. The geophysical results of this interpretation will later be use to improve the hydrological model – MODFLOW-SWI.

Interpretation of the North of Friesland helped identifying the signature of the tide during the ice age in the Saalian epoch. There is also present a high resistive area in the SE of the flight lines that may be considered to be percolation of the Magriget Channel due to the proximity.

Key-words: airborne TEM, SkyTEM System, interaction salt-fresh water, fresh water lenses, hydrogeophysics

Resumo

O tema das alterações climáticas é hoje de preocupação geral. Em 2008 foi iniciado um projecto Europeu CLIWAT (CLImate change and Ground WATer) com o objectivo de estudar possíveis cenários do impacto das alterações climáticas sobre os sistemas de águas subterrâneas e da forma como este poderá afectar o abastecimento de água nas regiões vizinhas do Mar do Norte. Este é um projecto multi-disciplinar e conta com a participação de um vasto grupo de geo-cientistas cujo principal objectivo é a criação de modelos hidrológicos para avaliação dos possíveis impactos hidrológicos em função de diferentes cenários climáticos.

O método eletromagnético aéreo no domínio do tempo é conhecido pela sua facilidade de cobrir grandes áreas num curto período de tempo, bem como a sua sensibilidade para detectar variações na geologia como seja o tipo de rocha, a porosidade, o tamanho do grão, as fracturas e o teor de argila. O sistema SkyTEM mantêm-se em desenvolvimento permanente pelo Grupo HGG (Universidade de Aarhus, Dinamarca) para investigações hidrológicas e ambientais. O sistema foi usado com vantagem, em Setembro de 2009, na província de Friesland e a Ilha de Terschelling, ao Norte da Holanda.

Todo o sistema SkyTEM está suspenso por um gancho no helicóptero. A leve estrutura do sistema transporta os instrumentos de transmissão e recepção, dois GPS, dois lasers que medem num modo continuo a altitude durante o voo, assim como inclinómetros na parte da frente e de trás da estrutura para medir a sua inclinação. Um gerador é transportado entre o helicóptero e a estrutura para providenciar energia ao sistema.

A configuração é um *loop* central, com um deslocamento vertical, pois este tipo de configuração é insensível às inomogeneidades locais na resistividade próxima à superfície assim como é indiferente a pequenas alterações na distância entre o transmissor e o receptor. O sistema SkyTEM é configurado por dois momentos: um momento magnético baixo (LM) de cerca de 12.000 Am^2 e um momento magnético alto (HM) de cerca de 200.000 Am^2. A altitude de voo recomendada é de cerca de 30 metros.

O desenvolvimento da exploração turística e hoteleira na Ilha de Terschelling levou a um aumento do consumo de água potável. O abastecimento é actualmente feito através de uma conduta submarina que garante 64% das necessidades. Os restantes 36% são obtidos de água subterrânea através de um furo existente no Oeste da ilha.

Estudos prévios indicam a presença de duas lentes de água doce localizadas a Norte da localidade de Hoorn e na parte Oeste da ilha, subjacentes a dunas protegidas o que impede a sua exploração. A interpretação geofísica dos dados do sistema SkyTEM confirma a localização das duas lentes de água doce. Devido à sensibilidade deste método foi possível localizar a interface água doce/salgada com uma grande precisão como se verificou depois da comparação com outros métodos geofísicos como CPT's, VES, CVES e TEM. Foi também possível identificar camadas finas de argila de extrema importância, dado o seu papel de protecção de águas subterrâneas devido à impermeabilidade. Em certas zonas, a Norte da ilha, nota-se uma transição gradual de alta resistividade para baixa resistividade o que poderá ser explicado por um processo de descarga de água subterrânea para o oceano. A interpretação destes dados geofísicos será posteriormente usada para o melhoramento do modelo hidrológico da ilha – MODFLOW-SWI.

No caso da área em estudo, a Norte da província de Friesland, o objectivo era a obtenção de conhecimentos adicionais sobre a área. Foi possível identificar vestígios da última época glaciar na Holanda, constituída por depósitos da formação de Drent. A Sudoeste da área em estudo encontra-se uma zona com alta resistividade possivelmente consequência de percolação do Canal de Magriet devido à sua proximidade.

Palavras-chave: Métodos electromagnéticos aéreos, sistema SkyTEM, interacção água doce/salgada, hidrogeofísica

Acknowledgments

I would like to express my gratitude to my supervisors, Professor Fernando Santos and Professor Esben Auken for all their support. Without the motivation and encouragement from Professor Santos I would have not gotten this far. For the opportunity at early stage of my academic studies to be able to participate on field works, that made me realize that Applied Geophysics was the scientific area I would like to follow.

I would like to thanks Professor Auken for the loop of faith on taking in a student that he had never heard of, and that according to him it was just due to my perseverance on sending him emails. For giving me the opportunity to work with several researchers from the Hydrogeophysics Group from Aarhus University, Denmark.

A special thanks goes out to Msc. Nikolaj Forge, without whose guidance and endurance the process of working on the thesis would have been much harder.

I am heartily thankful to my mum, grandparents, brother, close friends and family for all their unconditional love and support that made it easier working on this thesis as well as sharing my experiences of living this past year abroad.

I am indebted to several colleagues for providing a stimulating and fun environment in which to learn and grow. I am especially grateful to João Plancha, James Ramm, João Macedo and Ivo Bernardo

Lastly, I offer my regards and blessings to all of those who supported me in any respect during the completion of this thesis.

"The only place where success comes before work is in the dictionary"

- Albert Einstein

Contents

Table of figures

List of symbols

$\vec{E}$	Electric field	$[V/m]$
$\vec{B}$	Magnetic induction	$[Weber/m^2]$ or $[Tesla]$
$\vec{H}$	Magnetic field	$[A/m]$
$\vec{D}$	Electric Displacement	$[C/m^2]$
$\vec{J}$	Electric current density	$[A/m^2]$
ρ	Electric charge density	$[C/m^3]$
σ	Electric conductivity	$[S/m]$
ε	Dielectric permittivity	$[F/m]$
μ	Magnetic permeability	$[H/m]$
σ_w	Conductivity of water	$[S/m]$
σ_l	Conductivity of formation	$[S/m]$
F	Formation factor	Adimencional
I	Index of resistivity	Adimencional
ϕ	Porosity	Adimencional
S	Saturation	Adimencional

1. Introduction

In the North Sea region is being conducted a study on the influence of the climate changes in the groundwater system – CLIWAT project (CLImate change and Ground WATer). The aim of this project is to determine the effects of climate changes on groundwater systems and through this on the surface water and water supply.

Although this thesis is using the data of this project, the main goal is to learn how to process and interpreter geophysical data of the airborne time domain electromagnetic method – SkyTEM System. The areas in this thesis will be focus on the region of the North of The Netherlands: North of the province of Friesland and Island of Terschelling.

In the early times the Island of Terschelling was known to be an island for agriculture porpoise, but now it is getting known for its offering of a getaway from the city, especially during the summer. The tourism has been growing every year, and therefore the consumption of drinking water has been increasing as well. The main water supply comes from a pipe line from the mainland (about 64% of the total consumption of drinkable water) and the others 36% is explored in a well located on the Western part of the dune area on the island (Groen et al., 2009).

From previous studies there is evidence of two fresh water lenses, one located at the Western part of the Island, and the other one at North of Hoorn. These two lenses are below an area of protected dune, and therefore the extraction of water is limited due to possible damage to the dunes.

It is also expected to obtain information from the geophysical results that will reinforce the confirmation of the areas where it exist fresh water lenses, to help on delimiting the interface of fresh/salt water boundary, as well as to be able to characterize the thin clay layer. These geophysical results will later on be used to improve the hydrological model - MODFLOW - on the Island.

Dutch are known to conquer land from the sea since the early 16^{th} century, which means that the country may be considered as lowland due to its shallow topography. The province of Friesland is not a stranger of this process. The objective for this area is to obtain a better knowledge of the geology. It will be done an experience to try adding geological layers to the inversion to see if it is possible to obtain a better model. This part will be done together with Rik Noorlandt (DELTARES, Netherland).

1.1 CLIWAT - CLImate change and Ground WATer

Since the early 90's a global concern about the climate changes and its consequences started to focus more and more an environmental, economic and political issue.

The world climate is changing and it is every day more important to try to understand what the causes are, the possible consequences and how to prevent its disastrous cost. The global climate change may raise the sea level up to/over one meter in the next century and, in some areas, increase the frequency and severity of storms. Hundreds of thousands of square meters of coastal wetlands and other lowlands could be inundated. Beaches could retreat as much as a few hundred meters and protective structures may be breached. Flooding would threaten lives, agriculture, livestock, buildings and infrastructures. Salt water would advance landwards into aquifers and up estuaries, threatening water supplies, ecosystems and agriculture in some areas.

The European project CLIWAT (CLImate change and Ground WATer) focuses on the study of the influence of this climate changes on the groundwater systems and how it would affect on the surface water and water supply in the North Sea region.

The CLIWAT project started in September 2008 and it's a multi-disciplinary project that counts a wild range of Geo scientists with the main objective to present groundwater and integrated hydrological models for an evaluation of the possible hydrological impacts for different climate scenarios.

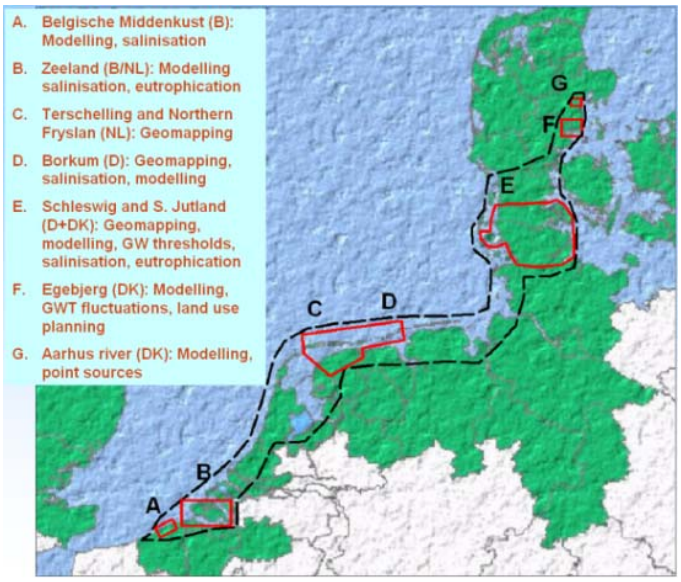

Fig. 1: CLIWAT pilot areas of study (in www.cliwat.eu)

2. Survey overview

This survey is part of the CLIWAT project and it will focus on the study of the area at North of the province of Friesland and the Terschelling Island (Netherland). The field work took place on the 14th to the 18th of September, 2009.

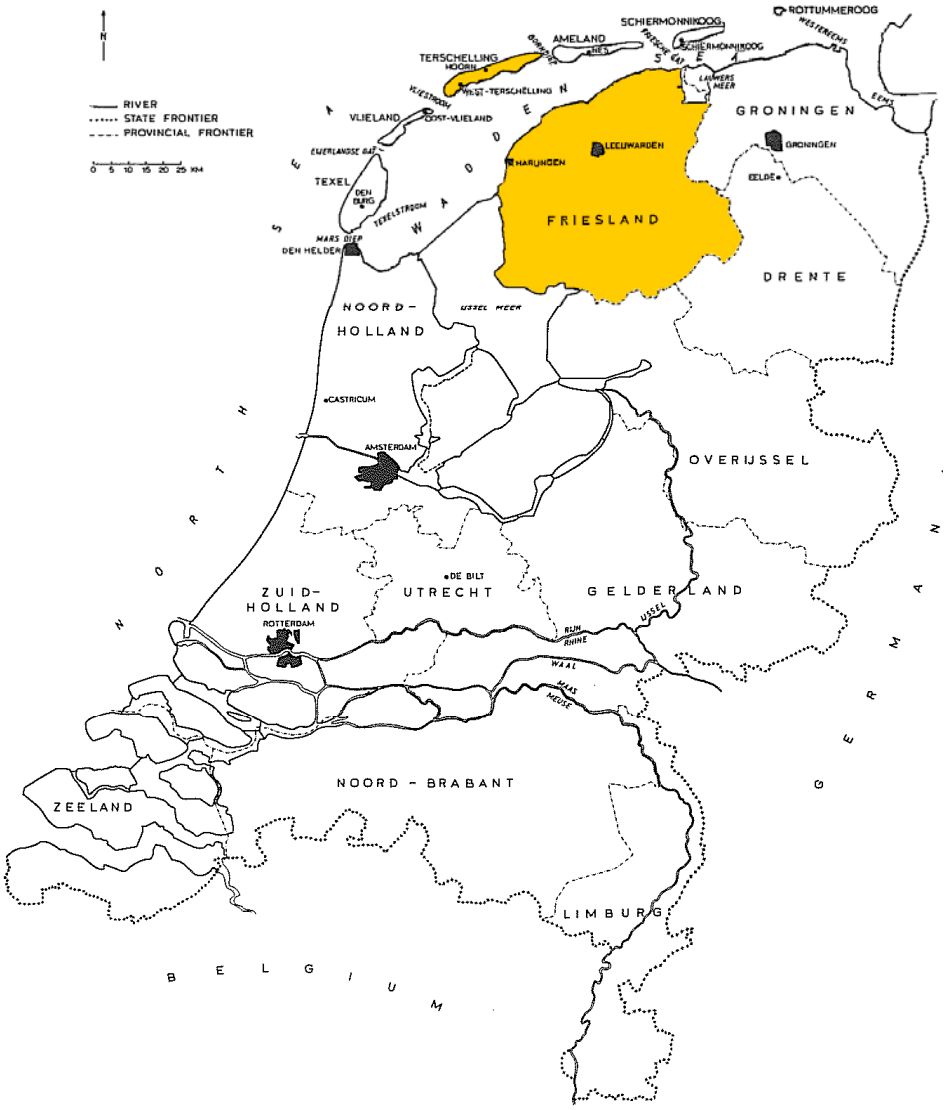

Fig. 2: Map of Netherland (areas in colour are the provinces of study)

Fig. 3 and Fig. 4 show the areas of study. The survey on North of Friesland had a total area of approximately 125 × 10^3 km^2 and Tershelling Island approximately 450 line km. In both cases, the line spacing was approximately of 200 meters.

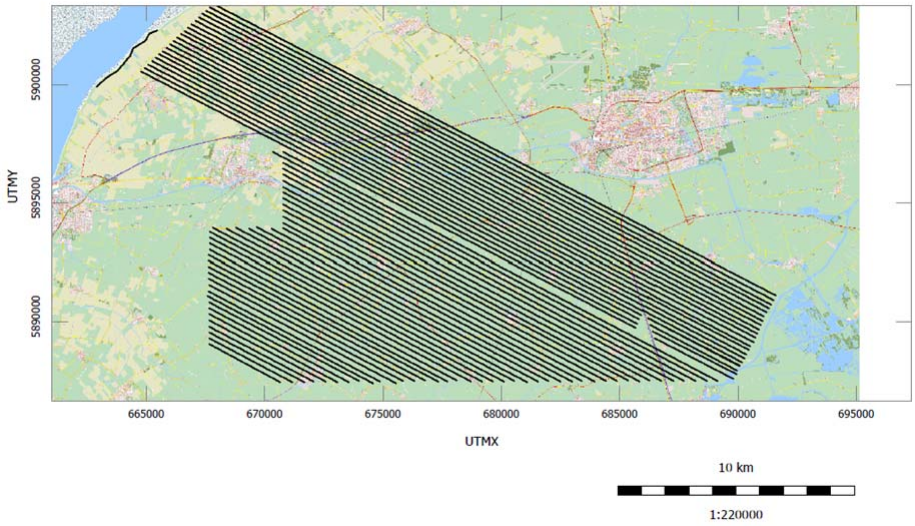

Fig. 3: Overview of the flight lines at North of Friesland

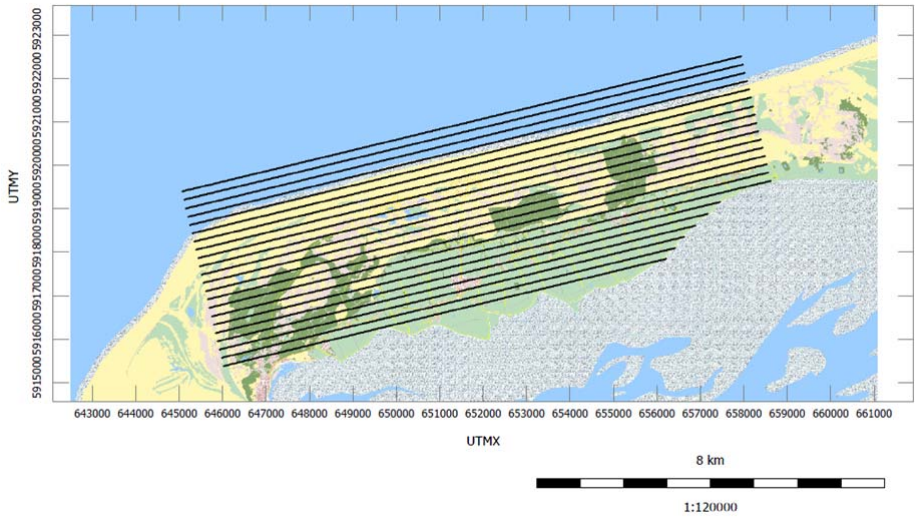

Fig. 4: Overview the flight lines on Terschelling Island

3. Electromagnetic properties of rocks

This chapter intends to give a brief explanation of what are the electromagnetic properties of the rocks and how do they vary according to the medium in question.

3.1 Conductivity

Ohm's Law is a constitutive relationship of Maxwell equations, this is, it an equation that relates the force field and the effect created in the medium by the force field (Zhdanov and Keller, 1994). The Ohm's Law states that $\vec{J} = \sigma\vec{E}$, which $\vec{J}$ is the current density in $\left[A/m^2\right]$, $\vec{E}$ is the electric field in $\left[V/m\right]$ and σ a tensor that relates the two fields, called conductivity in $\left[S/m\right]$. In a cartesian system, the conductivity tensor is a matrix of 3×3, having therefore 9 elements. It is a symmetrical tensor and if it is expressed in the principal directions of conductivity, it will have nonzero elements only in the main diagonal:

$$\sigma = \begin{bmatrix} \sigma_{xx} & 0 & 0 \\ 0 & \sigma_{yy} & 0 \\ 0 & 0 & \sigma_{zz} \end{bmatrix}$$

If the diagonal elements are the same, we are in the presence of an isotropic material, this is the electrical field vector and the current density is collinear, and therefore the electric conductivity is a scalar. This is very useful because we can then define the electrical resistivity as $\rho = \frac{1}{\sigma}$.

It is necessary to have in mind that the conductivity is not a constant parameter; it changes with time, temperature, pressure and others environmental factors.

3.2 Dielectric permittivity

The second main constitutive equation states that there is a relationship between the electric field intensity and the displacement. For this equation it's introduced another electrical property of the medium, the dielectric permittivity, ε, measured in $\left[F/m\right]$.

$$\vec{D} = \varepsilon \cdot \vec{E} \tag{3.1}$$

On the contrary of the conductivity, the dielectric permittivity has a defined value of 8.854×10^{-12} $\left[F/m\right]$.

3.3 Magnetic permeability

The relation between the magnetic field strength and the magnetic induction is done by the third constitutive relation of the Maxwell equations:

$$\vec{B} = \mu \cdot \vec{H} \tag{3.2}$$

Where μ is the magnetic permeability of the medium measured in $[H/m]$. On the contrary of the other two parameters of electrical properties of the medium, the magnetic permeability is not dependent on the applied field strength. When not in presence of material, the magnetic permeability assumes the value for the free-space, $\mu = 4\pi \times 10^{-7}\ H/m$.

3.4 Mechanism of conduction of electric current

There are three mechanism of conduction of electric current: electronic conduction, electrolyte and semiconductor. In a rock, there exists or can exist all these three processes, which means that the classification of the type of conduction of a rock only tell us which is the most important conduction process.

The electronic conductions occur in metals and depend directly on the number of free electrons present on the metal and the mean time between the collisions of the electrons with the atoms of the metallic net. This type of conduction is the one that allows having lower conductivities, although it is rare to be the predominant mechanism on the crustal rocks.

In the case of the semiconductors the conduction is made by movement in the gaps; it increases with the raising of the temperature due to the release of valence electrons and the appearing of more available gaps for conduction. The geological materials behave normally as semiconductors unless if they are pure metals, as such, insulators.

Finally, we have the mechanism by electrolyte conduction that occurs in the presence of an ionic solution inside the rock. When a salt dissolves in water, the ions that form it will split up. In the presence of an external electric field, the anions will move towards the applied field and the cations on the opposite way, existing thus a conduction of electrical current. This mechanism depends on temperature; an increase in temperature promotes a decrease on viscosity of the fluid, thus increasing the mobility of ions which implies the decrease in resistivity. However, if the temperature is very high, it may occur vaporization of the ionic solution, leading to an abrupt increase of the resistivity.

The last mechanism is the dominant conduction mechanism in most cases at the upper crust. In this case the factors that influence the conductivity of the rock, beyond the conductivity of the rock matrix

itself, is the: quantity of fluid, the porosity, that can be intergranular or of fracture, the salinity of the ionic solution, the temperature, the saturation, the pressure and the clay content.

- Intergranular porosity: the more pore exits in the rock, bigger is the quantity of the ionic solution that the rock can have, and naturally diminishing its resistivity. The pores may have others preferred directions, that means that the resistivity depends on the direction that it is measured. However, there is the possibility that the rocks containing other solution not aqueous, which is the case of the hydrocarbonates.
- Porosity of fracture: a rock may have plans of fracture, that when they are full with ionic solution, it behaves almost as a short circuit when the measurement is made parallel to the plan of fault. If it is measured perpendicularly it barely registers any kind of effect in the resistivity.
- Salinity: the more salinity a rock has, bigger will be the electrical conductivity because it exits more available conductors (ions).
- Temperature: influences the mobility of the ions and therefore the conductivity of the electrolyte.
- Saturation: is defined as the fragment of the pore space occupied by water. A pore that is not completely filled has a resistivity much higher than when it is full, this is because the air is a very bad conductor.
- Pressure: increasing of the pressure may have three distinct effects on the conductivity of the rock. The most common situation is the increasing of the resistivity due to the fact of the diminution of volume of the pores, and therefore, it leads to the diminution of the interstitial fluid available for conduction. However, if the rock does not expel the fluid when it is being compressed the pressure inside the pores increases, it is said to be over-pressurized, observing a decrease in the resistivity. Another effect may have to do with the fractures. In the case of existing perpendicular fractures and are collinear with the direction of compression, the rise in the pressure causes that the anisotropy coefficient of the rock changes significantly; if it has a perpendicular direction, the gaps closes causing a increase in the resistivity if it has previously filed with water.
- Clay content: the presence of clay causes a diminishing of the resistivity and its dependence in frequency. The effect of the diminishing of the resistivity has to do to the fact that the clay possesses an active electronic surface.

There are still other factors that can influence the conductivity, such as the compression of the material. For example, the sands are very resistive, but when in contact with water, as they are slightly compressed its resistivity is reduced.

3.5 Archie Law

The Archie Law (1942) is a mathematical relation between the electrical proprieties of the rocks and its hydrogeological proprieties, and it's given by:

$$\sigma_w = IF\sigma_I \tag{3.1}$$

if we are not in the presence of clay. σ_w represents the conductivity of water, σ_I the electrical conductivity of formation, F the factor of formation and I the index of resistivity. F and I are expressed in terms of porosity ϕ and S_w saturation and have the following expression:

$$F = a\phi^{-m} \tag{3.2}$$

$$I = S_w^{-n} \tag{3.3}$$

Where a, m and n are empirical constants. Thereby, expressing the Archie Law in function of this parameters and transforming the conductivity into resistivity we have:

$$\rho_f = \rho_w \cdot \phi^{-m} \cdot S_w^{-n} \cdot a \tag{3.4}$$

This formula is only valid if we are not in the presence of clay. But for the case of being in the presence of clay, it has to be summed a corrective term that encounters this fact. Waxman and Smits (1968) obtained experimentally an expression that takes in account the clay factor:

$$F_a = \frac{\rho_w}{\rho_f} = \frac{F}{1 + \rho_w BQ} \tag{3.5}$$

Where F_a is the formation factor with the presence of clay, Q the capacity of the clay to do an ionic exchange per unit of volume and B is a factor that takes in account the variation of the ions mobility with the solution concentration.

4. Transient electromagnetic method

Electromagnetic techniques were originally developed for locating conductive ore bodies, but in the last 20 years are used for environmental investigations, in particularly groundwater contamination. This is due to the fact that this method is sensitive to changes in resistivity which is related to such as type of rock, type of porosity, grain size, fractures and clay content.

The instrumentation consist of a transmitter (Tx) and a receiver (Rx) placed on the surface of the earth or up in the air at a certain altitude, as it is the case for airborne EM System. Using a source of alternating field (the primary field) it induces currents into the ground, where these currents generate a secondary magnetic field. When measured in a frequency domain, the receiver measure both primary and secondary field (EM34, VLF). The intensity of the secondary field diminishes with the depth which makes it harder to distinguish in the presence of the primary field. On the other hand, measuring in a time domain the secondary field is detected without the presence of the primary field (TEM).

Theoretically a time domain response is mathematically transformable to a frequency domain response using the Fourier transform and vice-versa.

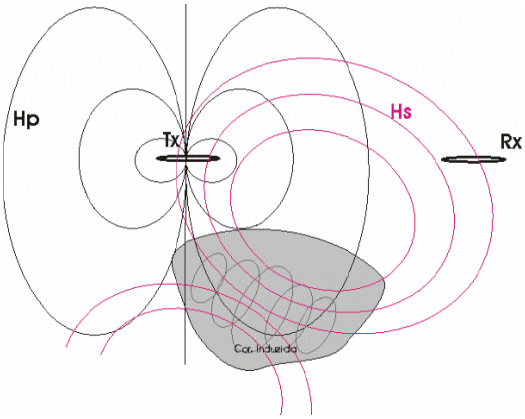

Fig. 5: Magnetic dipole. Primary field (H_p) and secondary field (H_s)

4.1 The principle of the Time Domain Electromagnetic Method (TEM)

The TEM method is a time-domain method and it uses a direct current which normally is passed through a wire loop. When the current is turned on it creates a primary field that is constant, Fig. (6a), and therefore there is no induction present. After turning off abruptly the current, it is observed a decay on the electric field that will originate a magnetic field which in turn will induce currents on the subsoil, eddies, Fig. (6b). According to the Lorentz law, this variation will create a secondary magnetic field that tends to cancel the variation (diminishing) the primary field.

The measurements are done during the off-time by time gates, which are basically field integrations that have a logarithmically increasing length so that it allows to enhance the signal/noise (S/N) rate at late times – log-gating (Christiansen et al., 2006).

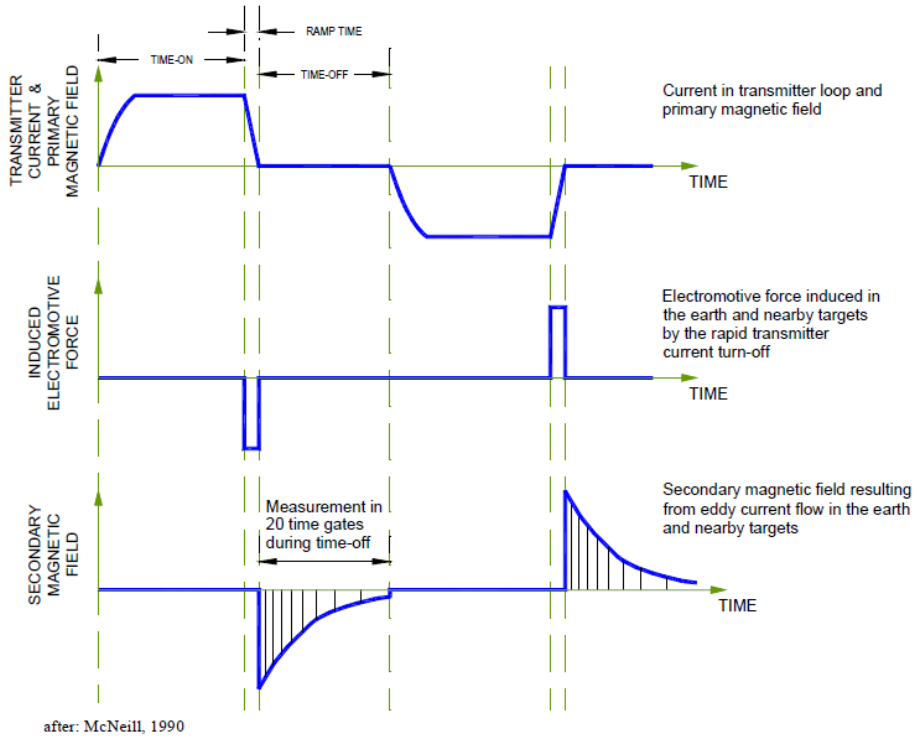

Fig. 6: Basics principals of TEM

The induced currents are initially concentrated immediately below the transmitter loop, Fig. (7a).With time, those currents will diffuse down and away from the transmitters, Fig. (7b). To describe the behavior of the currents in the ground it is often made an analogy with “smoke rings” (Nabighian, 1979), where initially strong currents form in the ground close to the transmitter loop. Then, the “smoke ring” will expand, fade and travel down through the subsoil. The rate of diffusion depends on the conductivity of the subsoil. In the case of resistive mediums the currents will diffuse very rapidly. In contrary, in conductive mediums the currents will diffuse more gradually.

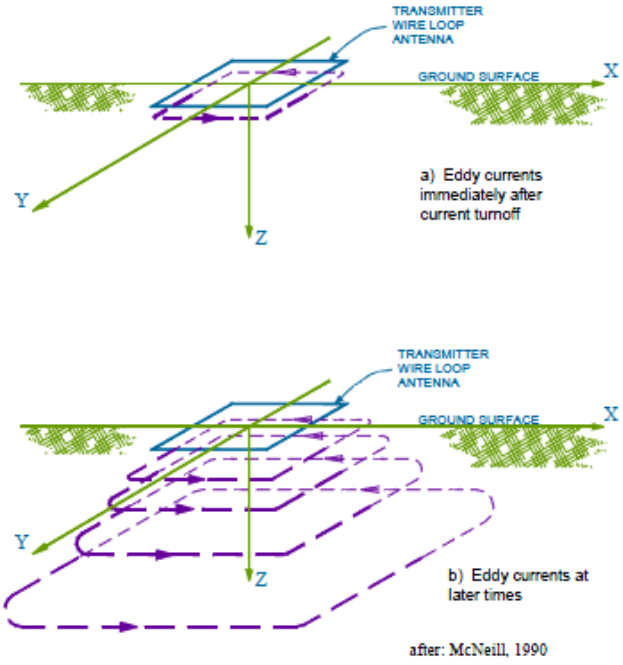

Fig. 7: TEM eddy current flow

4.2 Coherent and incoherent noise

When studying TEM two types of noise occur: coherent noise and incoherent noise. The incoherent noise, sometimes referred to as random noise, is temporally uncorrelated with the transmitter source current and it's commonly known as electromagnetic noise; it is a consequence of electrical currents formed on the Ionosphere. The most known electromagnetic noise, mainly common in the tropical areas, is a result of thunderclouds and the lightning discharge, denominated as spherics. It has a typical frequency of 1 Hz that can be removed from the raw data by stacking[1]. Another electromagnetic noise, although not relevant enough to be considered a source of noise in the transient methods, is originated by fluctuations on the Earth magnetic field.

Coherent noise is a temporally noise correlated with the transmitter source current and can include transmitter or receiver loop misalignment or instrumental drift. It can be divided into two categories: geological noise and cultural noise. Geological noise is associated to the interaction of electrical current with the inhomogeneous geoelectrical properties of the rock (Fitterman and Labson, 2005). See chapter 3.4.

[1] Stack: it is used to improve the S/N rate; measures the transient signal in gates and after it averages the gate values.

Cultural noise is defined as the electromagnetic field generated by currents induced in man-made conductors such as pipe lines, buried tanks, steel fences or other objects. This kind of noise is also known as coupling and can not be accurately removed by stacking. The way to avoid it is to try to keep a safe distance, about a minimum of 100 meters, from the source of coupling.

There are two types of coupling: galvanic and capacitive. The galvanic coupling is characterized by a LR circuit that has a galvanic return path. It has a decay that decreases exponentially. This kind of coupling can be very hard to identify it can be easily be confused with a low resistive layer. This type of coupling may be found near high voltage power-lines, fences, metal roads guard, etc, Fig. (8).

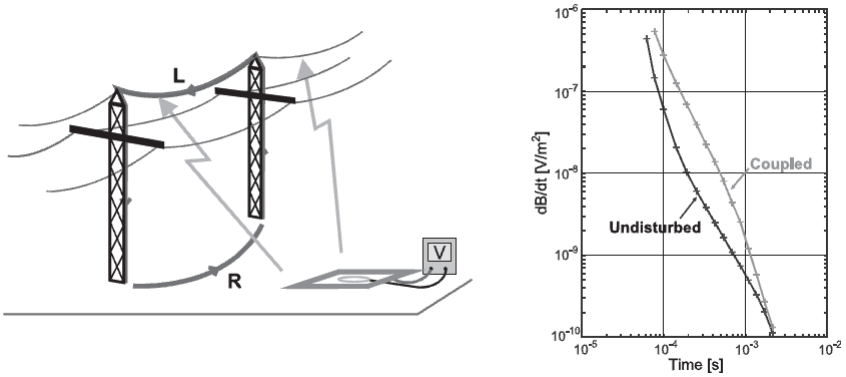

Fig. 8: Example of a galvanic coupling (Christiansen, 2006)

A capacitive coupling is characterized as a LCR circuit and it is easier to be identified as it is seen as an oscillating decay as a consequence of having an induced current that interacts with a coaxial cable and the soil subsurface creating a large capacitor, Fig. (9). This phenomenon is associated with long isolated wires, telephones cables, buried cables, etc.

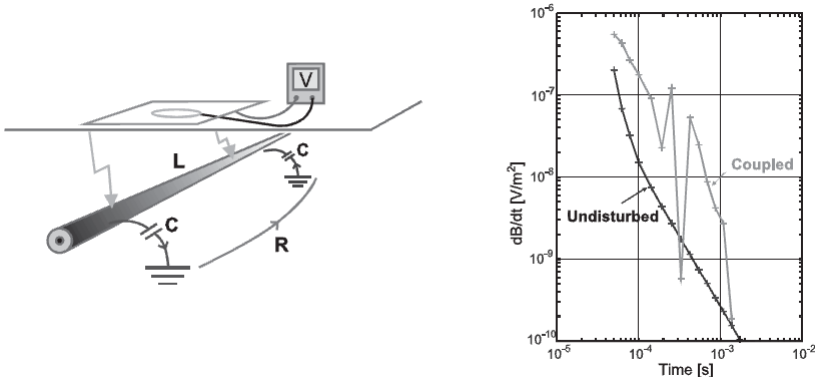

Fig. 9: Example of a capacitive coupling (Christiansen, 2006)

5. Electromagnetic theory

The nomenclature for the equations used in this chapter is that capital letters usually represents frequency-domain and the small letter represents time-domain.

5.1 Maxwell equations

Maxwell, James Clerk (1831 – 1879), was a British physicist that explained the proprieties of electromagnetism. He published a set of four differential equations in which he describes the nature of electromagnetic fields in terms of time and space.

We can define the electromagnetic field in terms of five vector functions: electric field intensity ($\vec{e}$), magnetic induction ($\vec{b}$), magnetic field intensity ($\vec{h}$), dielectric displacement ($\vec{d}$) and electric current density ($\vec{j}$) all in the time domain as:

Faraday's Law:
$$\nabla \times \vec{e} + \frac{\partial \vec{b}}{\partial t} = 0 \tag{4.1}$$

Ampere's Law:
$$\nabla \times \vec{h} - \frac{\partial \vec{d}}{\partial t} = \vec{j} \tag{4.2}$$

Gauss's Law for magnetic field:
$$\nabla \cdot \vec{b} = 0 \tag{4.3}$$

Gauss's Law for electric field:
$$\nabla \cdot \vec{d} = \rho \tag{4.4}$$

Where ρ is the electric charge density.

In a brief description Faraday's Law states that a circulating electric field is produced by a magnetic field that changes with time; the Ampere's Law that a circulating magnetic field is produced by an electric current and by an electric field that changes with time; and on the other hand Gauss's Law for magnetic field stated that the magnetic field has divergence equal to zero, i.e., the magnetic field is a solenoidal vector field; the Gauss's Law for electric field states that the divergence of the displacement current is equal to the electric charge density.

Relations between the electric fields ($\vec{e}$) and magnetic ($\vec{h}$) and the displacement fields ($\vec{d}$ and $\vec{b}$) depend on the state of polarization of the medium, characterized by the quantities ε , μ and σ such that:

$$\vec{d} = \varepsilon \cdot \vec{e} \tag{4.5}$$

$$\vec{b} = \mu \cdot \vec{h} \tag{4.6}$$

$$\vec{j} = \sigma \cdot \vec{e} \tag{4.7}$$

Where ε , μ and σ are the dielectric permittivity, the magnetic permittivity and the electric conductivity.

Using the Fourier transform allow us to convert equation written in the time domain to frequency domain. Applying this to the equation (4.1) and (4.2), we obtain the Maxwell's equations in the frequency domain:

$$\nabla \times \vec{E} + i\mu\omega\vec{H} = 0 \tag{4.8}$$

$$\nabla \times \vec{H} - (\sigma + i\varepsilon\omega)\vec{E} = 0 \tag{4.9}$$

According to Harrington (1961), he defined impedivity ($\hat{z} = i\mu\omega$) and admittivity ($\hat{y} = \sigma + i\varepsilon\omega$), therefore equations (4.8) and (4.9) can be re-written as:

$$\nabla \times \vec{E} + \hat{z}\vec{H} = 0 \tag{4.10}$$

$$\nabla \times \vec{H} - \hat{y}\vec{E} = 0 \tag{4.11}$$

5.2 Schelkunoff potential

When in a region there are sources it is necessary to compensate the Maxwell Equations, transforming them into inhomogeneous equations:

$$\nabla \times \vec{E}' \hat{z}\vec{H} = -\vec{J}_m^s = i\mu_0\omega\vec{H}^s \tag{4.18}$$

$$\nabla\vec{H} - \hat{y}\vec{E} = \vec{J}_e^s = i\omega P^s \tag{4.19}$$

Where $\vec{J}_m^s$ is a magnetic current and $\vec{J}_e^s$ is an electric current.

The use of Schelkunoff potentials, A and F, helps to simplify the calculation of the derivation by differentiation of $\vec{E}$ and $\vec{H}$ (Ward and Hohmann, 1988).

The electric and magnetic field can be written as a superposition of electric and magnetic sources:

$$\vec{E} = \vec{E}_m + \vec{E}_e \tag{4.20}$$

$$\vec{H} = \vec{H}_m + \vec{H}_e \tag{4.21}$$

For fields that have magnetic sources it is assumed that $\vec{J}_e^{\,s}$ is zero, and for electric sources the same assumption is made for $\vec{J}_m^{\,s}$.

For the specific case of a TEM system, it uses a magnetic source and therefore the fields due to magnetic sources can be written as (Christiansen et al., 2006):

$$\nabla \times \vec{E}_m = -\vec{J}_m^{\,s} - \hat{z}\vec{H}_m \tag{4.22}$$

$$\nabla \times \vec{H}_m = \hat{y}\vec{E}_m \tag{4.23}$$

Calculating the divergence of equation (4.23) we obtain:

$$\nabla \vec{E}_m = 0 \tag{4.24}$$

This means that $\vec{E}_m$ can be represented as the curl of a vector function:

$$\vec{E}_m = \nabla \times \vec{F} \tag{4.25}$$

Substituting equation (4.25) in equation (4.23) we have:

$$\vec{H}_m = -\hat{y}\vec{F} - \nabla U \tag{4.26}$$

Where U is an arbitrary scalar function due to the fact that is not mandatory that the curl of the vector is equal to the vector itself.

Using the two previous equations, equation (4.22) transforms into:

$$\begin{aligned} &\nabla \times \nabla \times \vec{F} = \vec{J}_m^{\,s} - \hat{y}\hat{z}F - \hat{z}\nabla U \\ &\Leftrightarrow \nabla \nabla \cdot \vec{F} - \nabla^2 \vec{F} = \vec{J}_m^{\,s} - \hat{y}\hat{z}F - \hat{z}\nabla U \end{aligned} \tag{4.27}$$

Arbitrarily imposing the Lorentz Condition:

$$\nabla \cdot \vec{F} = -\hat{z}U \tag{4.28}$$

Solving the equations just in terms of $\vec{F}$, this means transforming equation (4.27) into the inhomogeneous Helmholtz equations:

$$\nabla^2 \vec{F} + k^2 \vec{F} = -\vec{J}_m^s \tag{4.29}$$

Where according to the quasi-static approximation, the wave number, k, is given by:

$$k \approx -i\mu_0 \sigma w \tag{4.30}$$

The wave number is an important parameter in determining the behavior of an electromagnetic field travelling in a conductive medium.

To determine the equations in the case of only one source being used, it is necessary to combine the Helmholtz equations with the Lorentz Conditions as well as with the equations of continuity. Resulting for the case of using a magnetic source, $\vec{J}_m^s$:

$$\vec{E}_m = -\nabla \times \vec{F} \tag{4.31}$$

$$\vec{H}_m = -\hat{y}\vec{F} + \frac{1}{\hat{z}}\nabla\left(\nabla \cdot \vec{F}\right) \tag{4.32}$$

Assuming that the Earth is 1-D, the Schelkunoff potential, F, only was z-component, therefore:

$$\vec{F} = F_z \vec{u}_z \tag{4.33}$$

Where, F_z is the scalar function of x, y, z and $\vec{u}_z$ is a unit vector in the z-direction.

Substituting this equation on equation (4.31) and (4.32) and knowing that for a TEM system it only transmits a transverse electric field, this is a field that propagates in the xy-plane, we get:

$$\begin{aligned} E_x &= -\frac{\partial F_z}{\partial y} \\ E_y &= \frac{\partial F_z}{\partial x} \\ E_z &= 0 \end{aligned} \tag{4.34}$$

5.3 Transient response for a half space

For a TEM system the current source has a shape of a square loop where it is a good approach of a circular loop. This means that for calculation of the integration of the vertical magnetic dipoles over a circular loop, the equation for the Schelkunoff potential F between the source at $P(x, y, z)$ and the earth is given by:

$$F(\rho, z) = \frac{\hat{z}m}{4\pi}\int_0^{\infty}\left[e^{-u_0|z+h|} + r_{TE}e^{u(z-h)}\right]\frac{\lambda}{u_0}J_0(\lambda\rho)d\lambda \tag{4.35}$$

Where:

m – Magnetic moment in the z direction

J_n – Bessel function of order n

$\lambda = \sqrt{k_x^2 + k_y^2}$ and k_n^2 is the wave number under the quasi-static approximation

$u_n = \sqrt{\lambda^2 - k_n^2}$

$\rho = \sqrt{x^2 + y^2}$ – Radial distance from the source to the receiver

r_{TE} – Reflection coefficient

h – Transmitter height

z – Receiver height

Integrating the previous equation over a circular loop with radius a and a I current, we obtain the following result:

$$F(\rho, z) = \frac{\hat{z}_0 Ia}{2}\int_0^{\infty}\frac{1}{u_0}\left[e^{-u_0|z+h|} + r_{TE}e^{u(z-h)}\right]J_1(\lambda a)J_0(\lambda\rho)d\lambda \tag{4.36}$$

When substituting the calculated Schelkunoff potential for a circular loop in the equation (4.32), the vertical magnetic field is:

$$H_z = \frac{Ia}{2}\int_0^{\infty}\left[e^{-u_0|z+h|} + r_{TE}e^{u_0(z-h)}\right]\frac{\lambda^2}{u_0}J_1(\lambda a)d\lambda \tag{4.37}$$

Considering that we are in a homogeneous half-space, the reflection coefficient is given by:

$$r_{TE} = \frac{\lambda - u}{\lambda + u} \tag{4.38}$$

Therefore we have:

$$H_z = \frac{Ia}{2}\int_0^\infty \left[e^{-u_0|z+h|} + r_{TE}e^{u_0(z-h)}\right]\frac{\lambda^2}{u_0}J_1(\lambda a)d\lambda$$

Assuming the quasi-static conditions $u_0 = \lambda$:

$$\Leftrightarrow H_z = \frac{Ia}{2}\int_0^\infty \left[e^{-\lambda|z+h|} + \frac{\lambda - u}{\lambda + u}e^{\lambda(z-h)}\right]\frac{\lambda^2}{\lambda}J_1(\lambda a)d\lambda$$

$$\Leftrightarrow H_z = \frac{Ia}{2}\int_0^\infty \left[e^{-\lambda|z+h|} + \frac{\lambda - u}{\lambda + u}e^{\lambda(z-h)}\right]\lambda J_1(\lambda a)d\lambda$$

Because the source or receiver is on the surface of the earth:

$$\begin{aligned}
&\Leftrightarrow H_z = \frac{Ia}{2}\int_0^\infty \left[e^0 + \frac{\lambda - u}{\lambda + u}e^0\right]\lambda J_1(\lambda a)d\lambda \\
&\Leftrightarrow H_z = \frac{Ia}{2}\int_0^\infty \left[\frac{\lambda + u + \lambda - u}{\lambda + u}\right]\lambda J_1(\lambda a)d\lambda \\
&\Leftrightarrow H_z = \frac{Ia}{2}\int_0^\infty \left[\frac{2\lambda^2}{\lambda + u}\right]J_1(\lambda a)d\lambda \\
&\Leftrightarrow H_z = Ia\int_0^\infty \frac{\lambda^2}{\lambda + u}J_1(\lambda a)d\lambda
\end{aligned} \tag{4.39}$$

Using the simple relation described on equation (4.6), and evaluating the integral and applying an inverse Laplace transform, we obtain:

$$b_z = \frac{\mu_0}{2a} I\left[\frac{3}{\sqrt{\pi}\theta a} e^{-\theta^2 a^2} + \left(1 - \frac{3}{2\theta^2 a^2}\right) erf\left(\theta a\right)\right] \tag{4.40}$$

Where:

$$\theta = \sqrt{\frac{\mu_0 \sigma}{4t}}$$

μ_0 - Magnetic permeability

a - Radius of the loop

I - Current

σ - Conductivity of the half-space

erf - Error function

When measuring the field, what is in fact being is the time-domain decay of the magnetic field intensity in the centre of the circular loop, $\partial b_z / \partial t$, that can be obtain by differentiating equation (4.40):

$$\frac{\partial b_z}{\partial t} = -\frac{I}{\sigma a^3}\left[3erf\left(\theta a\right) - \frac{2}{\sqrt{\pi}}\theta a\left(3 + 2\theta^2 a^2\right)e^{-\theta^2 a^2}\right] \tag{4.41}$$

For late times the following approximation $\theta \to 0$ is applied and the time-derivative of the magnetic field becomes:

$$\frac{\partial b_z}{\partial t} \approx -\frac{M}{20}\left(\frac{\sigma}{\pi}\right)^{3/2}\left(\frac{\mu_0}{t}\right)^{5/2} \tag{4.42}$$

Where:

$M = I\pi a^2$ - Magnetic moment of the transmitter

6. SkyTEM System

Airborne electromagnetic systems (AEM) have been explored since the 1990's for the purpose of metal exploration in Canada. Until the 70's, this kind of systems were dominated by Canada and Nordic countries. By the 90's, the AEM systems was divided into two categories: fixed-wing time-domain for the detection of deep conductive targets, and frequency-domain for high-resolution, near surface, conductivity mapping. These systems are cost efficient due to the fact that it allows covering large areas in a short period of time.

As an example of currents fixed-wing time-domain there is the GEOTEM, MEGATEM and TEMPEST, where the system is wound around the nose, wing tips and tail of the aircraft.

New systems of airborne TEM have been developed where the system is carried as a suspended weight on the cargo hook of the helicopter. As an example of these kind systems there is the AeroTEM, the NEWTEM, the HoisTEM, the VTEM and the SkyTEM. The first four systems were designed primarily for mineral exploration. The SkyTEM system is developed by the HGG Group at Aarhus University, Denmark for the purpose of groundwater investigations and environmental investigations (Sørensen and Auken, 2004).

Fig. 10: SkyTEM System in operation – Netherland fieldwork (Set. 2009)

6.1 Instrument

This system has the same principles as a ground-based TEM system, with the obvious difference that the entire system is carried as a sling load on the cargo hook of the helicopter. The light weight wooden lattice six-sided frame of the system caries the transmitter and receiver instruments, two GPS, two lasers that measure in a continuous mode the altitude while flying , and also inclinometers on the front and back of the frame to measure the tilt (pitch and roll) of the frame. A generator is carried between the helicopter and the frame in order to provide power to the system.

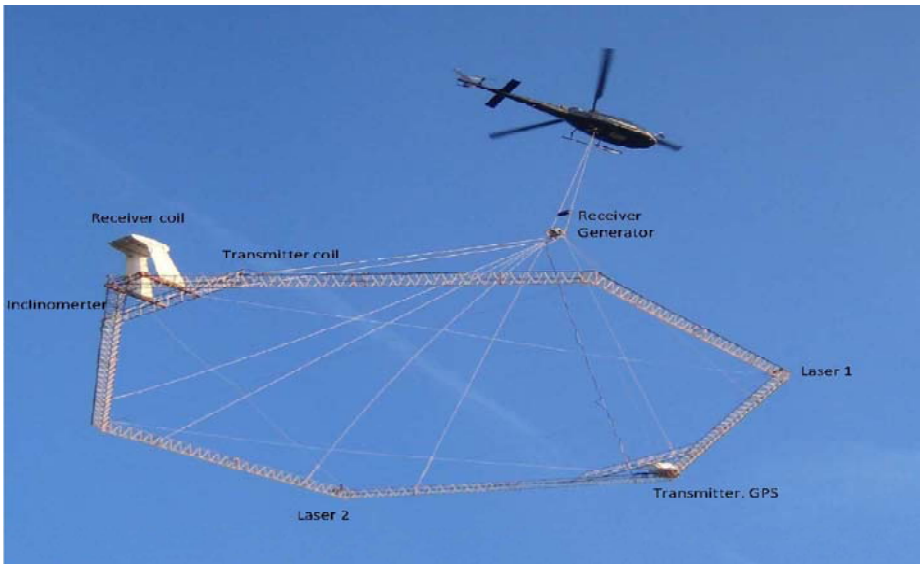

Fig. 11: SkyTEM configuration

6.2 Measurement procedure

The transmitter is a four-turn 300 m^2 loop divided into segments to allow transmitting with a low moment (LM) using one turn, and high moment (HM) using all four turns. The LM as a magnetic moment of approximately 12.000 Am^2 and the HM of roughly about 100.000 to 200.000 Am^2.

Configuration is a central loop with a vertical offset, as this kind of configuration is insensitive to local inhomogeneities in the near-surface resistivity was well as it is indifferent to small changes in the distance between the transmitter and the receiver.

In general the mean flight altitude was around 50 meters, with the exception when the helicopter was passing through, for example, a village or city, power lines, forests, etc. The helicopter flew at a mean speed of 16-20 m/s.

The SkyTEM System was configured in a two moment setup (low and high moment), with an approximate maximum transmitter moment of 122.000 Am^2. Where a full sounding curve covered a time interval from 3,5 μs to 8,84 ms.

6.2.1 Calibration

The SkyTEM System is an absolute calibrated system; this means that it is possible to reduce the interaction between the transmitter and the receiver, which the distortion of the measured off-time is negligible (Christiansen et al., 2006).

This calibration is done on the test-site at Lyngby (Denmark), where the layered earth model is known along a line and therefore it can then be compared with the response of the SkyTEM system.

6.2.2 Altitude

The altitude is a parameter that has a influence in the resolution, as the Earth response tends to decrease with the altitude. Therefore for higher altitudes the resolution at near surface tends to reduce. Therefore the operation altitude recommended is low, around 30 to 35 meters on flat fields and higher when passing trough forests.

Another consequence of decreasing of signal with the altitude, is that the coupling by man-made is intensified and therefore it is necessary to increase the safe distance to this kind of installations.

7. Geology

This chapter presents a brief description of the geology of the areas of study.

There is a known saying that goes like: "*God created the world but the Dutch made the Netherland*". Over the centuries the Netherlands have been constantly flooded either by the ocean or either by the three main rivers: Rhine, Wall and Meuse. The only effective way to protect the country from these floods was by building massive man-made sea dikes and creating chains of dunes barriers along the coast line.

This chapter will focus on the Holocene, Quaternary and young Tertiary Epoch due to its importance for the porpoise to hydrological studies.

7.1 North of Friesland

The Netherlands is part of the subsiding basing of the North Sea, therefore is characterized by sedimentary deposits, mainly fluvial and marine origin (Westerhoff and Mulder, 1984). At a depth of about 500 meters it can be found traces of clay from the Miocene. The overlaying Oosterhout Formation is from the late Tertiary – the Pliocene, and contains fine sand and clay. The Plieocene was a transitional stage between the Miocene and the Pleistocene, which started about 1.8 million years ago.

Between the Lower Pleistocene and the Cromerian epochs there was a period which occurred the transportation of sediments by the rivers Rhine and Meuse.

During the Pleistocene period occurred three ice ages. The first one took place during the Elsterien epoch that manage to interfere with the processing of a fluvial sedimentation. In the course of this epoch, it was observed the deposition of glacial melting-water clay. While still in the Elsterien epoch started a renewal fluvial sedimentation of the Rhine that continued to the Holsteinnian. The compositions of these deposits were coarse and fine sand that belong to the Urk Formation.

As a consequence of the second ice age in the Saalian epoch it was formed melting-water channels, which were filled with deposits of the Drente Formation (fluvial-glacial sand with ground moraine deposits). Once this ice age ended, Eemian epoch followed where the channels formed were filled up with marine deposits, predominantly sand with clays, and some peat to origin – Eem Formation. A third ice age, the Weichelien, did not arrive to the Netherland. However, strong winds manage to transport large quantities of sand all over the country.

In the Holocene, erosion occurred removing some of the formations formed during the Pleistocene. In this epoch, the sedimentation was influenced by the post-glacial sea level rise. As a result, a peat landscape was developed in the lowlands (topographically speaking). Because the sea level continued to rise, the sea flooded this peat landscape depositing a clay layer.

Era	Period	Epoch			Formation	Facies	Lithology
Cenozoic	Quaternary	Holocene			Westland	marine, aeolian, organic	tidal flat deposits, dune sands, peat, clay
		Pleistocene	Upper	Weichselian	Twente	aeolian	fine sands
				Eemian	Eem	marine	fine sands, clay
			Middle	Saalian	Drente	fluivioglacial,glacial	sand and gravel, glacial till
					Urk II	marine, fluivial	coarse sands, gravel
				Holsteinian			
				Elsterian	Peelo	fluivioglacial, glaciolimnic	coarse sands, gravel, heavy textured clay
				Cromerican complex	Urk II	marine, fluivial	sands
					Enchede	fluivial	sands
			Lower	Menapian			
				Waalian	Harderwijk	fluivial	sands
				Eburonian			
				Tiglian			
				Praetiglian	Maassluis	marine	fine sands
	Tertiary	Neogene	Pliocene		Oosterhout	marine	fine sands, clay
			Miocene		Breda	marine	clay

Fig. 12: Stratigraphy in the Northern Netherland

7.2 Terschelling

The Frisian Islands were formed during the old-Holocene and they are a consequence of the last ice age. Before this era, the Walden Sea was just an area of swampy lowland in the Rhine delta. Approximately 12.000 years ago the last glacial age ended and the melt down of the ice caps provoked a sea level rise about 60 meters, which flooded the area of Walden separating the lowlands from the continent.

Due to currents and tides, large quantities of sediments were carried to the lowland and consequently started to form sandy beaches. As a result of strong storms, the wind blew up the drifting sand into dunes. This natural costal barrier is a sort of protection of the inland lying behind against the sea.

Terschelling is one of the Frisian Walden Sea islands off the Northern coast of the Netherlands that separate the Walden Sea and the North Sea. It's also the longest of the islands with 30 km of length, with a total area of 91,59 km^2.

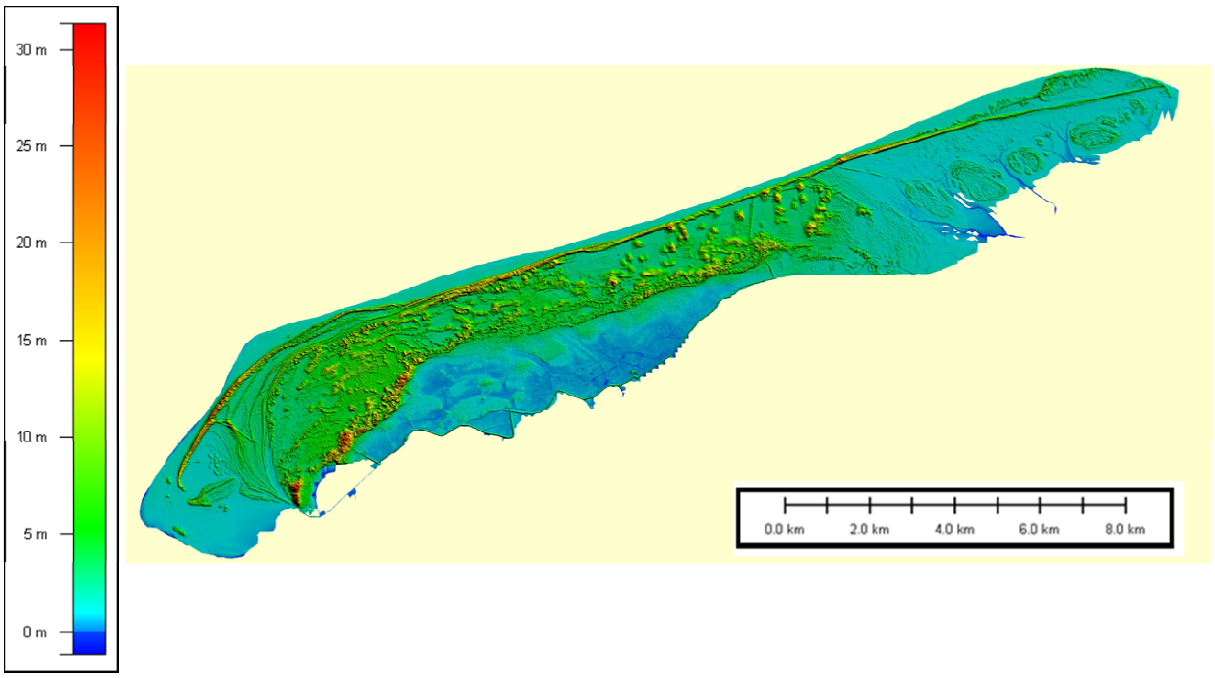

Fig. 13: Topography of Terchelling Island

As most of the Frisian Islands, Terschelling is characterized by Quaternary deposits such as sand, silt and clay. Being the oldest sediments found fluvial sands from the Harderwijk Formation – Lower Pleistocene.

There is a define dune along the North and west side of the island, with a maximum height of 31 meters. The polder area is found on the southern side of the island, where it is an embanked former salt-mash. This area was very low levels – 0 to 1 meter (Beukeboom, 1976).

7.2.1 Hidrology

In the 70th geoelectric surveys, the Schlumberger method (Hoogervost, 1970, Geinaert, 1974), have been used on the island for the purpose of delimiting the interface of salt/fresh groundwater, Fig. (14). On the western dune area we found the deepest interface at 100 meters depth. The other interface is found at 80 meter depth North of Hoorn.

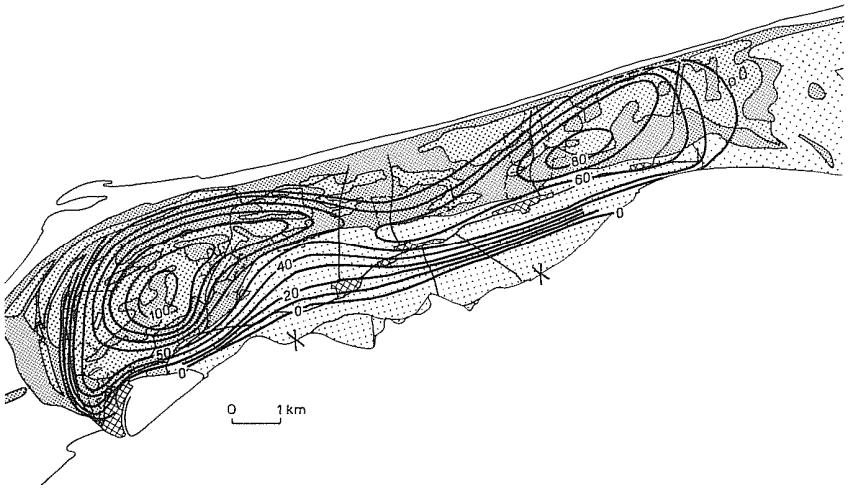

Fig. 14 : Contour-lines of the depth of the fresh/salt groundwater interface (Beukeboom, 1976)

The recharge of the lenses on a dune area is only done by precipitation, while the outflow is takes place mainly by groundwater flow.

According to the topography and shape of this island and also taking in account its subsurface factors, this particularly freshwater lenses under a dune area and adjacent polder is characterized to be a "semi-forced" asymmetrical freshwater lenses (Beukeboom, 1976).

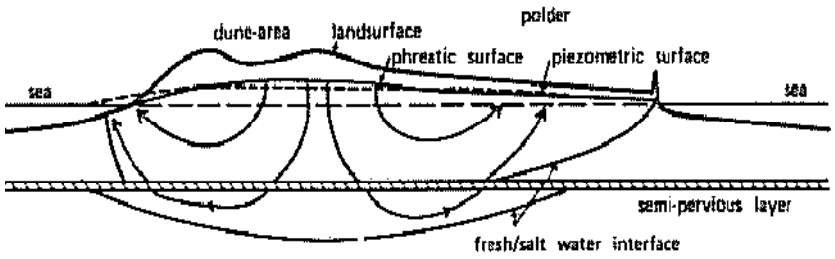

Fig. 15 :"Semi-forced" asymmetrical freshwater lenses under a dune-area and adjacent polder (Beukeboom, 1976)

8. Processing

The processing of the SkyTEM data was done using a software developed also by the HGG Group from Aarhus University, which is a program that allows working with geophysical, geological and GIS data – the *WORKBENCH*.

The data acquired on the field had a "*.rwb" files extension. These files need to be converted into two different extensions of files: the "*.skb", which contains the instrument data, the raw data and the averaged data; and the "*.sps", that keeps all the information about the GPS position, the altitude, the transmitter currents, the tilt, etc.

A geometry file contains system information about the loop size, the device positions, the calibration factors, etc.

After having these files it is possible to import the data to the *WORKBENCH* and start processing and inverting to finally be able to do a geophysical interpretation through the creation of thematic maps and profiles.

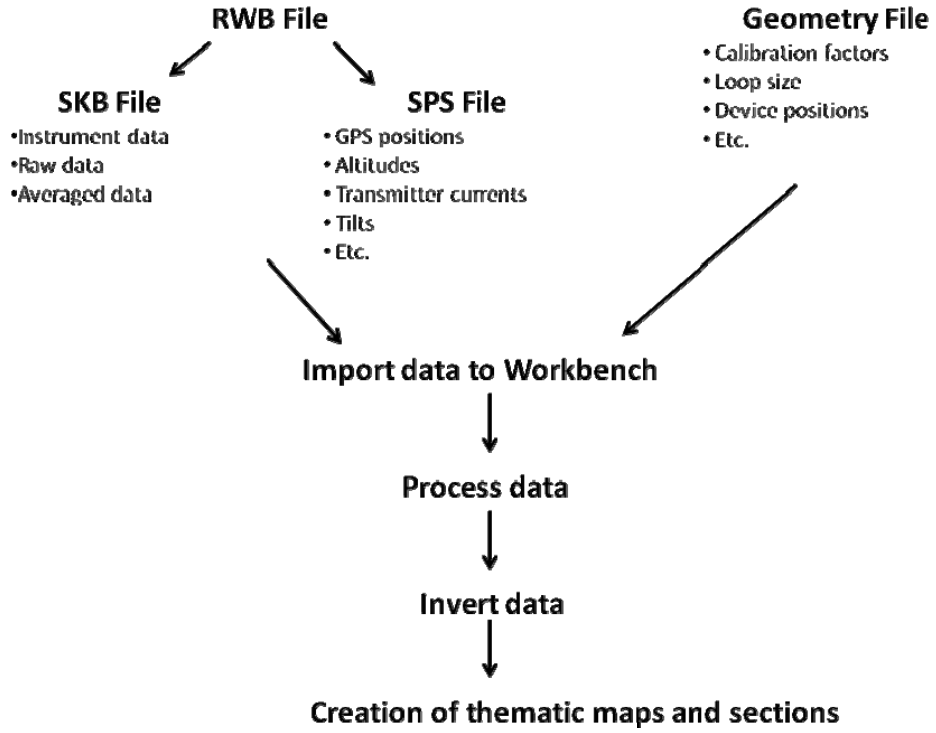

Fig.16: Schematic presentation of the procedure since the acquisition of the data until the geophysical interpretation

8.1 Navigation data processing

The first step of processing the SkyTEM data is stating by the evaluation of the navigation data. This data includes all the parameter acquired by the system, such as the tilt, altitude, voltage data, flight speed, topography, transmitter current, etc.

The navigation data is averaged and filtered automatically, although some manual processing of the altitude may be necessary.

Fig. (17) shows a 5 minutes time window of parameters of the navigation data from Friesland. The helicopter speed (light blue line) is more or less constant over the flights, where in this case it has a mean velocity of about 18 m/s. The raw altitude data collected from the 2 lasers are represented in light green and red, and the processed altitude (this is after the being filtered which the process is explained below) in black. The frame tilt, this is the pitch[2] (orange) and the roll[3] (blue), tends to oscillate naturally during the flight. On the figure where there is a big oscillation on the frame tilt corresponds when the helicopter is turning to proceed to the next flight line.

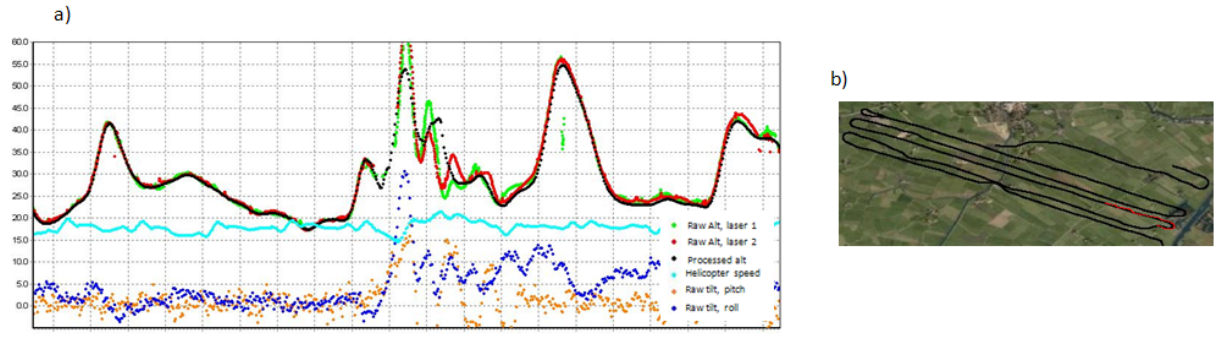

Fig. 17: Plot of the navigation data from North of Friesland in a time window of 5 minutes ~ 5.4 km a) shows the raw altitude of the two lasers in light green and red, the processed altitude in black, the helicopter speed in light blue, the tilt data in blue (roll) and orange (pitch); b) in black are represented the flight lines and in red the 5 min of the plot of the navigation data

[2] Pitch: oscillation around an axis perpendicular to the direction of the flight.

[3] Roll: oscillation around an axis on the direction of the flight.

8.1.1 Frame tilt – pitch and roll

The pitch and roll are measured by the two lasers on the frame. It is important to know this information because it may be necessary to correct the altitude of the frame caused by the wind, turning of the helicopter, etc, as the altitude is an input parameter of the inversion.

When the SkyTEM system is in production, this is when it is doing the acquisition of the data, the frame suffers an inclination of a certain angle, α. These needs to be correct in a way that the frame is parallel to the surface and therefore a correction of the angle of inclination is applied, Fig. (18).

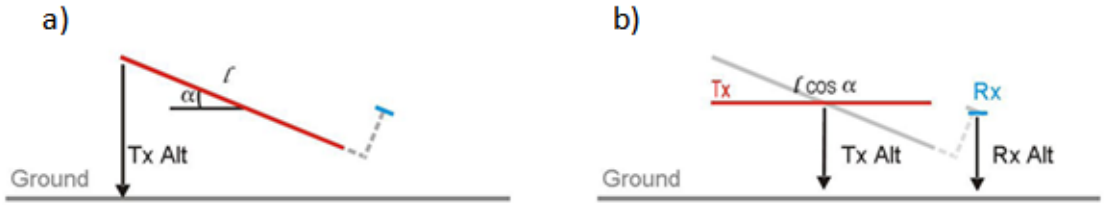

Fig. 18: a) Frame tilt angle, α, of the SkyTEM System in production, with the length l; b) Correction of the tilt frame (Auken, 2007)

8.1.2 Altitude

The lasers placed on the structure also measures the distance of the frame to the ground and therefore the altitude is influence also by reflection of the tree tops, resulting on a slightly lower altitude, Fig. (19). The correction of the flight altitude is made by using a repetition of cycles fitting a polynomial to the data while discarding outlying data.

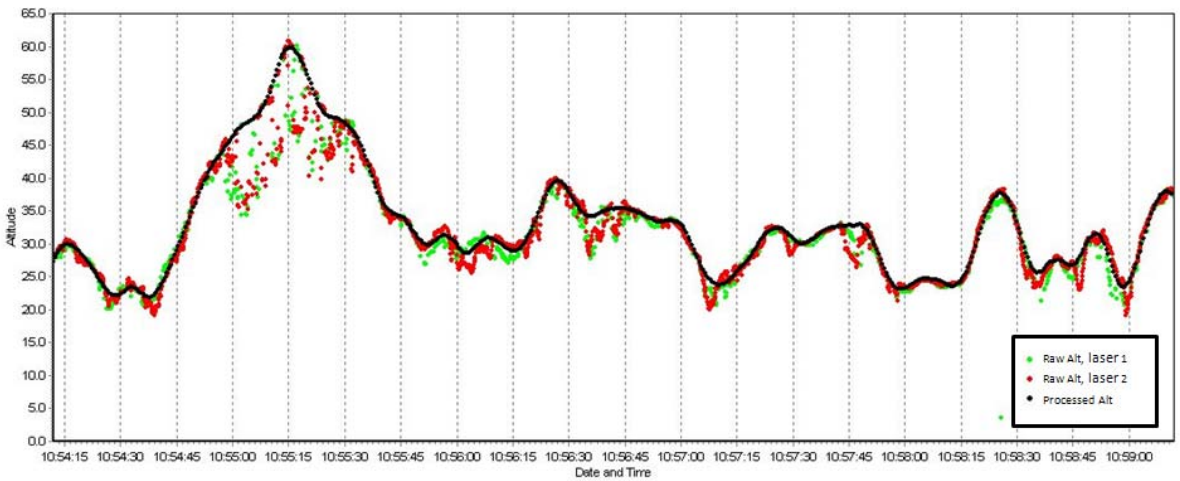

Fig. 19: Plot of the altitude data from Terchelling Island in a time window of 5 minutes ~ 4.8 km. Green and red dots represent the raw altitude data and the black line the polynomial altitude fit.

It is also important to have a precise measurement of the altitude as the Earth response tends to decrease with the increasing of the height. Increasing the altitude crosses the resolution in the near surface to be lost. In this particular case of the Netherlands, due to the fact that the Earth response has a high signal in this area, the admissible height of the frame was 55 meters. This means all the data above this height needs to be cut out. The *WORKBENCH* has a new feature that allows cut out all the raw data above a certain height.

8.2 Processing of voltage data

The procedure of processing the voltage data is considered the most time consuming step, as even thought there is an automatic process and there is filtering and averaging of the raw stack data, some manual processing is necessary especially when the area flew has a significant amount of infrastructure, e.g., cities.

It is important to remove all the coupling from the raw voltage data, otherwise they may cause a diminishing of the quality of the data. Most of the coupling can be removed by the application of filters. What these filters does is to find oscillations in the curve slope of the raw voltage data and then remove them. This means that the filter only helps to removes data in the situation where it has a capacitive coupling. As explained before, the detection of a galvanic coupling it is much harder to find, and therefore it's complicated to develop a filter for this kind of coupling.

Fig. (20) is an example of the time gates of Low Moment in the area of North of Friesland and its consequences of flying over a man-made conductor. In this plot is clear a pattern of good data as well as an example of coupled data. When the helicopter flies over a road, capacitive coupling, the imprint on the time gates (red line in Fig. (20.a)) as well as in the sounding curve is evident, Fig. (20.b); there is clear oscillation in the data. When flying over the advisable altitude (55 meters of this specific area) it is without a doubt visible a distortion on the data, and obviously this has to be cut out.

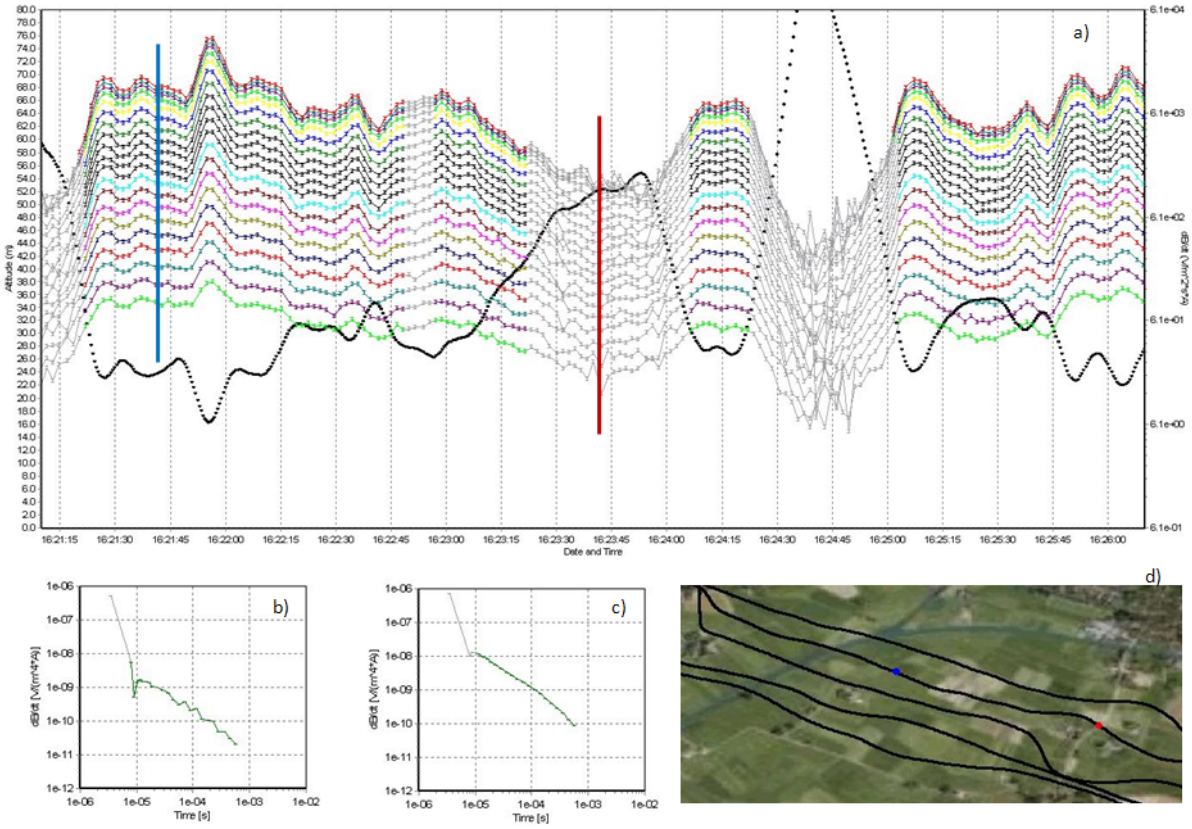

Fig. 20: a) Normalized raw LM data with a time window of 5 minutes ~ 6 km from North of Friesland. Each line represents a time gate. Grey lines have been excluded because they do not hold resistivity information. Black thick line represents the flight altitude. Example of soundings curves of a capacitive coupling (b) and in a "normal" situation (c). Having GIS information facilitate locating areas of coupling (d)

8.2.1 Data averaging scheme

In order to maintain the high resolution in the near surface, this is at the early times, as well as to be able to maximize the signal strength at late times (which implies that it also maximizes the penetration depth), the *WORKBENCH* uses a trapezoid filter as an averaging. The filter is designed in a way that it is narrowed at the top and wider as it goes to the bottom. The trapezoid shape is defined by 3 specific times and 3 specific widths chosen by the operator. In Fig. (21) shows the delimitation of the filter in a red line and the blue dots and line represents the raw data and its specific error bars, where the green dots represents the data being averaged. The trapezoid is a moving averaging filter that repeats at a determined time also chosen by the operator (red dashed line).

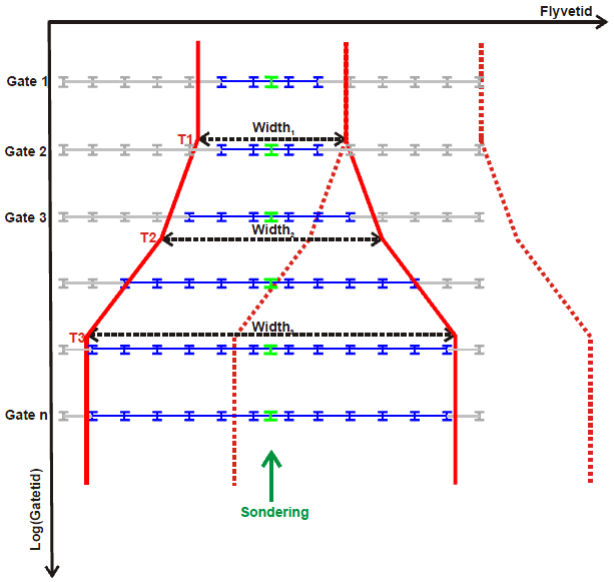

Fig. 21: Trapezoid averaging scheme (Hydrogeophysics Group, 2008)

In the practical case of the Terschelling Island, the trapezoid filter is repeated every 1.7 seconds in order to have a sounding about every 30 meters. For the Low Moment data the width were defined at the times 1e-5 s, 1e-4 s and 1e-3 s with the width of 3.5 s, 10 s and 16 s. This means that for a mean flight speed of 16 m/s the defined widths corresponds to 56 m, 160 m and 256 m. The width for the High Moment is a bit wider than for the Low Moment to allow to have a stronger signal strength. It was set up at 10 s, 16 s and 24 s, meaning that it corresponds to 160 m, 256 m and 384 m.

9. Inversion

The fundamental aim of geophysics is to "guess" the Earth's interior by collecting data on/or near surface. In general this is achieved by inverting the data assuming a more or less complex model for the Earth. This process is called the "inverse problem". It is generally a nonlinear problem and there is no unique solution to the problem. The concept of the inverse problem is a process of parameter estimation using constrains that can be applied to the model space in a way that the model or group of models are compatible with a particular set of observations. In sum the theory of inversion is simply a set of mathematical methods used to extract useful information about a set of observational physical measurements.

In opposition, in the forward problem the model and the parameters values are known. In this case we want to know the response of a specific model (and parameters). This response is unique.

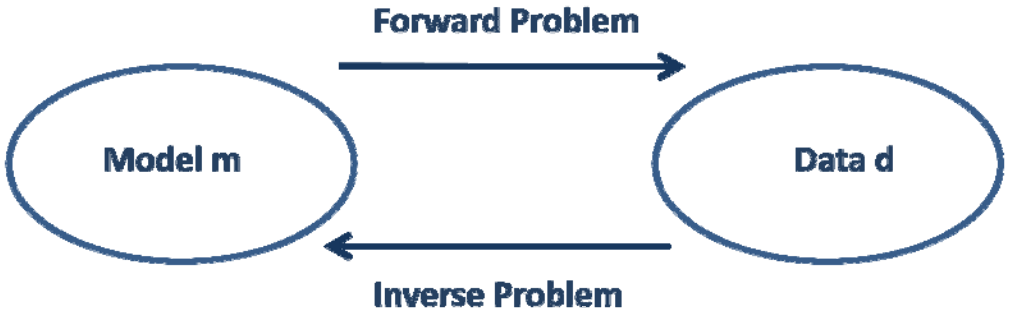

Fig. 22: Schematic explanation of the direct and inverse problem, where the data is the collected observations and the model is characterized by physical parameters.

9.1 Spatially Constrained Inversion

A constrained inversion methodology basically consists on the use of an algorithm that allows constraining parameters during the inversion in order to obtain a model with a smooth lateral variation. Auken and Christiansen (2004) and Santos (2004) publish an example of this algorithm that could create pseudo-2D images using a 1D forward solution.

The Spatially Constrained Inversion (SCI) is a quasi-3D modeling using 1D forward solution developed by the HHG Group (Aarhus University) in 2007. This new concept of inversion has the same basic principles as the LCI (Laterally Constrained Inversion), and the mathematical formulation is the same; a detailed description can be found in (Auken and Christiansen, 2004). It inverts using lateral constrains and sharp boundaries for continuous data but with the difference that it also allow to constrains information spatially. This is, the SCI does not constrain just laterally along the flight lines but constrains laterally in two dimensions (Viezzoli et al., 2008), Fig. (23). The advantage to have this

kind of laterally two dimensional constrain is that it resolves poorly determined parameters and spread a priori information.

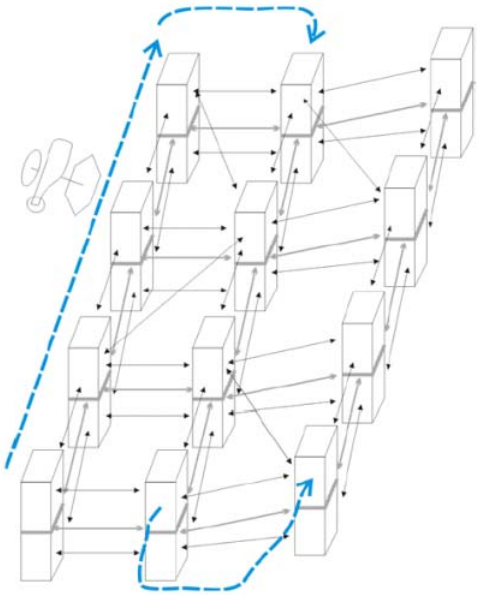

Fig. 23: Schematic presentation of the SCI concept (Viezzoli et al., 2007)

To be able to apply constrains laterally in two dimensions, it uses the Delaunay triangulation. This mathematical method also called nearest neighbors. For a given set of data point, the Delaunay triangulation is a set of lines connection each point to its natural neighbor. This means that every sounding is connected to the nearest neighbor, Fig. (24); sounding 'a' is connected to soundings 'b' to 'g', and consequentially this soundings will connect to their nearest neighbor giving origin to a continuum of interconnected soundings. Model parameter information spreads horizontally between nearest neighbors and then to the whole data set (Viezzoli et al., 2008).

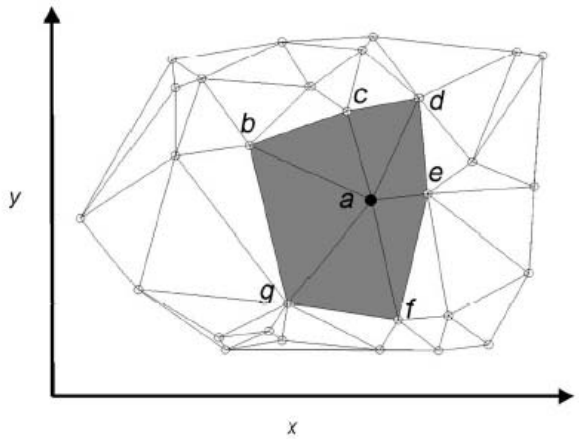

Fig. 24: Delaunay triangulation of random generated points on a plane (Viezzoli et al., 20008)

The process of the SCI is done in two runs. During the first run the data set is divided into smaller sub sets using the concept of the Delaunay triangulation. Once the first cell has been created, the second cell uses the points around the delimitation of the first cell to do an expansion using another process of nearest neighbor, Fig. (25.a). This process is repeated until each sounding of the data set is assigned to a cell .The cell size will vary according to the local data density.

The second run uses the results from the first run as a starting model. The grey line seen in Fig. (25.b) represents soundings that have a priori information from the first run, where the information will migrate toward the middle of the cells

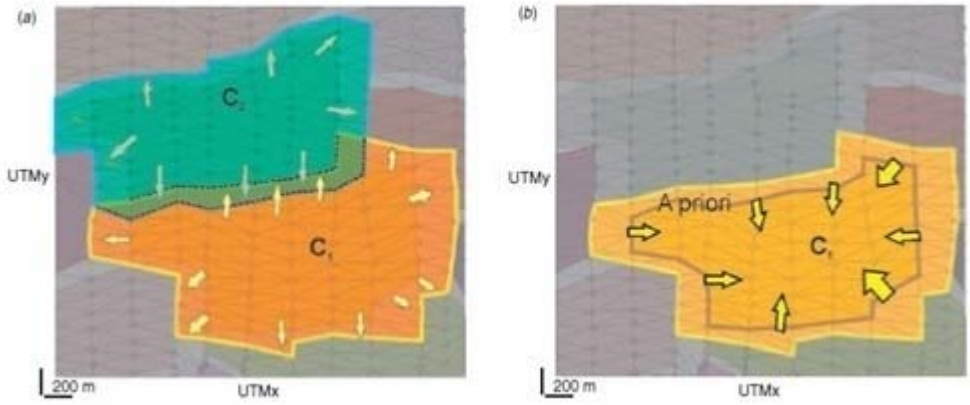

Fig. 25: a) Schematic representation of the first run of the SCI; b) Schematic representation of the second run of the SCI (Viezzoli et al., 2009)

9.2 Depth of investigation

The depth of investigation (DOI) was implemented recently in the *WORKBENCH*, and a paper is being prepared by its creator Anders Vest Christiansen. This new function allows us to have an estimate of how reliable the model is by giving us the minimum and the maximum of its penetration depth.

10. Discussion of results

In both areas of study, after processing the data they were inverted using the LCI setup, which allowed improving the data processing. After, the data was inverted with a smooth and a few layer SCI inversion setup. Here it will only be discussed the results of the SCI inversions.

The SCI setup for the smooth and few layer models can be found on Appendix 1.

All maps presented in this chapter were created using kriking[4] and pixel interpolation.

10.1 North of Friesland

The data residual for the North of Friesland was well fited, presenting values around or below 0.5 for the case of the 19 layer inversion, Fig. (26); where in the case of the few layer inversion (5 layers) the data residual was around 1 or less. It can be a bit hard for a first time user to be able to identify all the couplings in the data sets, but having a good GIS with the information of the location of the main roads and power lines helps. It is visible in Fig. (26) some cuts on the data, some due to detours of cities and another due to a big capacitive coupling at South of the profile, main highway.

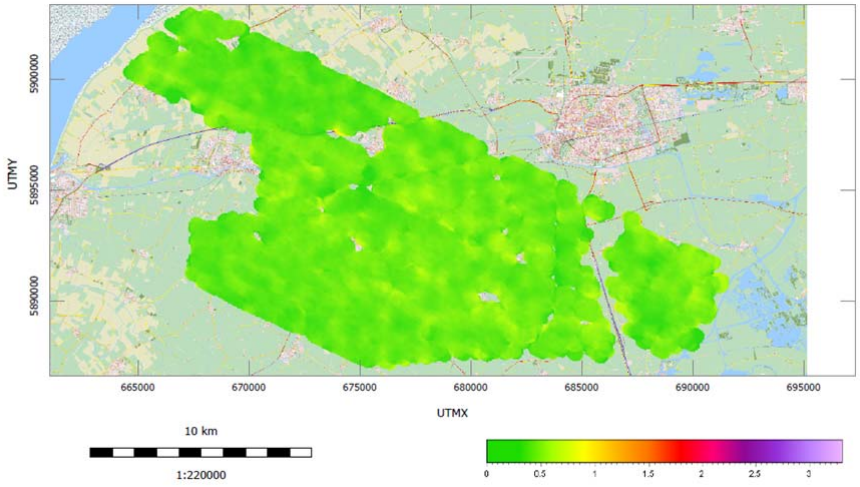

Fig. 26: Friesland data residual for the 19 layer SCI setup

[4] *Kriking*: weighted average of neighboring samples to estimate the "unknown" value at a given location

Analyzing the results of the depth of investigation (DOI) of the 19 layer inversion, there is a bigger penetration depth in the South East area with approximately 170 meters; meanwhile in the central area the penetration area is shallower with a maximum depth of 80 meters. The DOI for the few layer inversion does not vary much from these values.

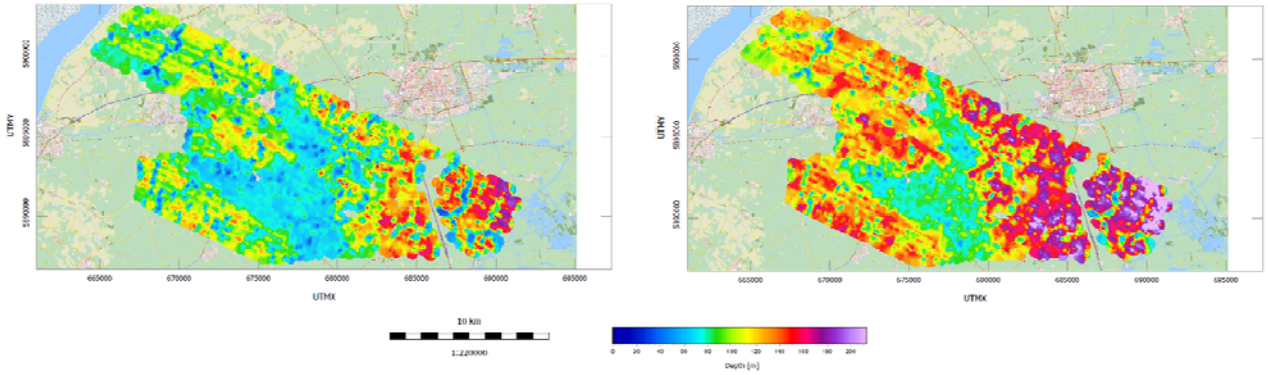

Fig. 27: DOI estimation on North of Friesland. On the left the Upper DOI and on the right the Low DOI

The geophysical results of the inversions for the smooth model as well as for the few layers are consistent with the geology of the area. Fig. (28) shows the thickness of the Holocene geological layer, where the traces of this unit can be found on the geophysical results, Fig. (29). Results from CPT's (Cone Penetration Test)[5] in the area indicate that the first 5 meters is saturated sand with fresh water. As we can see on Fig. (28) everything above 5 meters is in the tones of yellow/red, and in the horizontal resistivity map at the depth of -20 to -15 meters, Fig. (29), high resistivity (above 10 Ωm) represents fresh water. Comparing these two boundaries of high horizontal resistivity and geology above 5 meters, it can be found some similarity.

[5] *CPT*: it's an *in situ* method to determine the mechanical properties of the soil and delineating soil stratigraphy.

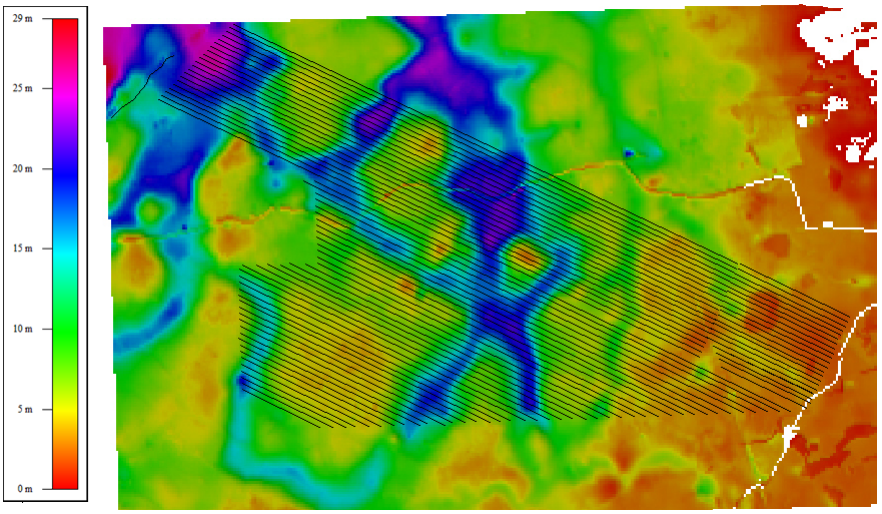

Fig. 28: Holocene thickness on the Friesland area (black lines represent the flight lines)

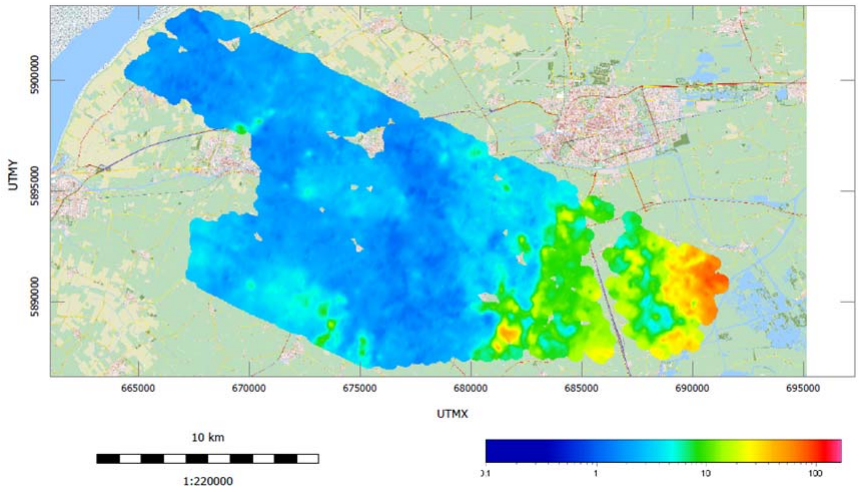

Fig. 29: Map of the horizontal resistivity for North of Friesland for the interval depth -20 to -15 meters of the SCI few layer inversion model

When comparing the geological layer – Eem layer, Fig. (29) – to the horizontal resistivity map presented in Fig. (28) some evidence of this Eem layer may be considered. It may be proposed that the prominence low resistivity next to the high resistivity in the SW part of the area is a consequence of the tides during that time.

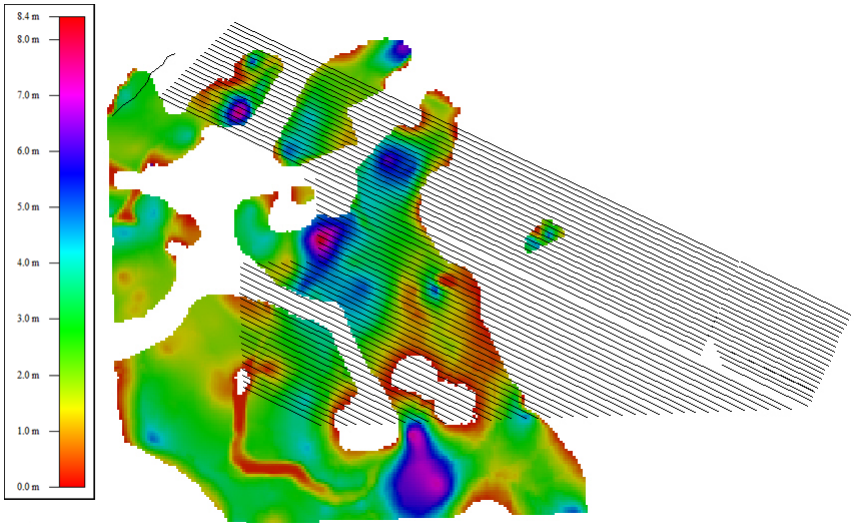

Fig. 30: Eem thickness on the Friesland area (black lines represent the flight lines)

Between the elevation -5 to -80 meters it is visible values of high resistivity on the SE of the profile. Analyzing the location of this more resistive area, in the proximity (about 200 meters from the flight lines) the big Magriet channel. Without having more information on the area, it is possible only to do assumptions. The relationship between the high resistivity and the proximity of the Magriet channel could be due to percolation, which is basically the movement of the water through the soil by gravity and capillary forces.

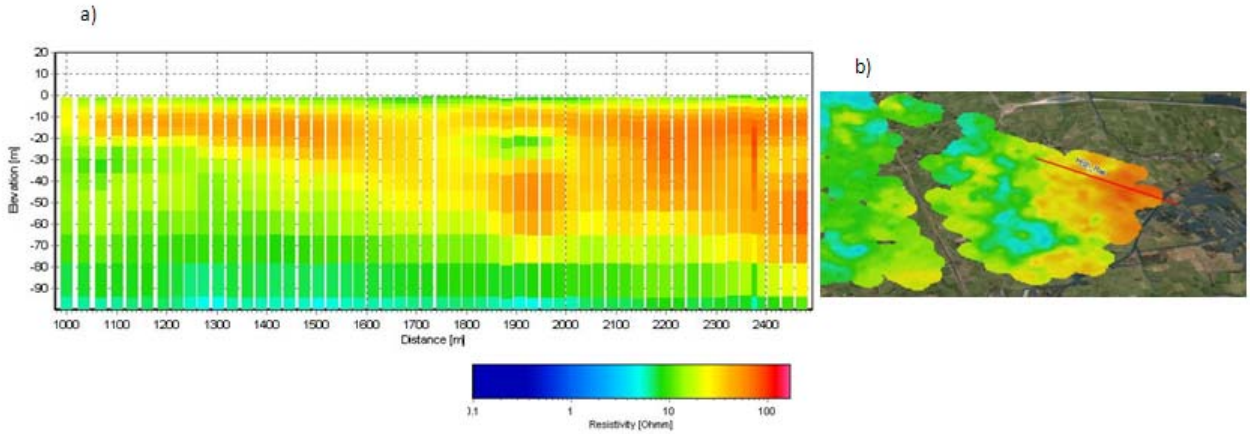

Fig. 31: a) cross section of the resistivity in the high resistive area in the North of the province of Friesland; b) horizontal resistivity map for the interval -20 to -15 meter of elevation, showing the location of the profile.

The purpose of the study of this area is to try to get a better knowledge of the geology and to combine SkyTEM data with CPT's and geological data. A small area, about 7% of the total area of acquisition, was defined to do some testing on inversion using constrains with CPT's and constrains with geological units to find out if it is possible to get better results of the inversions. This part of setup was done in collaboration with Rik Noorlandt from DELTARES (Netherland).

This new area of study was chosen considering the proximity of the CPT's to the SkyTEM flight lines, Fig (32). It was also taken in consideration on the choice of an area where it could have interference of the mains geological units: the Holocene Epoch and the Drente formation. The processed SkyTEM flight lines are represented in the map as black lines, the CPT's are as blue dots and the three profiles of study in red lines.

In this chapter it will be only showed some of the results for profile 2.

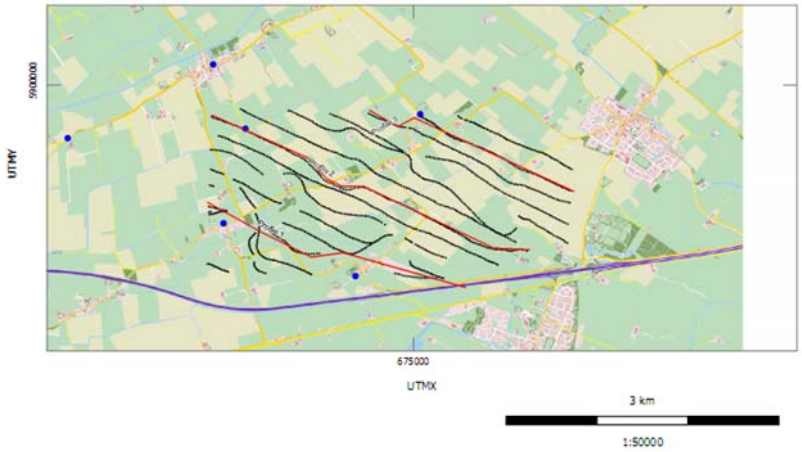

Fig. 32: Friesland profiles of study on the small area

Because a few layer inversion allow us to enhance the difference between the resistivities and therefore defining the major geological layers for the studies on this area it was used the few layer model.

According to the geology of the area, a 6 layer model fits the area better than a 5 layer model that was defined for the geophysical interpretation. Fig (33) shows the results of the inversion of the 5 and 6 layer inversion on profile 2. The data residual (represented as a black line on the profiles), as it was to be expected, is better in the 6 layer due to the fact that we have more parameters to allow the data to have more freedom to move. In the profiles it had been added the delimitation of the main geological units: in brown we have the Holocene that was divided in two, where the first 5 meters is characterized by saturated sand with fresh water (know through CPT's results), followed by sand saturated by salt water. The Drent Formation is limited by the grey lines. The CPT's results were also added to the profile just as a measure of comparison with the SkyTEM results, and as we can see this comparison is well fitted.

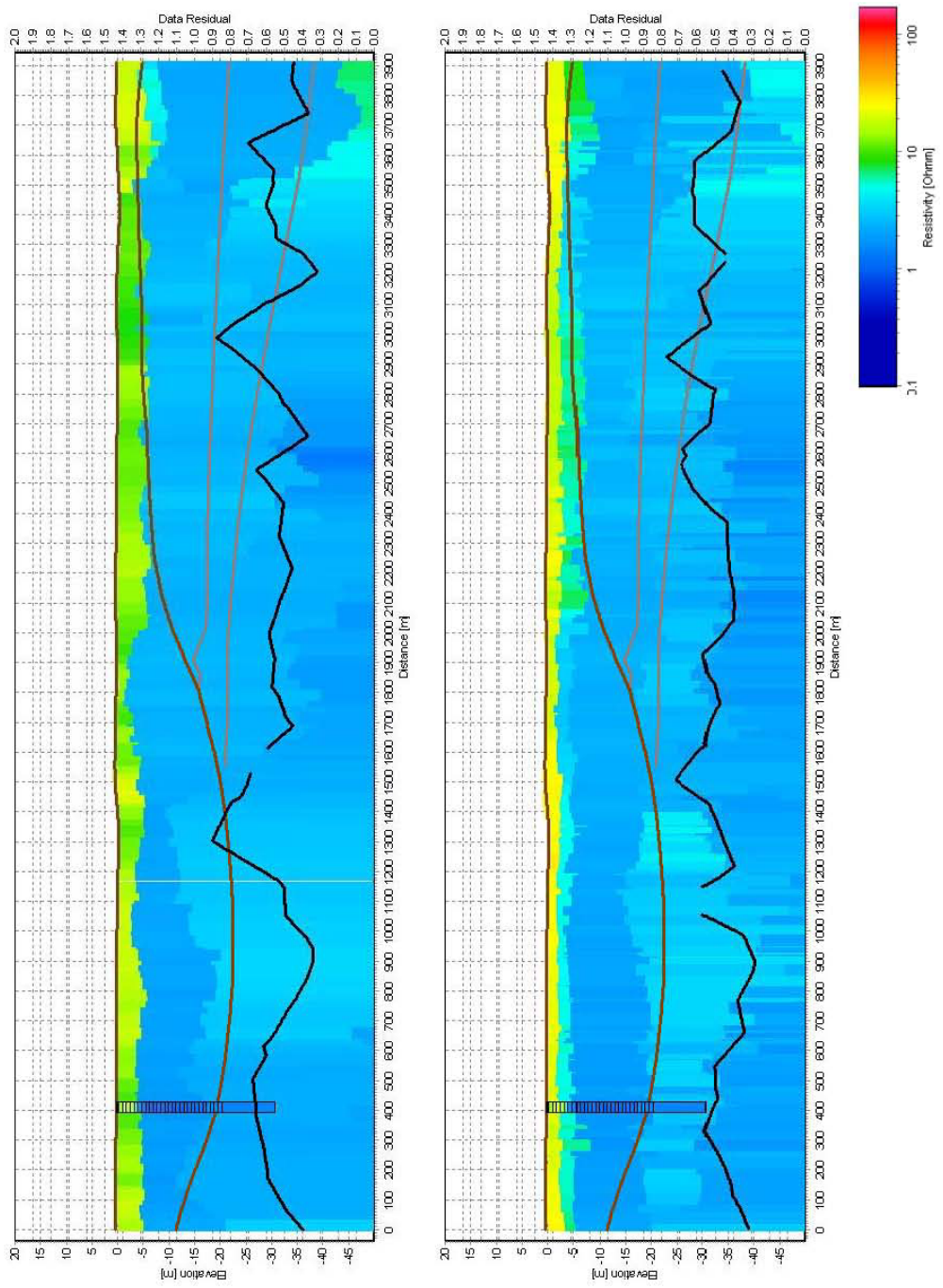

Fig. 33: Profile on the left represents the results of the SCI 5 layer inversion and on the right profile the SCI 6 layer inversion. Major geological units are represented on the profiles: the Holocene (brown line) an the Drent Formation (grey line)

On the East side of the profiles it is possible believe that it corresponds to the boundary of the Holocene, but on the West of the profile it is not clear the resemblance with the inversion and the delimitation of the geological unit.

Due to the fact that it was added an extra layer in the near surface (at 8 meters), allowed to distinguish the interface between the fresh and salt water, around 5 meters and coincident with the geological

interpretation. Another consequence of adding this extra layer is that it allows us to distinguish better also the delimitation of the 4th layer.

Even though on the results of Fig. (33) have been not applied any constrains with the CPT's, there is a good fit with the SkyTEM data and with the CPT's data.

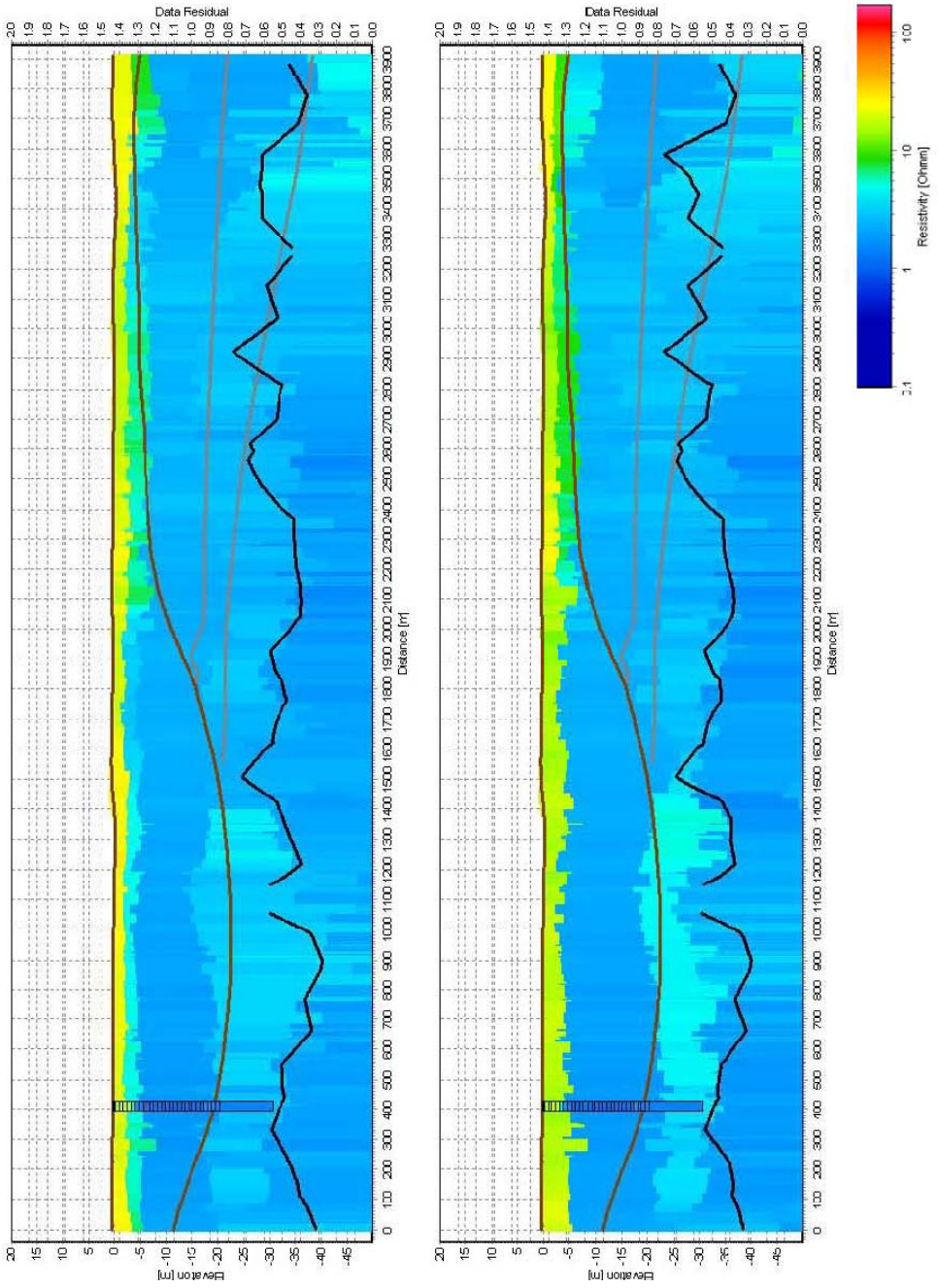

Fig. 34: Profiles represent the results of the SCI 6 layer inversion: on the left without any constrains and on the right whit constrains on the Holocene layer. Major geological units are represented on the profiles: the Holocene (brown line) an the Drent Formation (grey line)

On the figure above, Fig. (34), shows the comparison profiles for when the constrains to the Holocene layer are applied (right profile). One of the first things that is visible is that the on the layer just after the Holocene boundary is more distinct on the profile where the constrains on the geological unit was applied. However analyzing more carefully the first layers of the profile, it is observable the lost of resolution to distinguish the boundary between the fresh and salt water. Even though the data residual of the inversion is better when constraining with the Holocene there is the doubt that we might be forcing too much to have the desired outcome.

This lack of information of the delimitation of the brackish in the beginning of the profile is seen when we constrain de SCI 6 layer uniform with the Drent geological unit. This effect is seen also in the others two profiles. This leads me to conclude that it could be geophysical effect resulting of the constraining or a geological effect due to the fact that the smooth transition between the fresh/salt water is only verified on the beginning of the profiles.

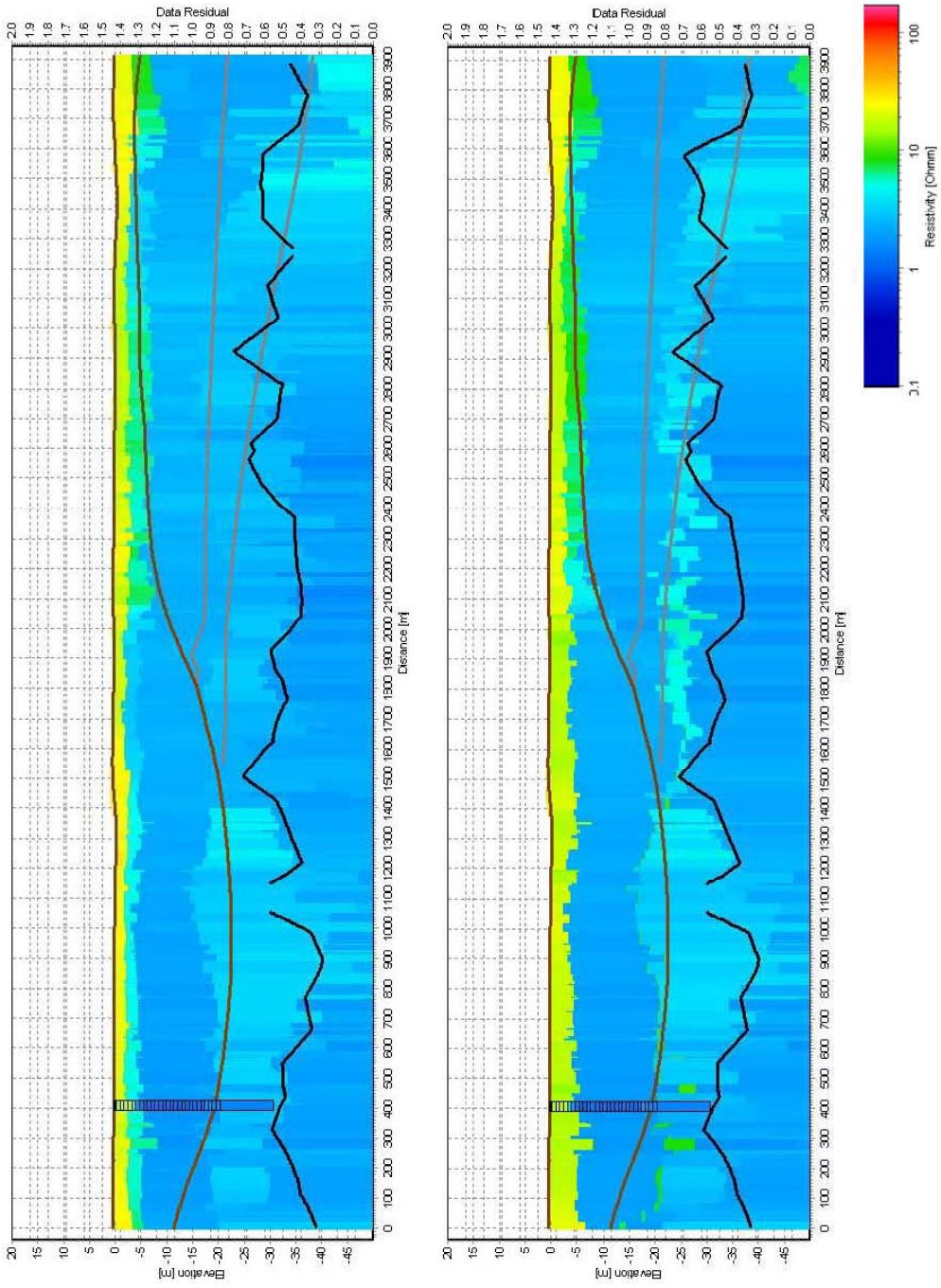

Fig. 35: Profiles represent the results of the SCI 6 layer inversion: on the left without any constrains and on the right whit constrains on the Drent Fomation layer. Major geological units are represented on the profiles: the Holocene (brown line) an the Drent Formation (grey line)

10.2 Terschelling

On the Terschelling Island was applied a smooth inversion with 19 layers and a few layer inversion with 4 layers. The inversions setup can be found on Appendix 1.

In this specific case of the Terschelling Island one of the goals, apart from determining the delimitation of the fresh – salt water interface, was also to be able to define the thin clay layers and for that it is more useful to use the results of the 19 layer inversion, as it has more parameters allowing the data to flow more freely and therefore to give more information.

The *WORKBENCH* has a feature that allows adding a priori information from the GIS. It was useful to use it in this case because it was necessary to change the starting model on the flight lines over the ocean and the coast line. The starting model on the island was started with 30 Ωm; due to the presence of salt in the ocean the resistivity is much lower. This means that starting the inversion over the ocean with such high resistivity would cause an increase on the data residual after because the data would try to fit a parameter that was "out of its league". The first 5 layers over the ocean where started with a very low resistivity of 2 Ωm and then increasing the resistivity softly over the others 4 layers until the resistivity of the half-space (30 Ωm) was reached. On the coast line the same process was applied but only to the three first layers. But even though there is still some effect that were not able to reduce; this is also reflected on the data residual, Fig. (36).

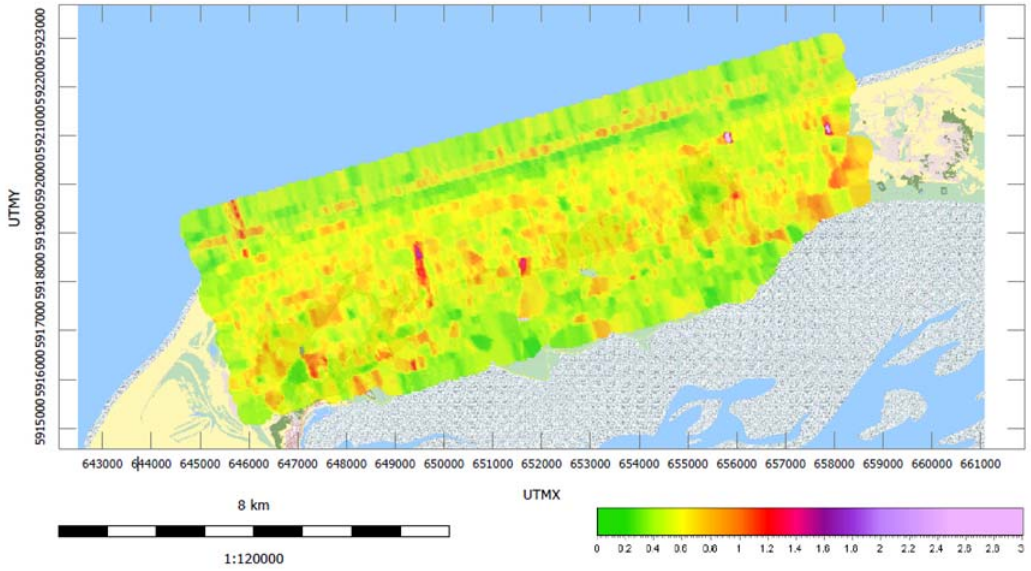

Fig. 36: Terschelling data residual for the 19 layer SCI setup

Processing the island was much easier comparing with the mainland, since it is not as much populated as the mainland, and consequently it has fewer infrastructures. As there are not many coupling, apart from the small villas, roads and electrical fences data residual is below 1 STD, Fig. (36), and total residual is bellow 0.5.

As said before, the purpose of the DOI is to give an estimation of the limitation of the penetration of the signal. For the island of Terschelling the penetration depth is bigger in the Western part of the island and the region of Hoorn, with a value in elevation of about -160 meters, Fig (37).

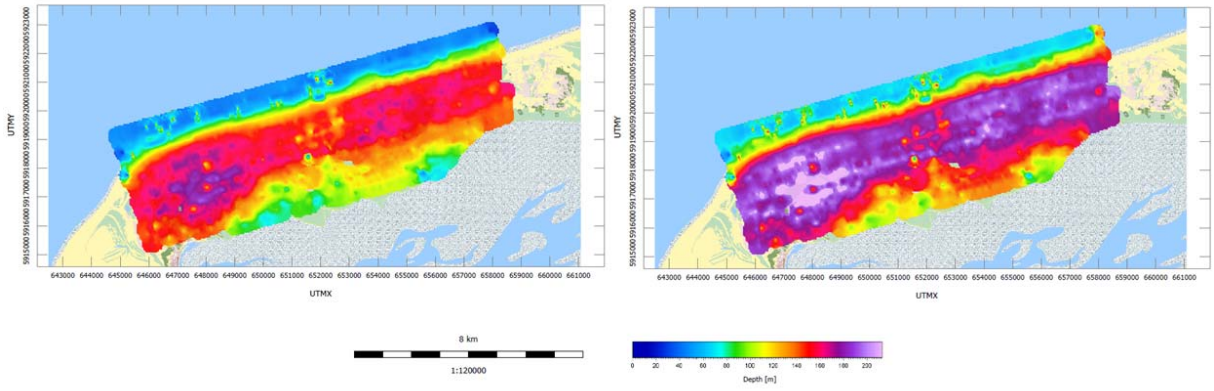

Fig. 37: DOI estimation on the Terschelling Island. On the left the Upper DOI and on the right the Low DOI

In a geophysical point of view, there is a high resistivity, above 150 Ωm, in the area of Hoorn. The area in the Western part that also presents a bigger DOI also presents a high resistivity about 80 – 110 Ωm, Fig. (38). Analyzing the hydrology presented by Beukeboom (1976), described in chapter 7.2.1 Fig. (14), these areas of high resistivity presented by the SkyTEM are the same previously identified as fresh water lenses.

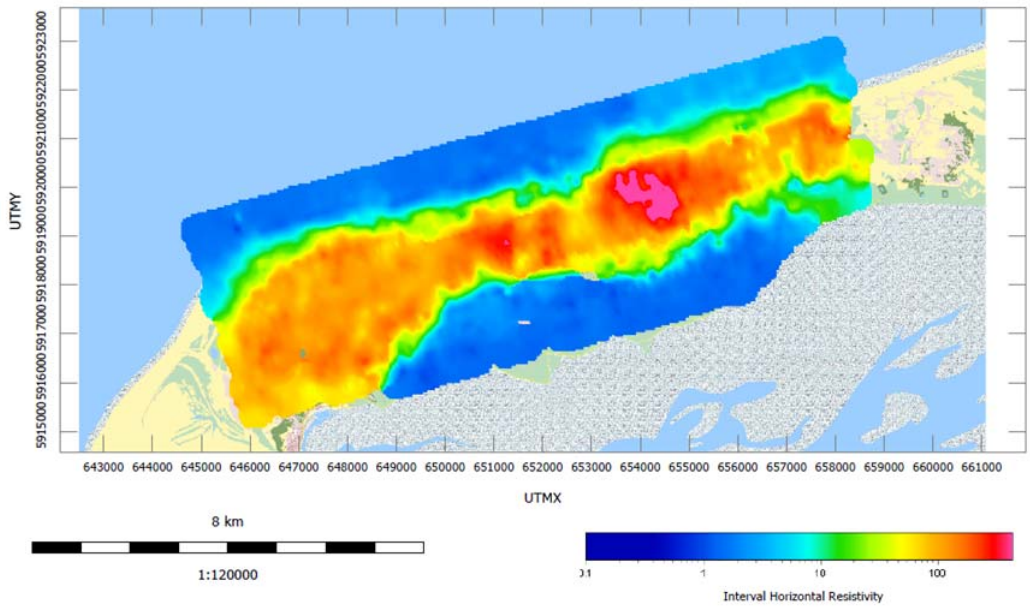

Fig. 38: Map of the horizontal resistivity of Terschelling Island for the interval depth -50 to -45 meters of the SCI 19 layer inversion model

Profiles on the areas of the fresh water lenses were done to try to obtain a more detail information. Here it will only be shown results of 2 profiles, the others may be visualized on Appendix 2. Fig. (39) shows the location of the cross section in terms of resistivity in the areas of the two fresh water lenses. Profile 1 is located on the Western part of the island. It shows a very high resistivity around 60 – 70 meters of depth of 70 – 90 Ωm. Profile 4 is situated on the area of Hoorn and it presents a higher resistivity around 130 – 150 Ωm at a depth of 50 – 70 meters.

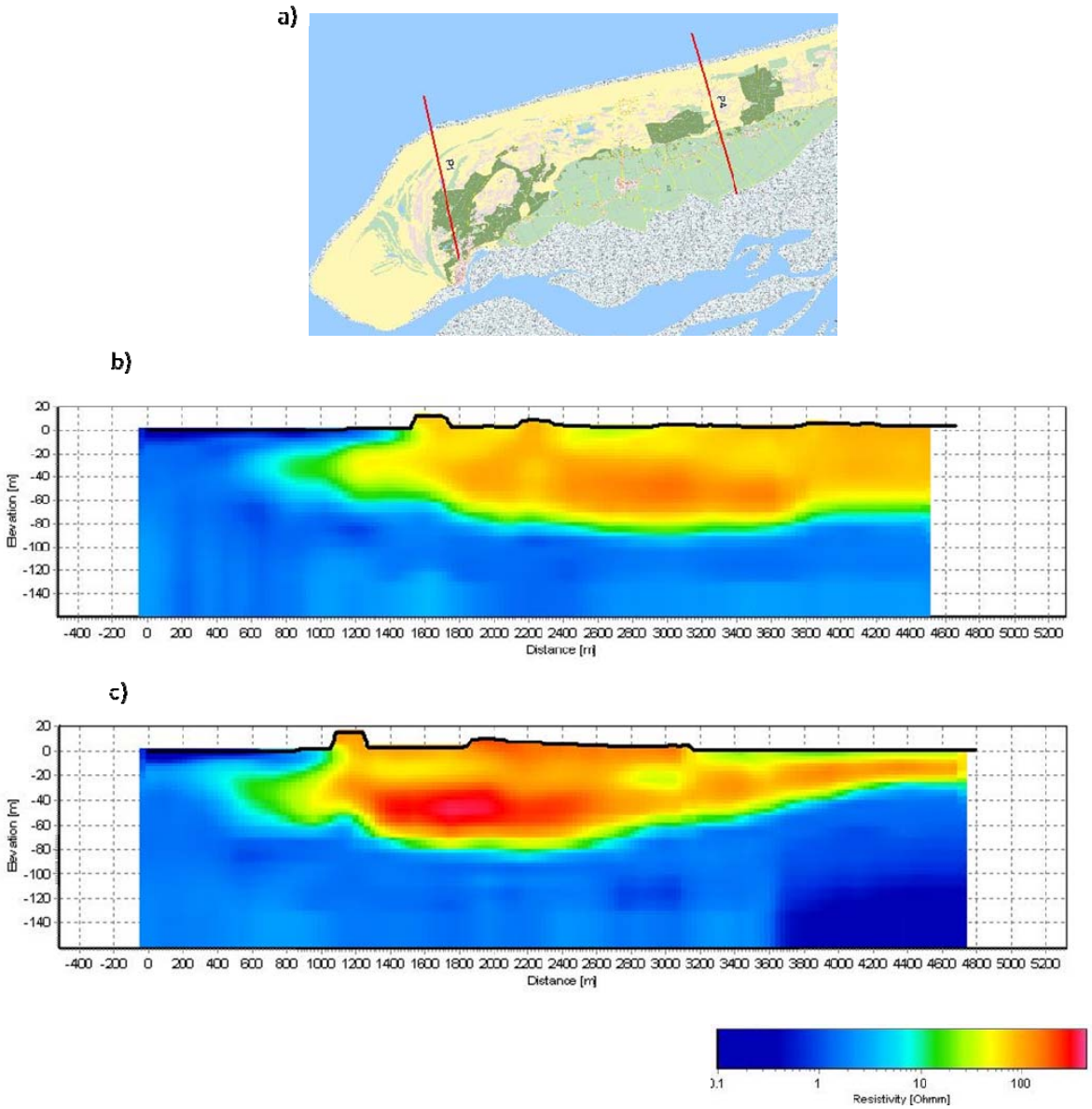

Fig. 39: Cross section of resistivity of profile P1 (b) and P4(c)

In a meeting in May, 2010 between the HGG group with Arjen Kork (Virens, Netherlands), Frans Schaars (Artesial, Netherlands) and Michel Groen (VU University, Amsterdam) the geophysical results were analyzed. According to CPT measurements it was possible to assume, with a certain certainty, that results over 70 Ωm was fresh water and it is known that resistivities bellow 60 Ωm are clay layers. With this new information new resistivity maps were created, now with the purpose to try to find the thin clay layers, Fig. (40). These clay layers are important because they have an effect of a cap layer; they are an important factor for the water infiltration as well as determining the

vulnerability[6]of the aquifer. A clay layer is considered to be one of the most efficient barriers for aquifer protection due to its impermeability factor.

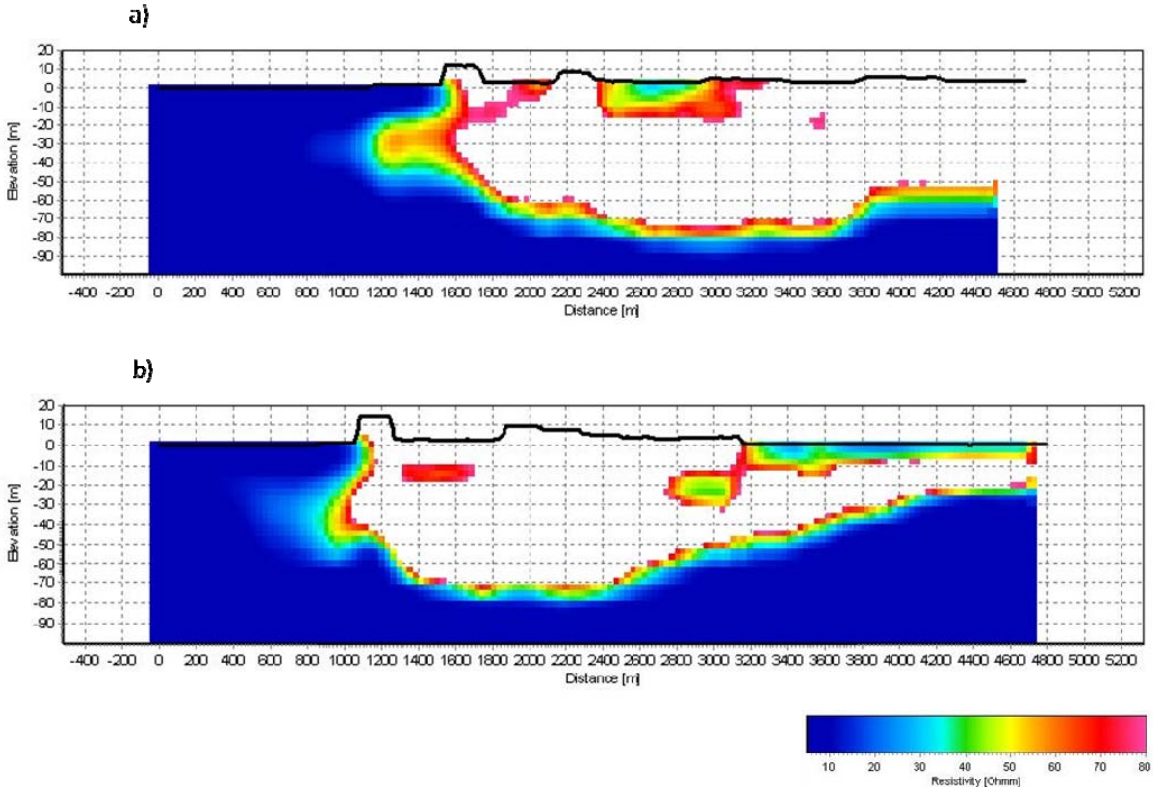

Fig. 40: Cross section of resistivity of profile P1 (a) and P4(b) with the purpose to locate the thin clay layers. Clay layers have a resistivity bellow 60 Ωm.

In both profiles shown in Fig. (40) the areas represented in white are areas that are filed with saturated sands with fresh water. A clay layer has typically resistivities bellow 60 Ωm, in this case it's represented in red. These two profiles represent the areas where the fresh water lenses are located. This shows that there is no significant clay layer to serve as a protection cap under the dune area, only on the polder area, as it is the case of the profile 4, Fig. (40.b).

In the two profiles presented of Fig.(39), it seems that it exists a sort of outflow of high resistivity towards the ocean. It might be plausible to admit that this could be a phenomenon denominated of Submarine Groundwater Discharge (SGD). SGD is generally described as groundwater provenient of coastal aquifers that drives flow water seeping towards the ocean. These have recently been given more importance due to the fact that it can be a source of contamination of the seawater with a variety of substances like nutrients, heavy metals, radionuclide and organic compounds (Burnett, 2006).

[6] *Vulnerability*: refers to the sensitivity of the groundwater to contamination, and it is determined by intrinsic characteristics of the aquifer.

This flow outwards to the ocean may be a consequence of an inland hydraulic consequence and as well as a marine process such as wave set-up, tidally driven oscillations, density-drive convections and thermal convection. The water seepage is not a constant phenomenon, it varies temporally and spatially.

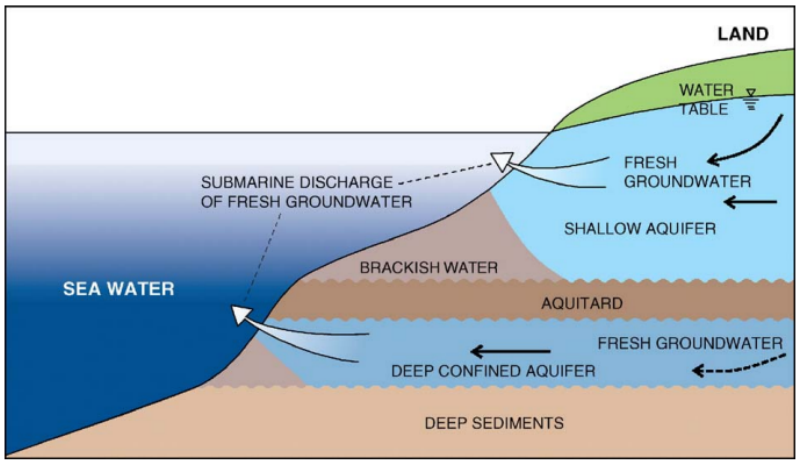

Fig. 41: Schematic description of the process associated with the SGD (Burnett, 2006)

Terschelling Island has a very low topography, Fig. (13); in the polder area mean topography is around 0 to 1 meters. Even though there are artificial coastal barriers in the South part of the island, it seems that it is not enough to protect from the saline intrusion. On the resistivity maps of -5 to 0 meters of depth it is visible the intrusion of salt water in the areas of Kaart and South of Hoorn, Fig. (42). In the region of Hoorn is located one on the fresh water lenses in the island. In a pessimist future scenario, if the sea level arises, this present small salt water intrusion may in the future contaminate the fresh water lenses of Hoorn's.

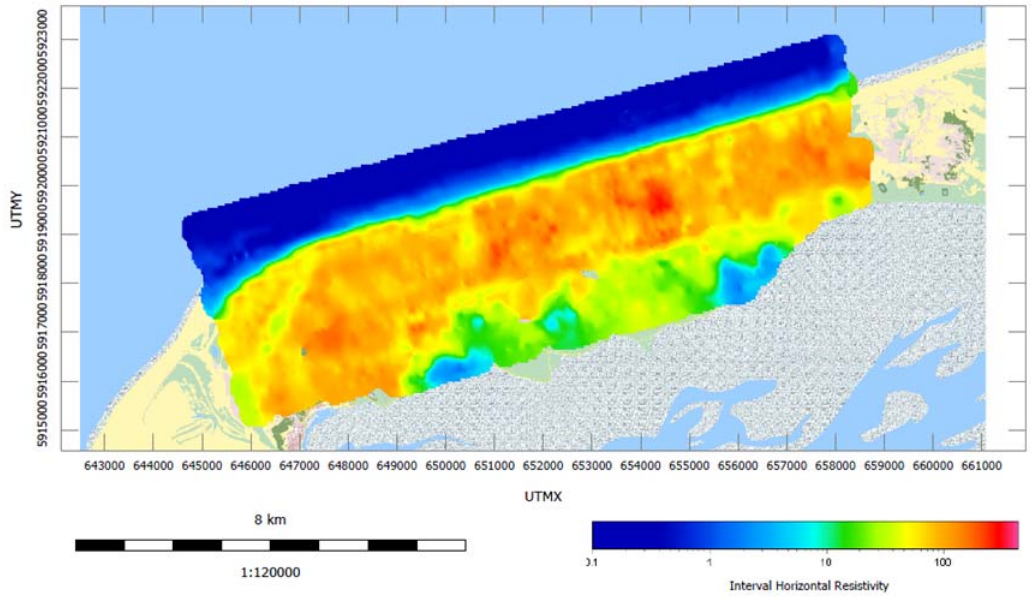

Fig. 42: Map of the horizontal resistivity of Terschelling Island for the interval depth -5 to 0 meters of the SCI 19 layer inversion model

Others geophysical measurements, such CPT (Cone Penetration Test), TDEM (Time Domain ElectroMagnetic sounding), VES (Vertical Electrical Sounding), CVES (Continuous Vertical Electrical Sounding), SkyTEM and borehole logging, as have been done in the island during the time. Frans Schaars (Artesia, Netherlands) created map collecting all this information with the purpose to verify the coherence with the different methods. The map show tall the data converted to the elevation o the fresh/salt water interface, Fig. (43). The data fit between the different methods is very well fit.

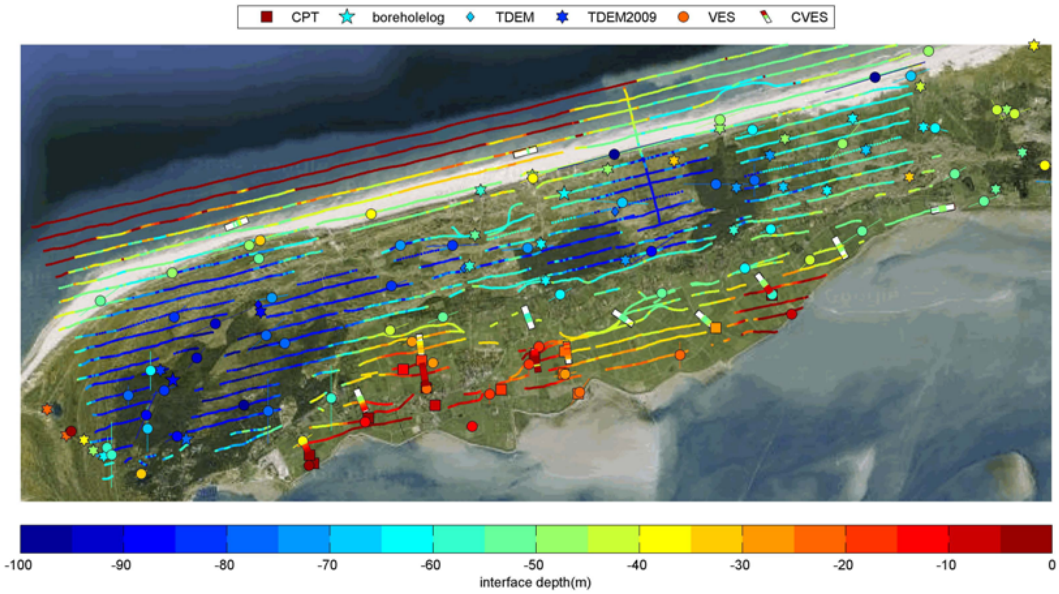

Fig. 43: A map with all data converted to the elevation of the salt groundwater interface (by Frans Schaars)

11. Conclusion

The main goals of this thesis have been achieved. I had the opportunity to see how the acquisition is done on fieldwork, have learned how to process and interpreter geophysical data from the SkyTEM system. An attempt to do some connection between the geophysical data and with the hydrology of the area was done but due to the fact that the access to the hydrology was limited and the lack of knowledge in this area this relationship was just based on bibliography about these areas and similar ones.

The SkyTEM System is an vital tool for hydrogeological and environmental investigations not just because it is a cost efficient method and can cover large areas (even sometimes areas with difficult range in the ground) in a short period of time but also as being a time domain electromagnetic method it has the sensibility to detect variations of the geology such as such as type of rock, porosity, grain size, fracture and clay content. This sensibility is very important especially for this thesis as it objective is to distinguish fresh/salt water interface as well as being able to detect the thin clay layers.

In the case of the Island of Terschelling the geophysical results were able to resolve the location of the two existence fresh water lenses on the Western part of the island and on the region of Hoorn. A delimitation of the fresh/salt water interface is seen on the results as well as the detection of the location of the thin clay layers. The knowledge of these parameters is important as they will be used by hydrologists to improve their hydrological model of the island and in the future be able to protect this fresh water lenses and explore the sustainability of drinkable water in the island.

The interpretation of the result of the province of Friesland focused more on the geology. In the study area there was not found hydrological signatures apart from the possible percolation on the SE of the flight lines near the Magriet Channel. This is not an unexpected result due to the known geology of the area; most of North region of The Netherland was conquered to the ocean. A small attempt to try to constrain the geological units in the inversion was tried. The outcome of this results I found it a bit complicated to analyze due to the fact that the boundary between achieving good results and forcing too much the data fit to a desirable result is very thin, and I don't have the sufficient knowledge to explore this matter.

12. References

Auken, Esben and Anders Vest Christiansen. "Layered and laterally constrained 2D inversion of resistivity data." Geophysics (2004): 752-760.

Auken, E., Christiansen, A.V., Westergaard, J.H., Kirkegaard, C., Foged, N., Viezzoli, A., 2009. An integrated processing scheme for high-resolution airborne electromagnetic surveys, the SkyTEM system. Exploration Geophysics, 184-192.

Auken, E., Nebel, L., Sørensen, K., Breiner, M., Pellerin, L., Christiansen, N.B., 2002. EMMA - A geophysical training and education tool for electromagnetic modeling and analysis. Journal of Environmental & Engineering Geophysics, 57-68.

Auken, E., Westergaard, J.H., Christiansen, A.V., Sørensen, K., 2007. Processing and inversion of SkyTEM data for high resolution hydrogeophysical surveys. SEG Conference, Perth (Australia).

Beukeboom, Theodorus Jozef, 1976. The hydrology of the Frisian Islands. Rodopi, 69-87.

Burnett, W.C., Aggarwal, P.K., Aureli, A., Bokuniewicz, H., Cable, J.E., Charette, M.A., Kontar, E., Krupa, S., Kulkarni, K.M., Loveless, A., Moore, W.S., Oberdorfer, J.A., Oliveira, J., Ozyurt, P., Provinec, P., Provitera, A.M.G., Rajar, R., Ramessur, R.T., Scholten, J., Stieglitz, T., Taniguchi, M., Turner, J.V., 2006. Quantifying submarine groundwater discharge in the coastal zone via multiple methods. Science of the Total Environment, 498 - 543.

Christiansen, A.V., Auken, E., Sørensen, K., 2006. Chapter 6 - The Transient Electromagnetic Method. Kirsch, Reinhard, Groundwater Geophysics - A Tool for Hydrogeology. Springer, 179 - 226.

Fitterman, D.V., Labson, V.F., 2005. Electromagnetic Induction Methods for Environmental Problems. Butler, Dwain K, Near-Surface Geophysics Part 1: Concepts and Fundamentals. Society of Exploration Geophysicists, 301 - 356.

Groen, M., Kok, A., Made, K.J., Post, V., 2008. The use of mapping the salinity distribution using geophysics on the Island of Terschelling for groundwater model calibration. 20th Salt Water Intrusion Meeting.

Hydrogeophysics Group, 2007. Guide to processind and inversion of SkyTEM data. Department of Earth Sciences - Aarhus University.

Hydrogeophysics Group, 2008. Spatially constrained inversion of SkyTEM data - concept and examples. Department of Earth Sciences - Aarhus University.

Reid, J.E., Macnae, J.C., 1998. Comments on the electromagnetic "smoke ring" concept. Society of Exploration Geophysicists, 1908-1913.

Santos, F.A.M., 2004. 1-D laterally constrained inversion of EM34 profiling data. Jornal of Applied Geophysics, 123-134.

Santos, F.A.M., 2006. Técnicas para investigação de estruturas superficiais - O método transiente. Apontamentos de Propecção Geofísica I.

Siemon, B., Christiansen, A.V., Auken, E., 2009. A review of helicopter-borne electromagnetic method for ground water exploration. Near Surface Geophysics, 629-646.

Sørensen, K., Auken, E., 2004. SkyTEM - A new high-resolution helicopter transient electromagnetic system. Exploration Geophysics, 194-202.

Steuer, A., Siemon, B., Auken, E, 2007. A comparison of helicopter-borne electromagnetics in frequency- and time-domain at the Cuxhaven valley in Northen Germany. Journal of Applied Geophysics, 194-205.

Viezzoli, A., Auken, E., 2007. Spatially constrained inversion for quase 3-D modelling of AEM data. SEG Conference, Perth (Australia).

Viezzoli, A., Auken, E., Munday, T., 2009. Spatially constrained inversion for quasi 3D modelling of airborne electromagnetic data - an application for environmental assessment in the Lower Murray Region of South Australia. Exploration Geophysics, 173-183.

Viezzoli, A., Auken, E., Sørensen, K., 2008. Quasi-3D modeling of airborne TEM data by spatially constrained inversion. Geophysics, Vol. 73, 105-113.

Ward, S.H., Hohmann, G.W., 1988. Electromagnetic Theory for Geophysical Applications. Nabighian, Misac N. Electromagnetic Methods in Applied Geophysics, Volume 1 - Theory. Society of Exploration Geophysicists, 131-307.

Westerhoff, W.E., Mulder, E.F.J., 1984. Quaternary geological framework of North-Holland and the markermeer (The Netherlands). Proceedings of the 3rd International Symposium on Land Subsidence, Venice, 877-883.

Zhdanov, M.S., Keller, G.V., 1994. Chapter 3 - Properties of rocks and minerals. The Geoelectrical Methods in Geophysical Exploration. Elsevier, 79 - 136.

Appendix 1 – Settings of the processing/inversions

North of Friesland

Processing parameters

Software	Aarhus WORKBENCH version:	3.3.10
Trapezoid filter	Sounding distance, LM [s]:	1.5
	Times, LM [s]:	1e-5 1e-4 1e-3
	With, LM [s]:	2 2 5
	Times, HM [s]:	1e-4 1e-3 1e-2
	With, HM [s]:	4 5 25

SCI-Inversion smooth model setup

Software	Aarhus *WORKBENCH* version:	3.3.10
SCI cells	Reference distance [m]:	30
	Constraints distance scaling:	$(1/\text{distance})^{1.5}$
Starting model	Number of layers:	19
	Thickness, 1st layer [m]:	1.5
	Depth of the last layer boundary [m]:	160
	Layer thickness distribution	Log with depth
	Resistivity [Ωm]:	20
Constraint factors	Horizontal resistivities:	1.6 (top) to 1.2 (bottom)
	Vertical resistivities:	3 (top) to 1.4 (bottom)
	Prior Thickness:	Fixed
	Prior resistivities:	None

SCI-Inversion 5-layer model setup

Software	Aarhus WORKBENCH version:	3.3.10
SCI cells	Aprox. Cell size (num. of models)	
	Reference distance [m]:	30
	Constraints distance scaling:	$(1/\text{distance})^{0.75}$
Starting model	Number of layers:	5
	Thickness, 1-5ayer [m]:	6, 14, 35, 60, inf
	Resistivity [Ωm]:	20
Constraint factors	Horizontal resistivities:	1.6 (top) to 1.2 (bottom)
	Horizontal depth:	~ +/- 7 m
	Prior, Thickness:	
	Prior, resistivities:	

Terschelling

Processing parameters

Software	Aarhus WORKBENCH version:	3.3.10
Trapezoid filter	Sounding distance, LM [s]: Times, LM [s]: With, LM [s]: Times, HM [s]: With, HM [s]:	1.7 1e-5 1e-4 1e-3 3.5 10 16 1e-4 1e-3 1e-2 10 16 24

SCI-Inversion smooth model setup

Software	Aarhus WORKBENCH version:	3.3.10
SCI cells	Reference distance [m]: Constraints distance scaling:	30 $(1/\text{distance})^{0.75}$
Starting model	Number of layers: Thickness, 1st layer [m]: Depth of the last layer boundary [m]: Layer thickness distribution: Resistivity [Ωm]:	19 4 130 Log with depth 30
Constraint factors	Horizontal resistivities: Vertical resistivities: Prior, Thickness: Prior, resistivities:	2 1.6 (top) to 1.2 (bottom) Fixed none

SCI-Inversion 4-layer model setup

Sotfware	Aarhus WORKBENCH version:	3.3.10
SCI cells	Aprox. Cell size (num. of models) Reference distance [m]: Constraints distance scaling:	 30 $(1/\text{distance})^{0.75}$
Starting model	Number of layers: Thickness, 1-4 layer [m]: Resistivity [Ωm]:	4 10, 25, 45, inf 20
Constraint factors	Horizontal resistivities: Horizontal depth: Prior, Thickness: Prior, resistivities:	1.6 (top) to 1.2 (bottom) ~ +/- 7 m

Appendix 2 – Mean resistivity maps

Mean resistivity maps in 10 meters interval from 50-160 m and in 5 meters interval from 0-50 m, generated from the smooth model inversion.

North of Friesland

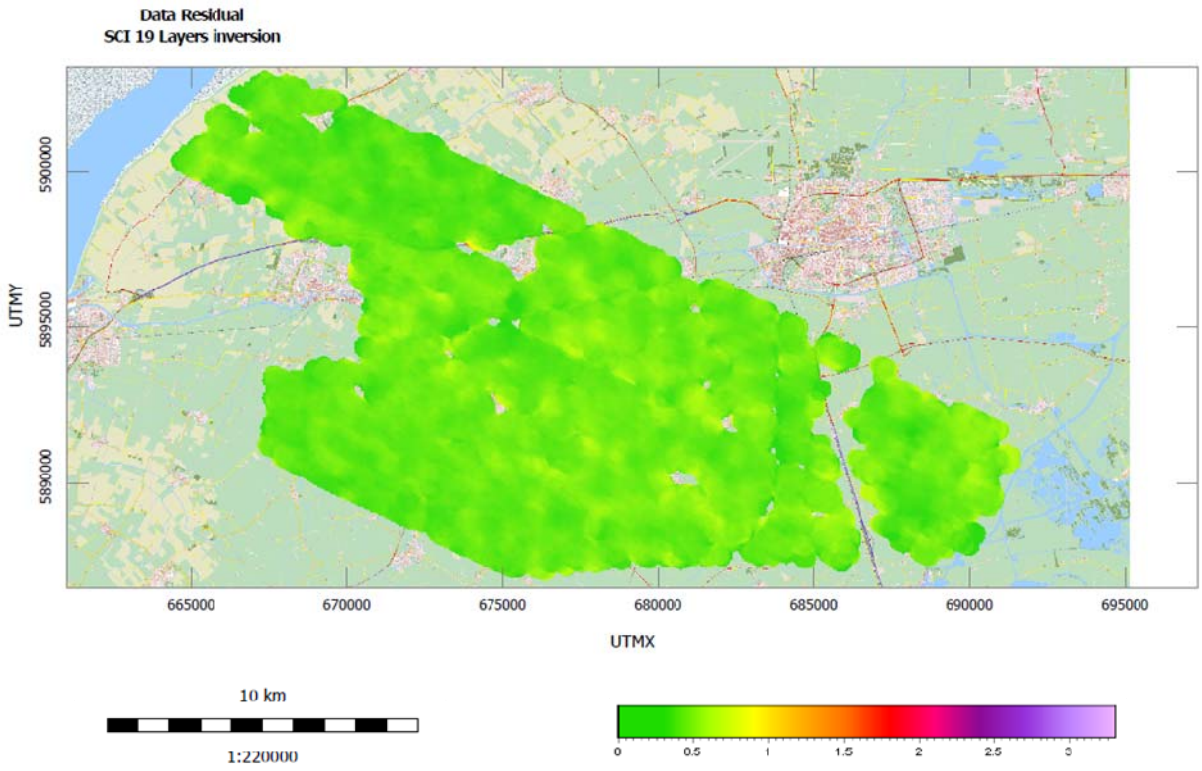

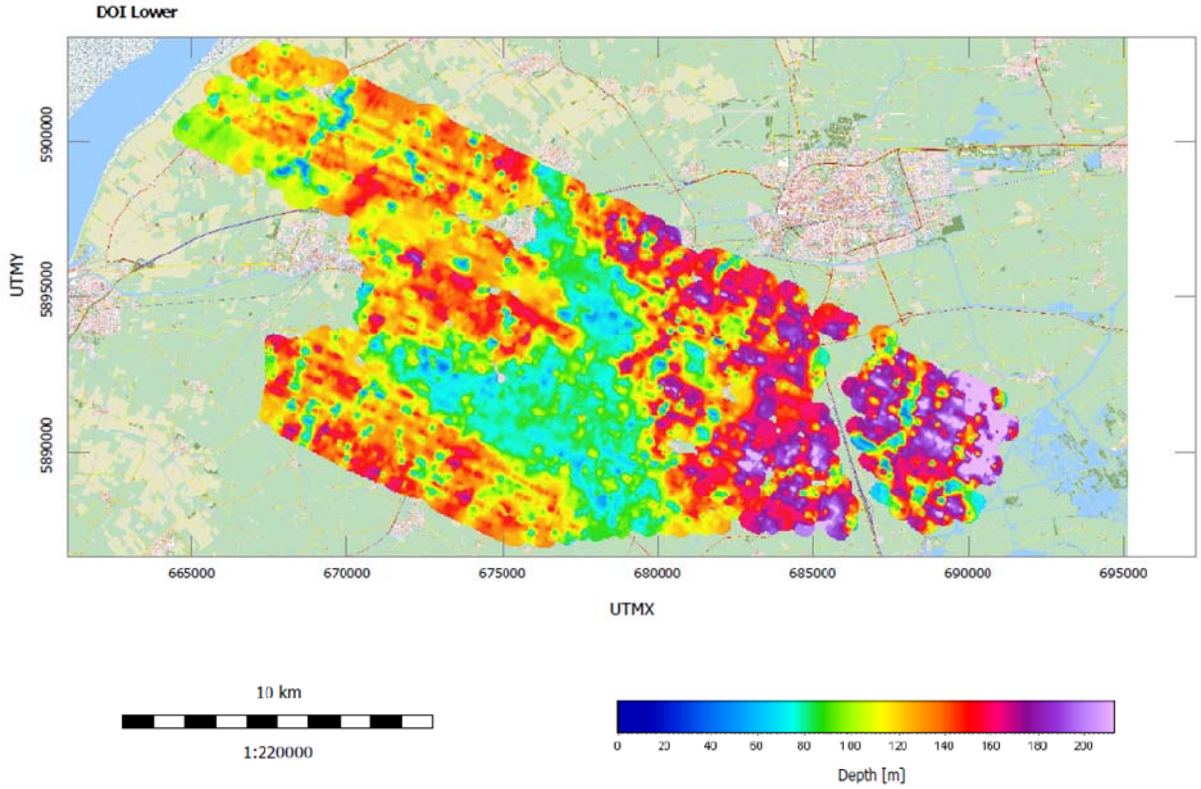
DOI Lower
UTMY
5900000
5895000
5890000
665000
670000
675000
680000
685000
690000
695000
UTMX
10 km
1:220000
0
20
40
60
80
100
120
140
160
180
200
Depth [m]

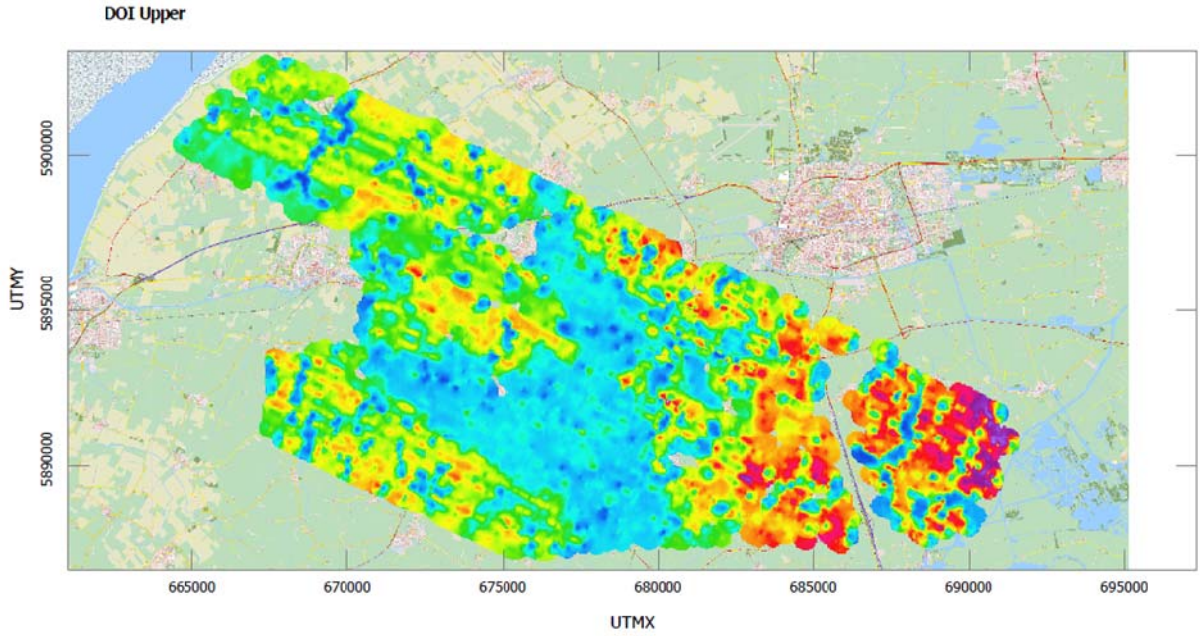
DOI Upper
UTMY
5900000
5895000
5890000
665000
670000
675000
680000
685000
690000
695000
UTMX

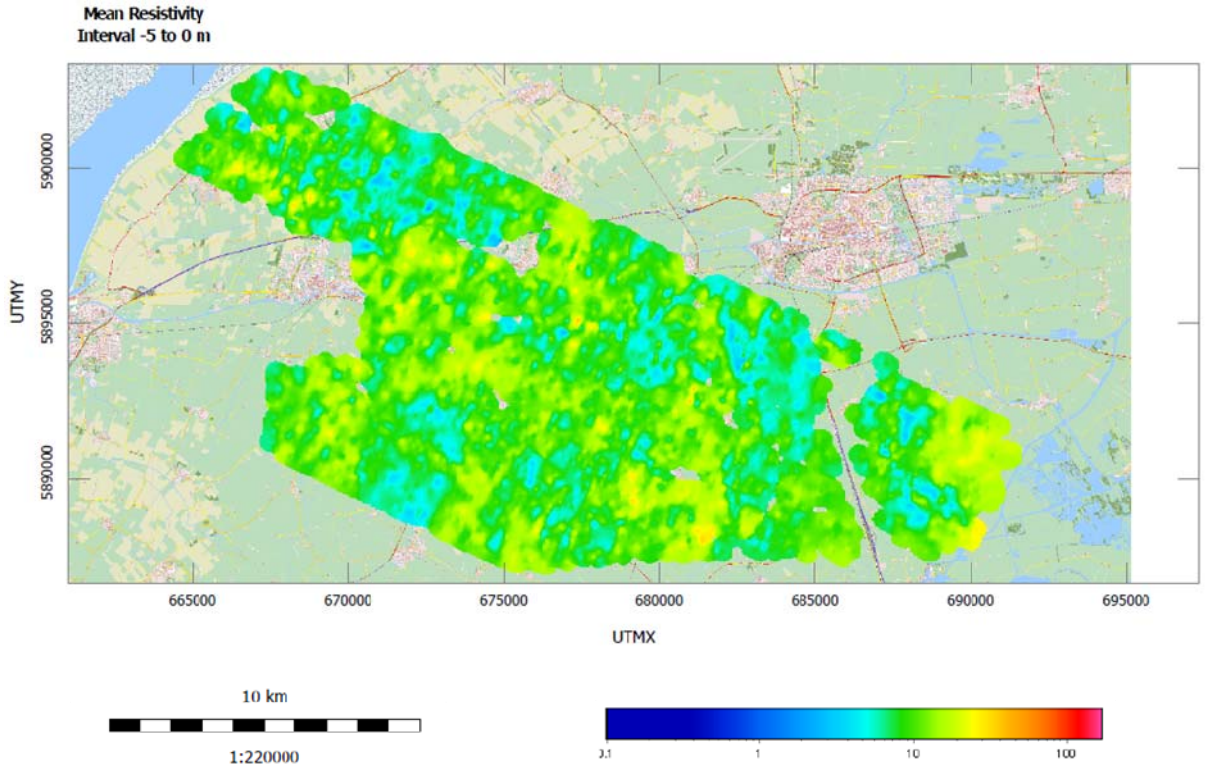
Mean Resistivity
Interval -5 to 0 m
UTMY
5900000
5895000
5890000
665000
670000
675000
680000
685000
690000
695000
UTMX
10 km
1:220000
0.1
1
10
100

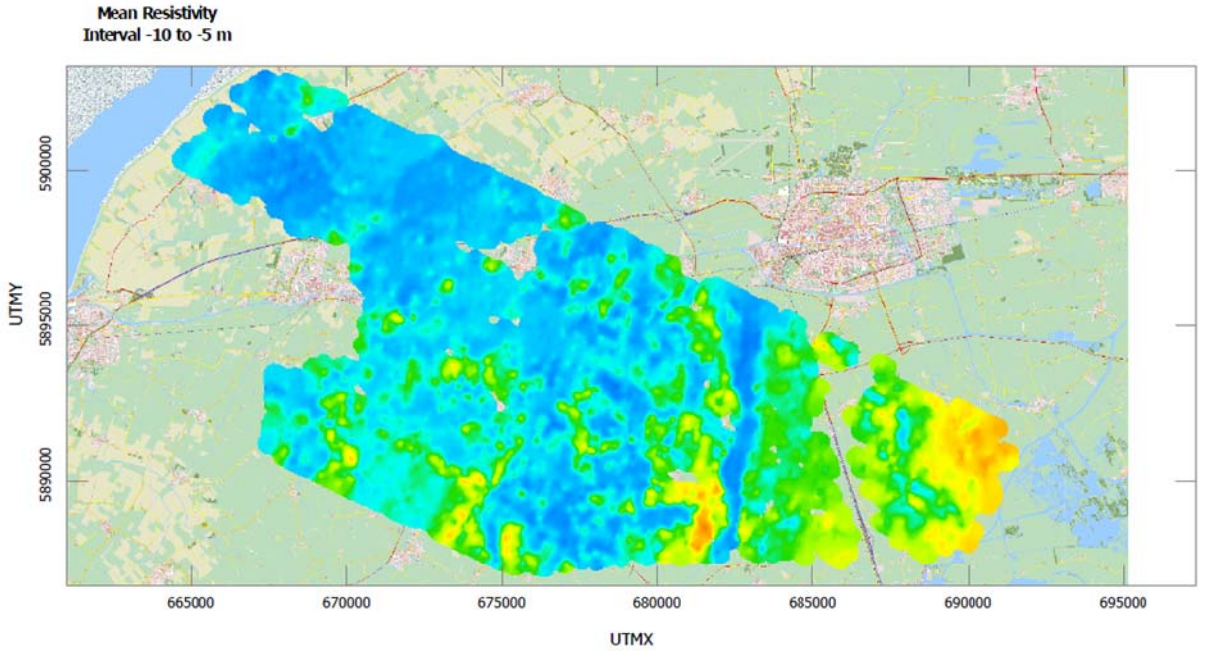
Mean Resistivity
Interval -10 to -5 m
UTMY
5900000
5895000
5890000
665000
670000
675000
680000
685000
690000
695000
UTMX

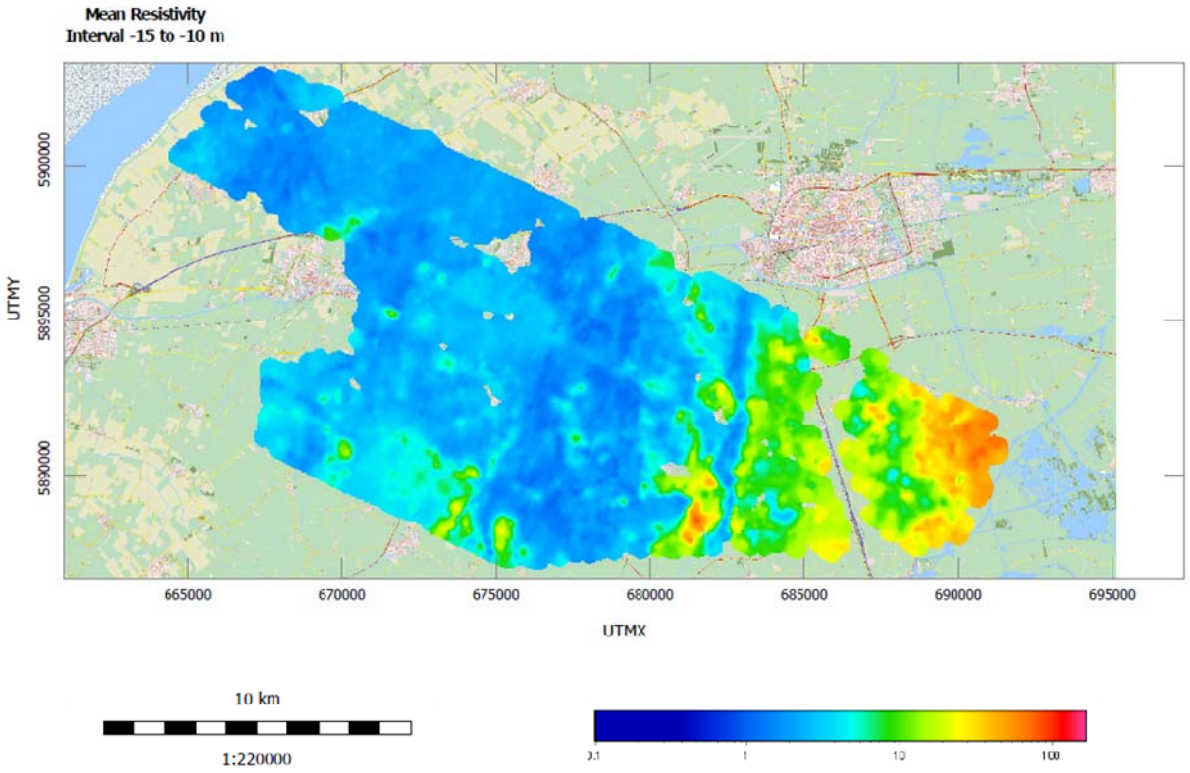
Mean Resistivity
Interval -15 to -10 m
UTMY
5900000
5895000
5890000
665000
670000
675000
680000
685000
690000
695000
UTMX
10 km
1:220000
0.1
1
10
100

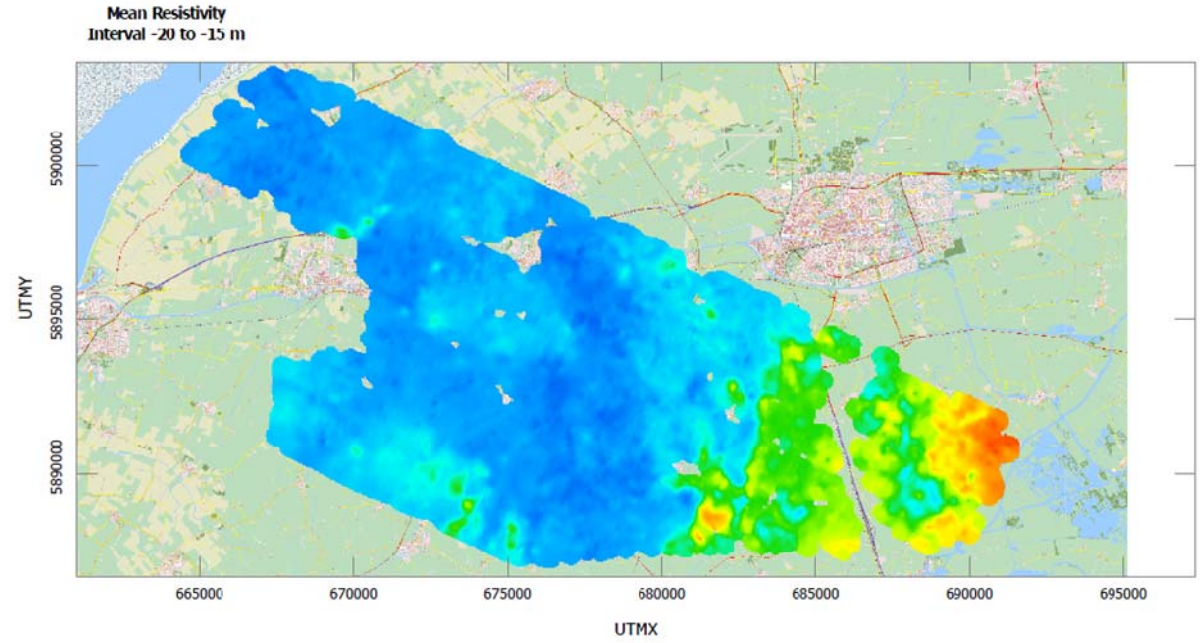
Mean Resistivity
Interval -20 to -15 m
UTMY
5900000
5895000
5890000
665000
670000
675000
680000
685000
690000
695000
UTMX

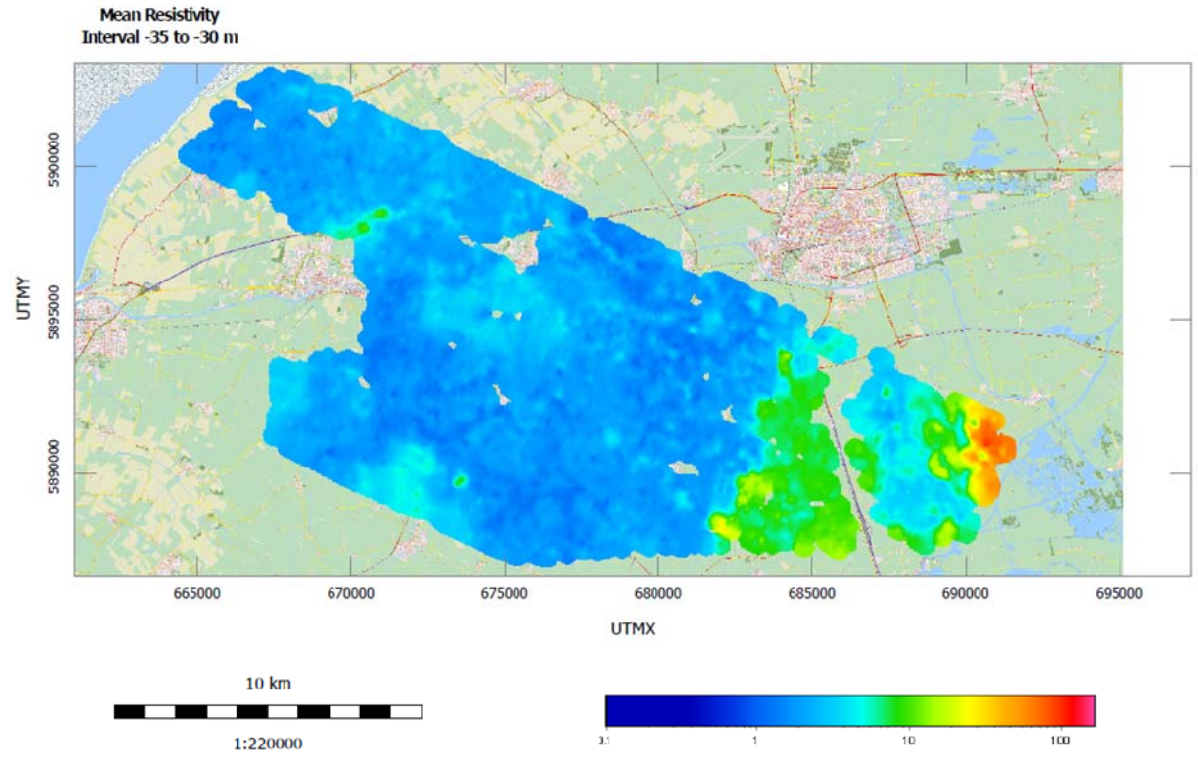
Mean Resistivity
Interval -35 to -30 m
UTMY
5900000
5895000
5890000
665000
670000
675000
680000
685000
690000
695000
UTMX
10 km
1:220000
1
10
100

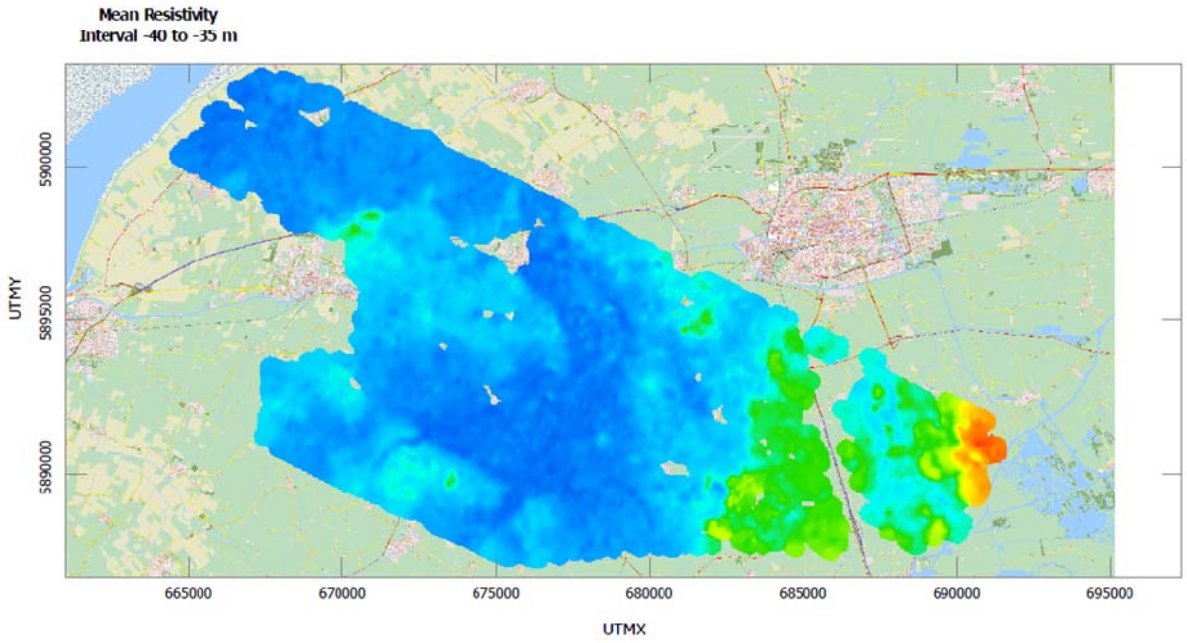
Mean Resistivity
Interval -40 to -35 m
UTMY
5900000
5895000
5890000
665000
670000
675000
680000
685000
690000
695000
UTMX

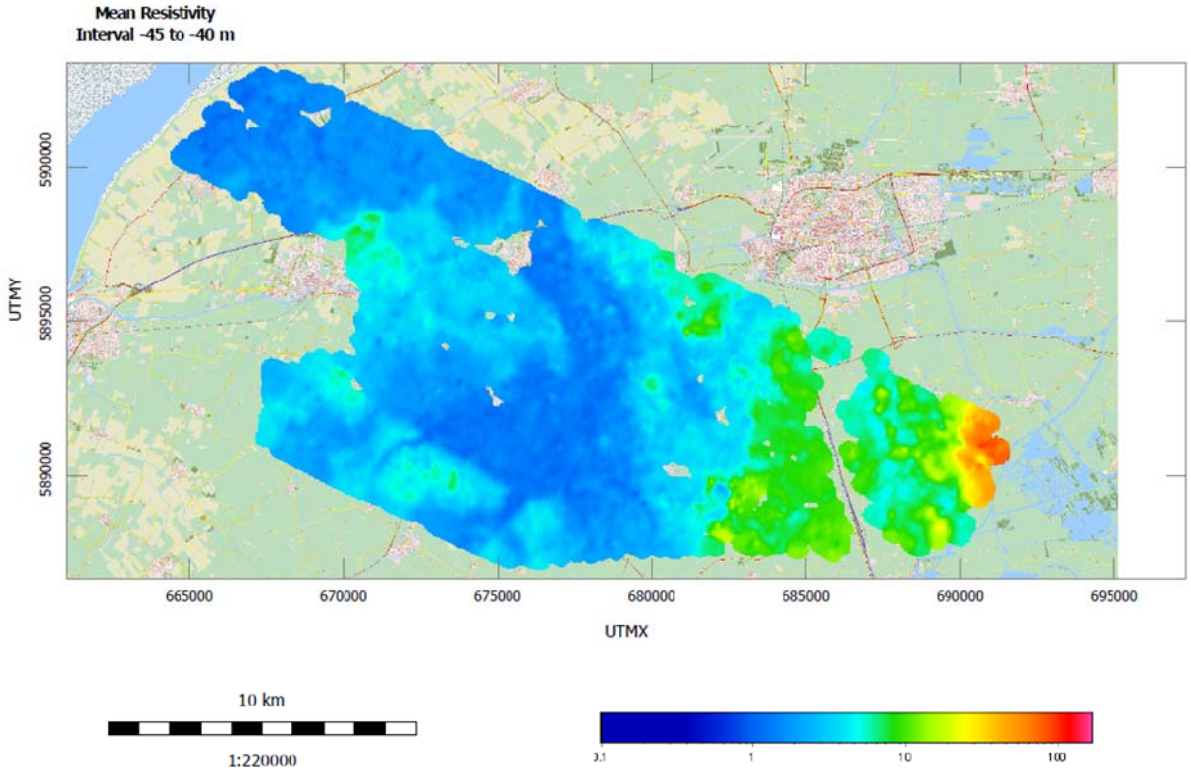
Mean Resistivity
Interval -45 to -40 m
UTMY
5900000
5895000
5890000
665000
670000
675000
680000
685000
690000
695000
UTMX
10 km
1:220000
0.1
1
10
100

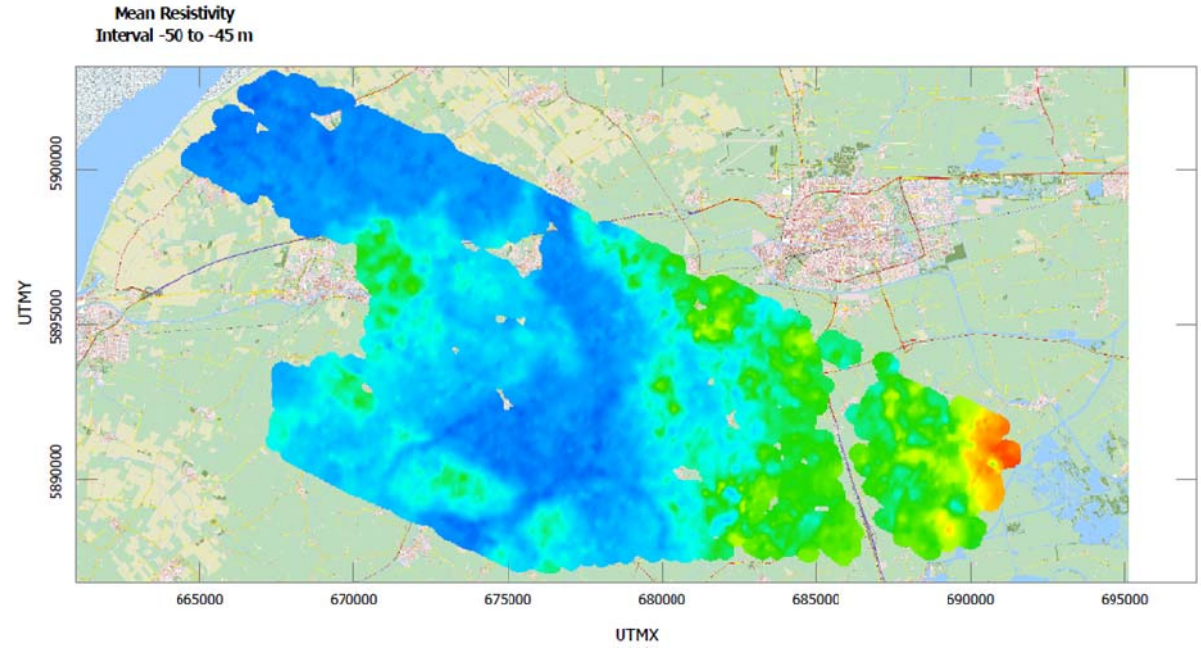
Mean Resistivity
Interval -50 to -45 m
UTMY
5900000
5895000
5890000
665000
670000
675000
680000
685000
690000
695000
UTMX

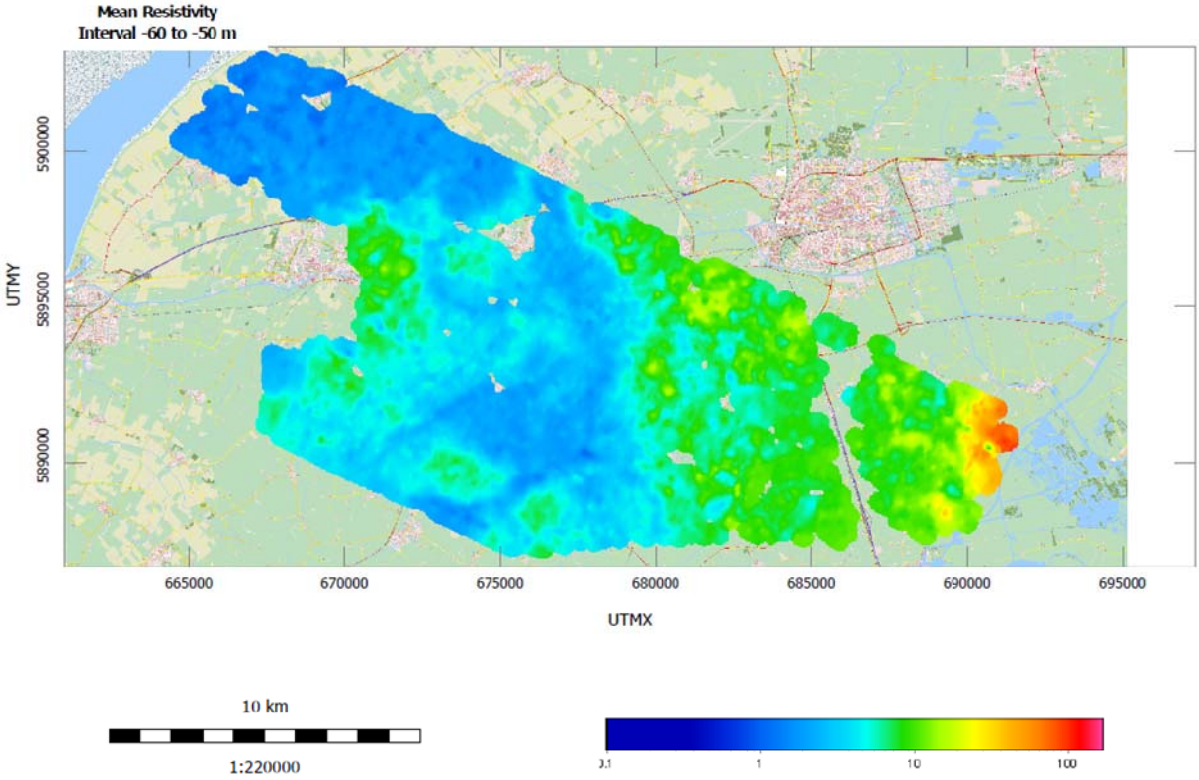
Mean Resistivity
Interval -60 to -50 m
UTMY
5900000
5895000
5890000
665000
670000
675000
680000
685000
690000
695000
UTMX
10 km
1:220000
1
10
100

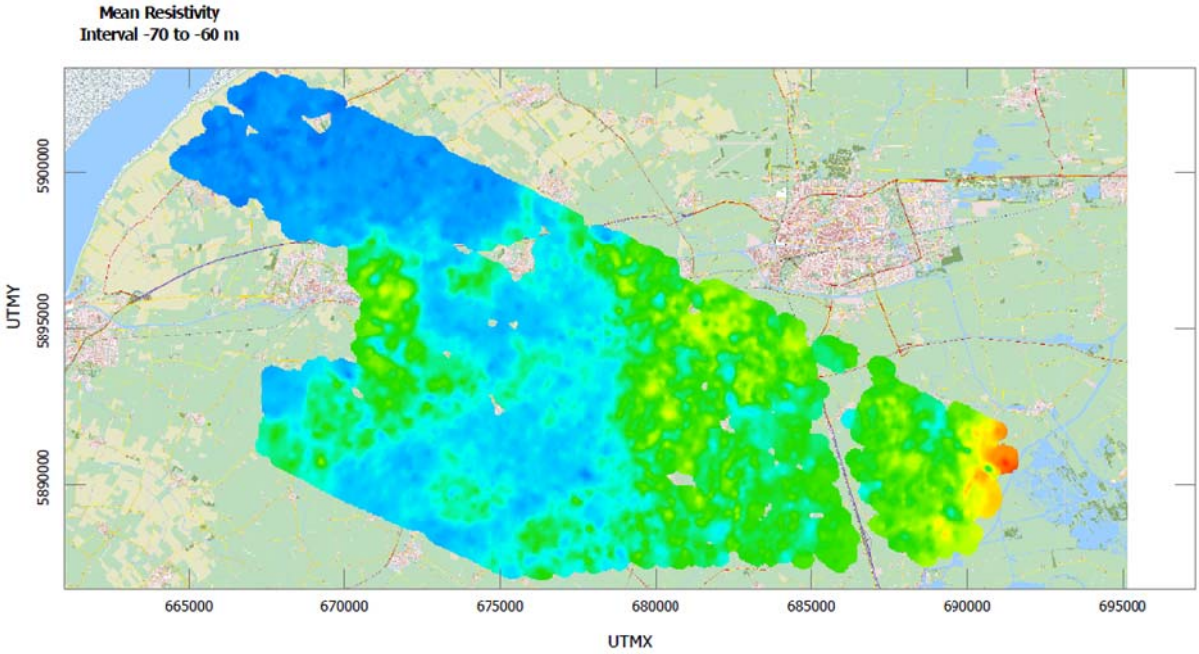
Mean Resistivity
Interval -70 to -60 m
UTMY
5900000
5895000
5890000
665000
670000
675000
680000
685000
690000
695000
UTMX

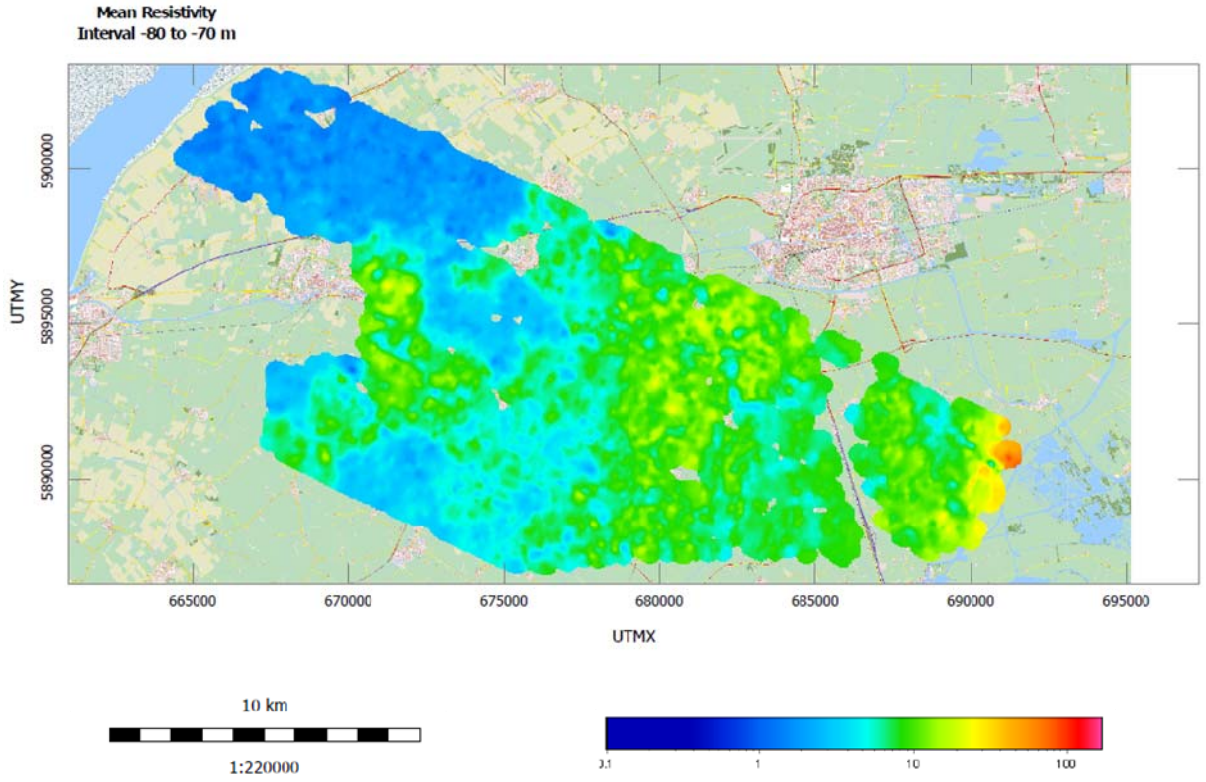
Mean Resistivity
Interval -80 to -70 m
UTMY
5900000
5895000
5890000
665000
670000
675000
680000
685000
690000
695000
UTMX
10 km
1:220000
0.1
1
10
100

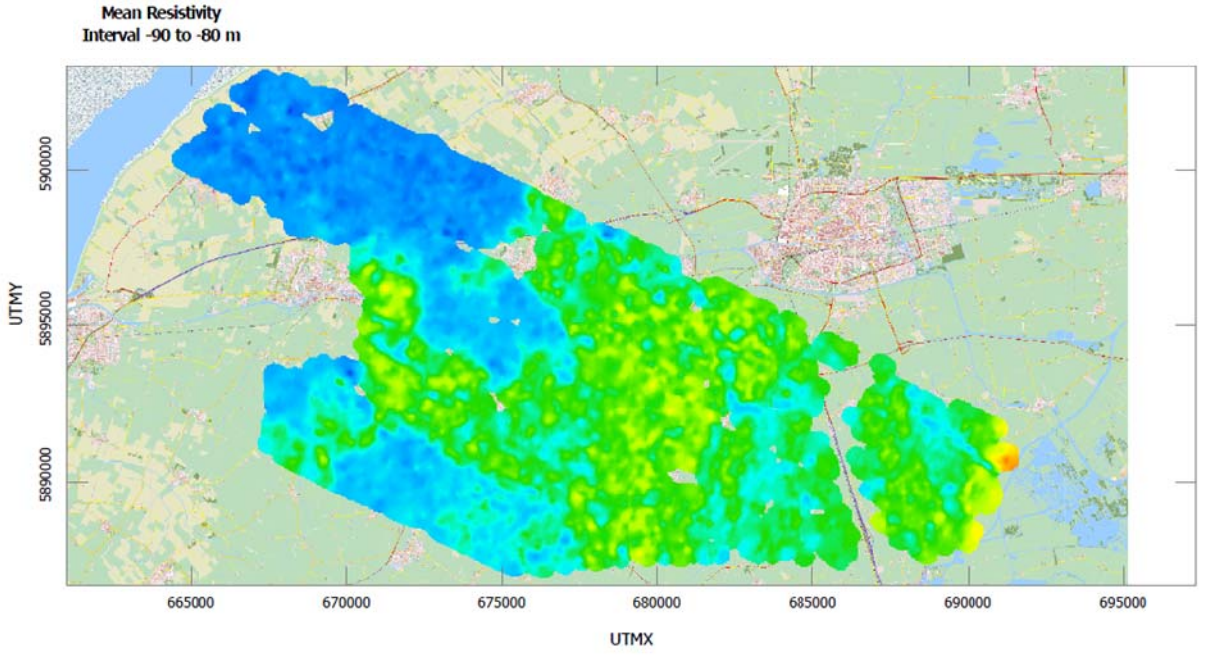
Mean Resistivity
Interval -90 to -80 m
UTMY
5900000
5895000
5890000
665000
670000
675000
680000
685000
690000
695000
UTMX

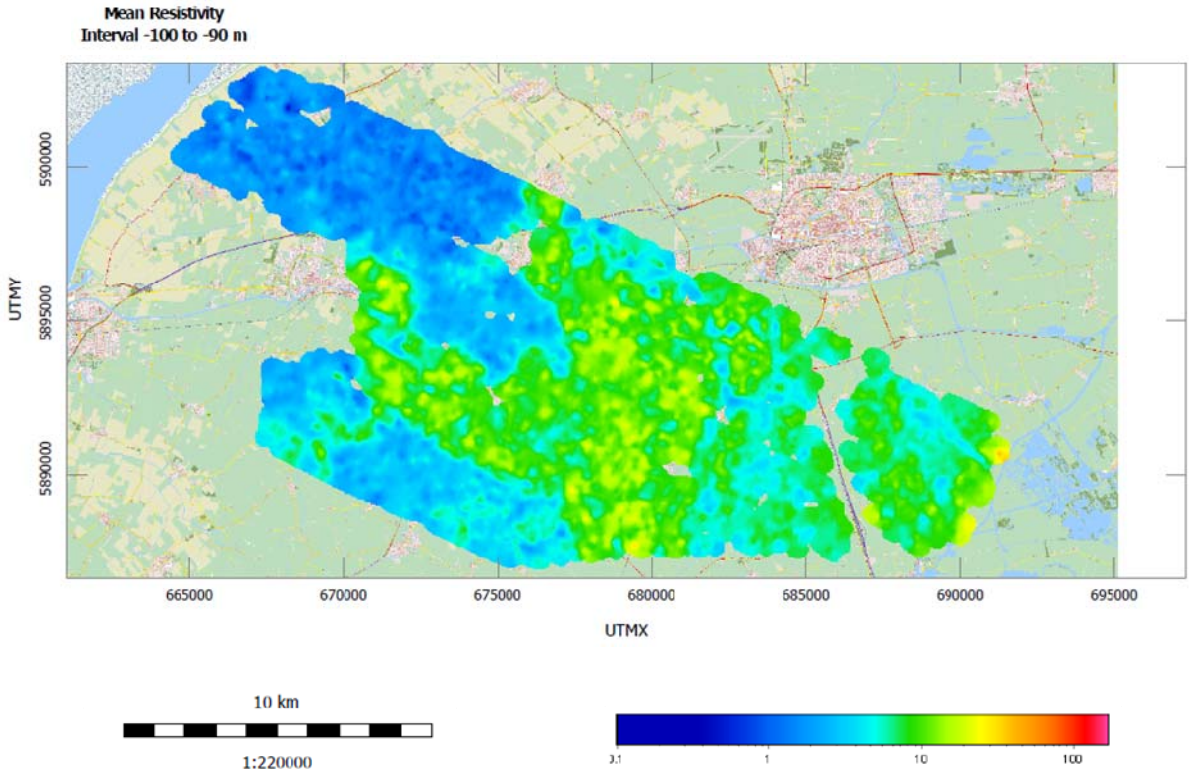
Mean Resistivity
Interval -100 to -90 m
5900000
5895000
5890000
UTMY
665000
670000
675000
680000
685000
690000
695000
UTMX
10 km
1:220000
3.1
1
10
100

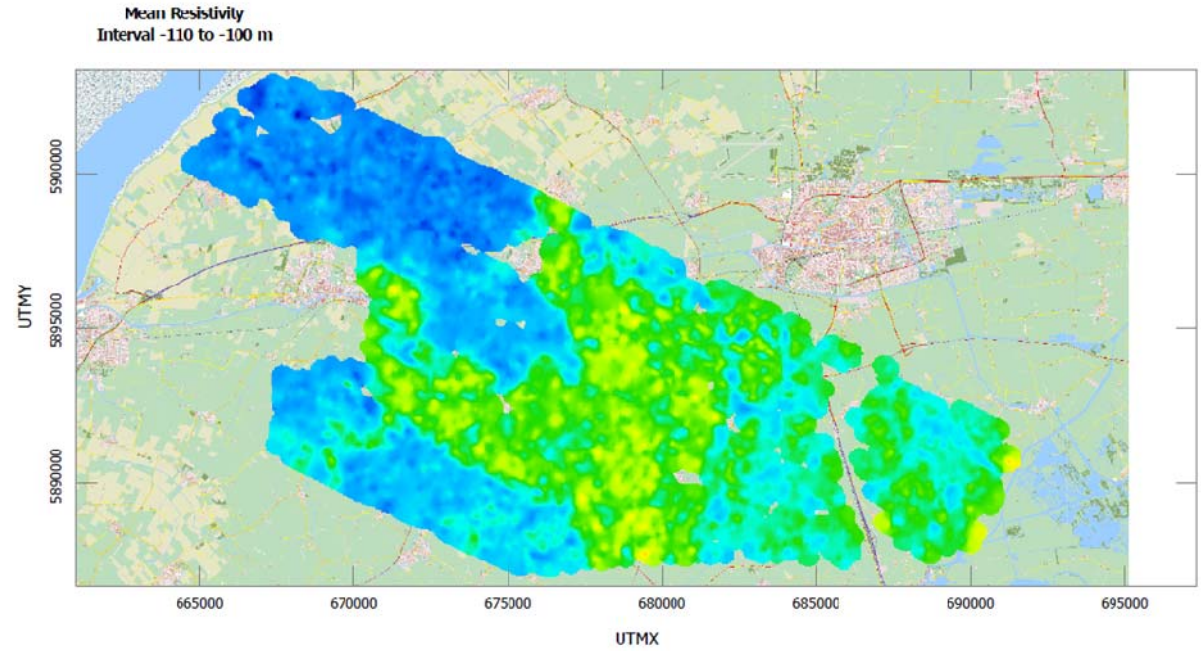
Mean Resistivity
Interval -110 to -100 m
5900000
5895000
5890000
UTMY
665000
670000
675000
680000
685000
690000
695000
UTMX

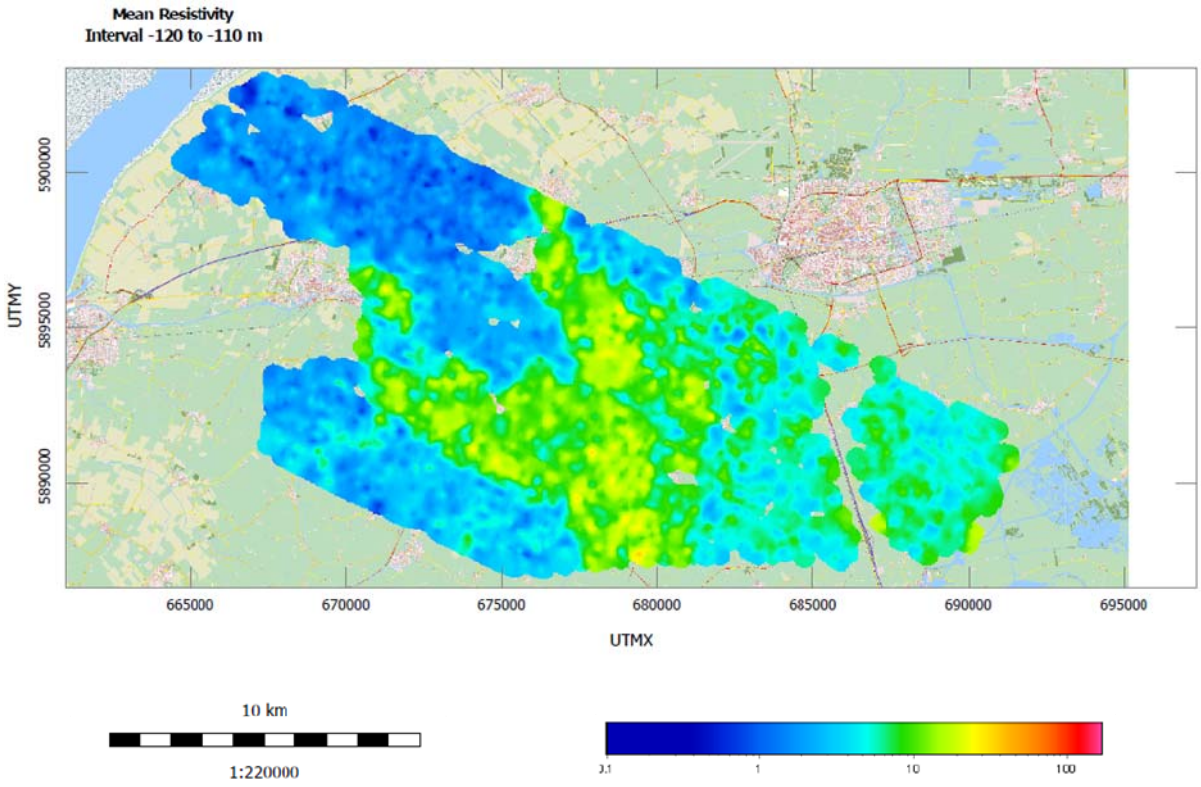
Mean Resistivity
Interval -120 to -110 m
UTMY
5900000
5895000
5890000
665000
670000
675000
680000
685000
690000
695000
UTMX
10 km
1:220000
0.1
1
10
100

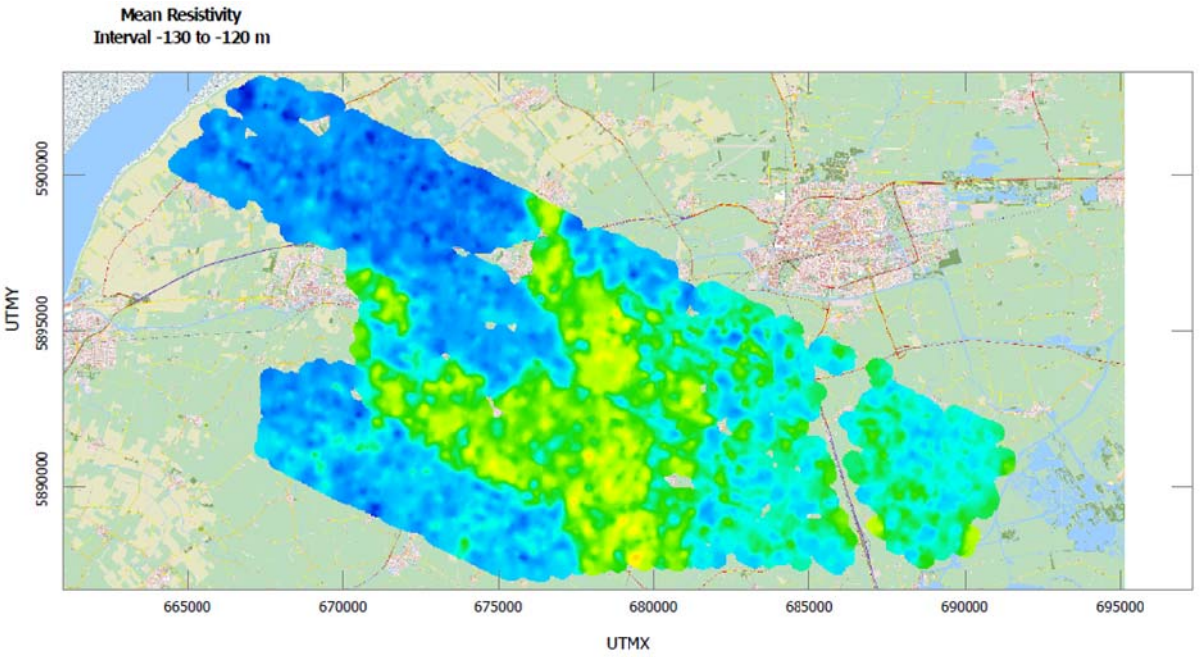
Mean Resistivity
Interval -130 to -120 m
UTMY
5900000
5895000
5890000
665000
670000
675000
680000
685000
690000
695000
UTMX

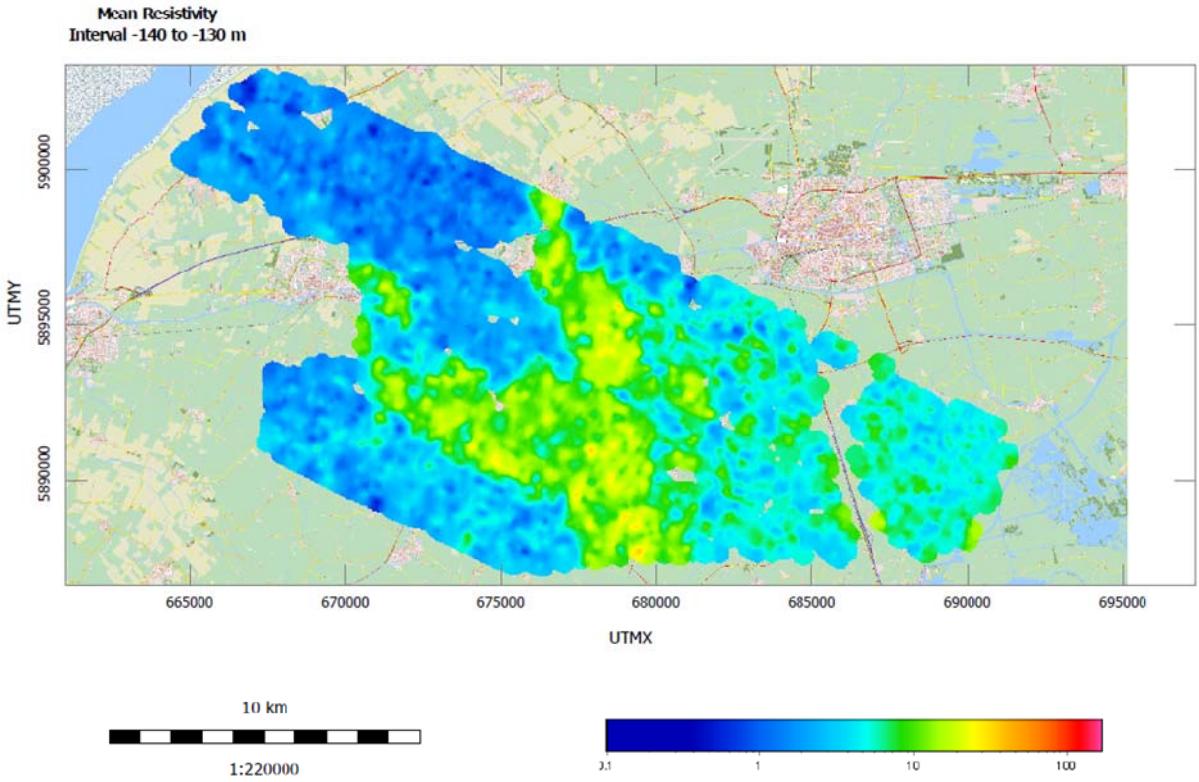
Mean Resistivity
Interval -140 to -130 m
UTMY
5900000
5895000
5890000
665000
670000
675000
680000
685000
690000
695000
UTMX
10 km
1:220000
0.1
1
10
100

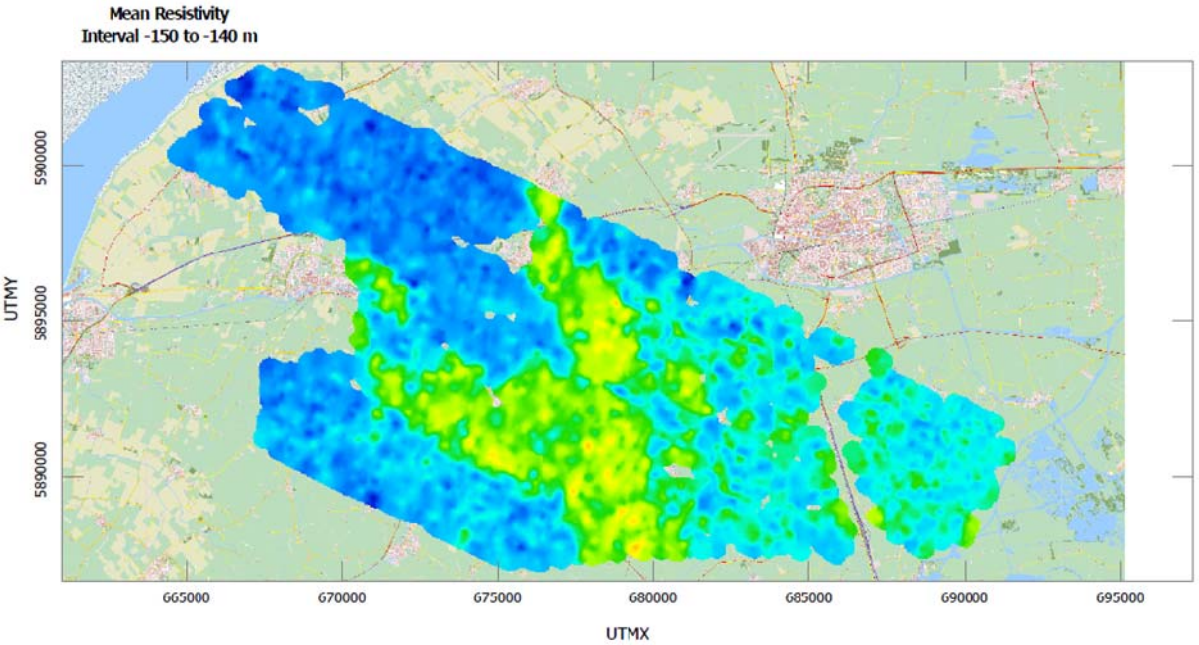
Mean Resistivity
Interval -150 to -140 m
UTMY
5900000
5895000
5890000
665000
670000
675000
680000
685000
690000
695000
UTMX

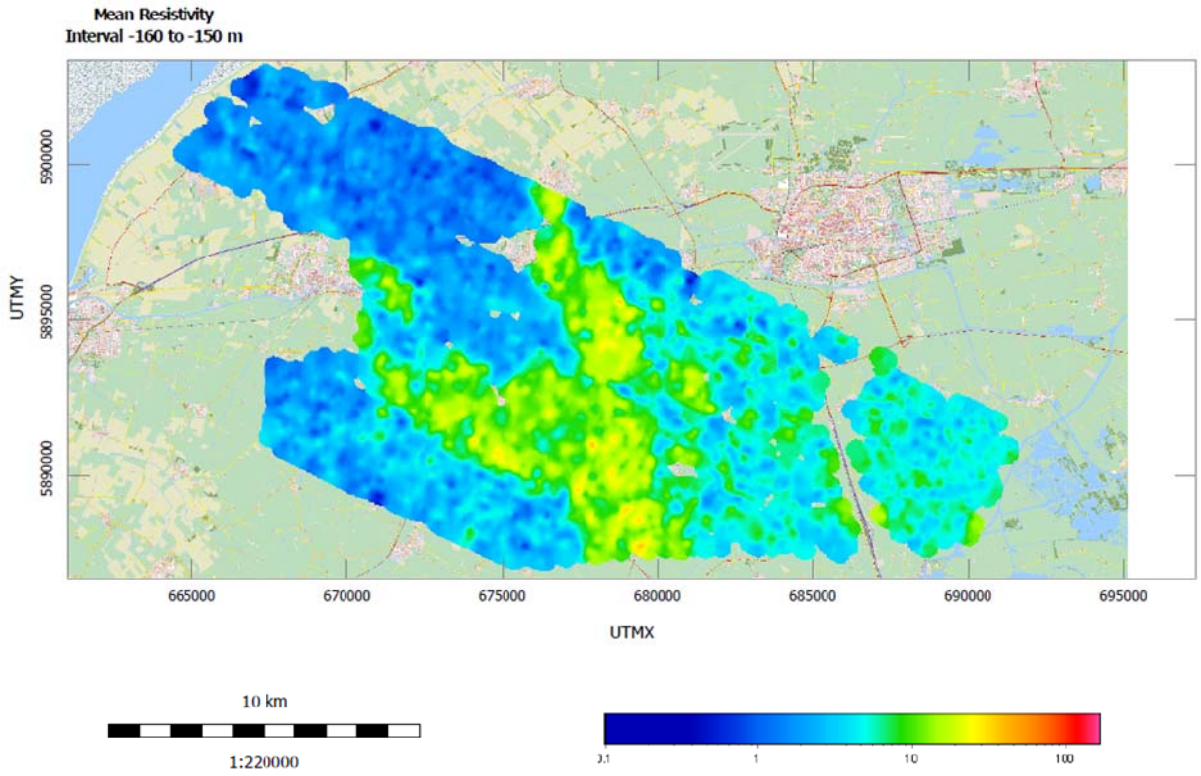
Mean Resistivity
Interval -160 to -150 m
UTMY
5900000
5895000
5890000
665000
670000
675000
680000
685000
690000
695000
UTMX
10 km
1:220000
1
10
100

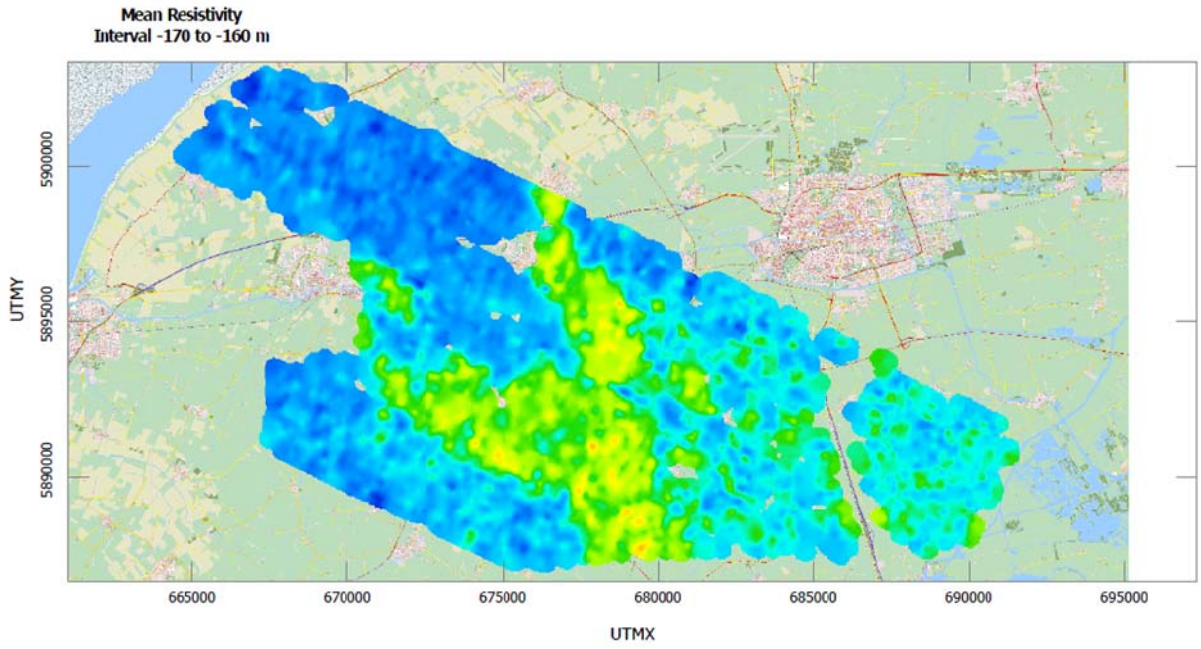
Mean Resistivity
Interval -170 to -160 m
UTMY
5900000
5895000
5890000
665000
670000
675000
680000
685000
690000
695000
UTMX

Terschelling

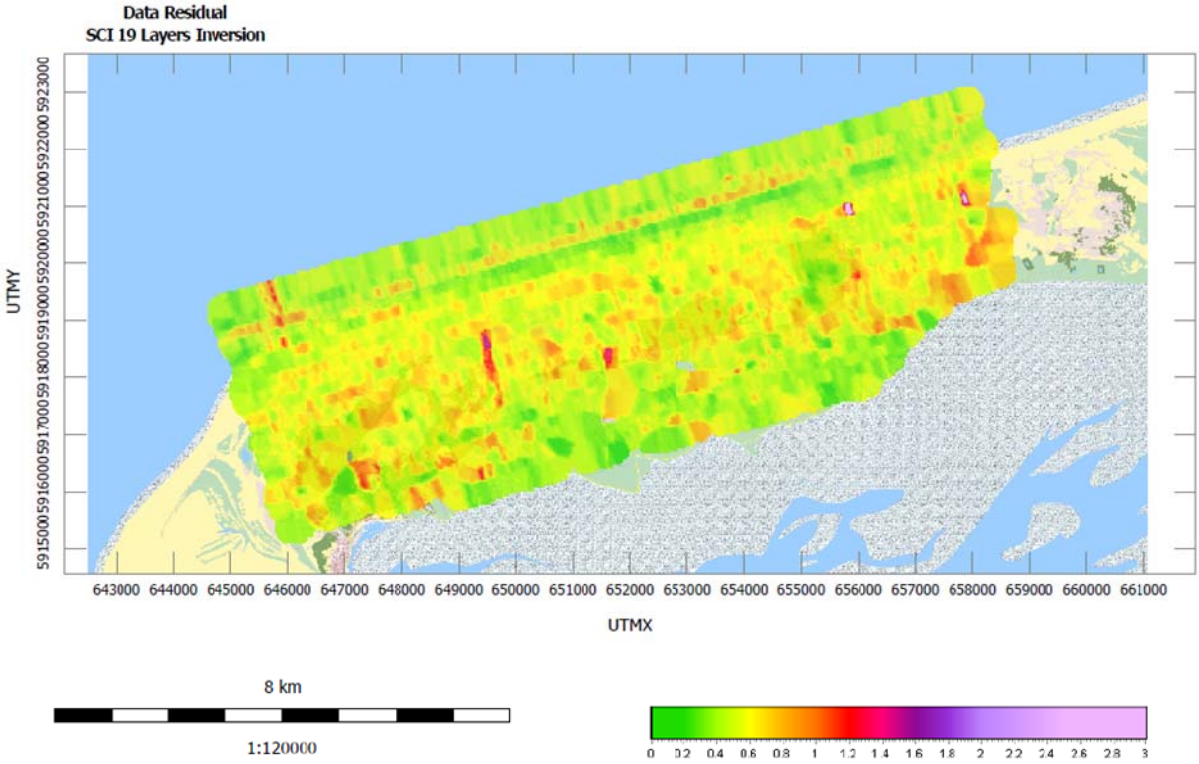

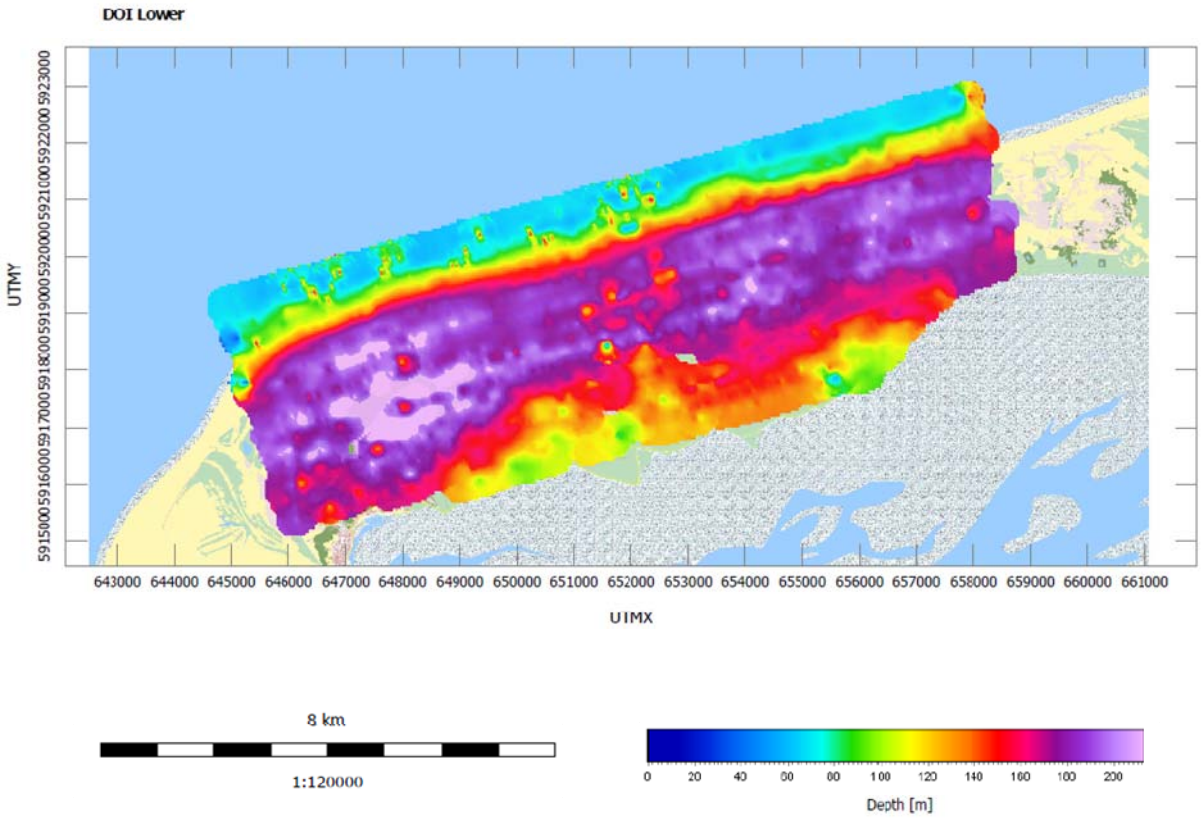
DOI Lower
UTMY
5915000 5916000 5917000 5918000 5919000 5920000 5921000 5922000 5923000
643000 644000 645000 646000 647000 648000 649000 650000 651000 652000 653000 654000 655000 656000 657000 658000 659000 660000 661000
UTMX
8 km
1:120000
0 20 40 60 80 100 120 140 160 180 200
Depth [m]

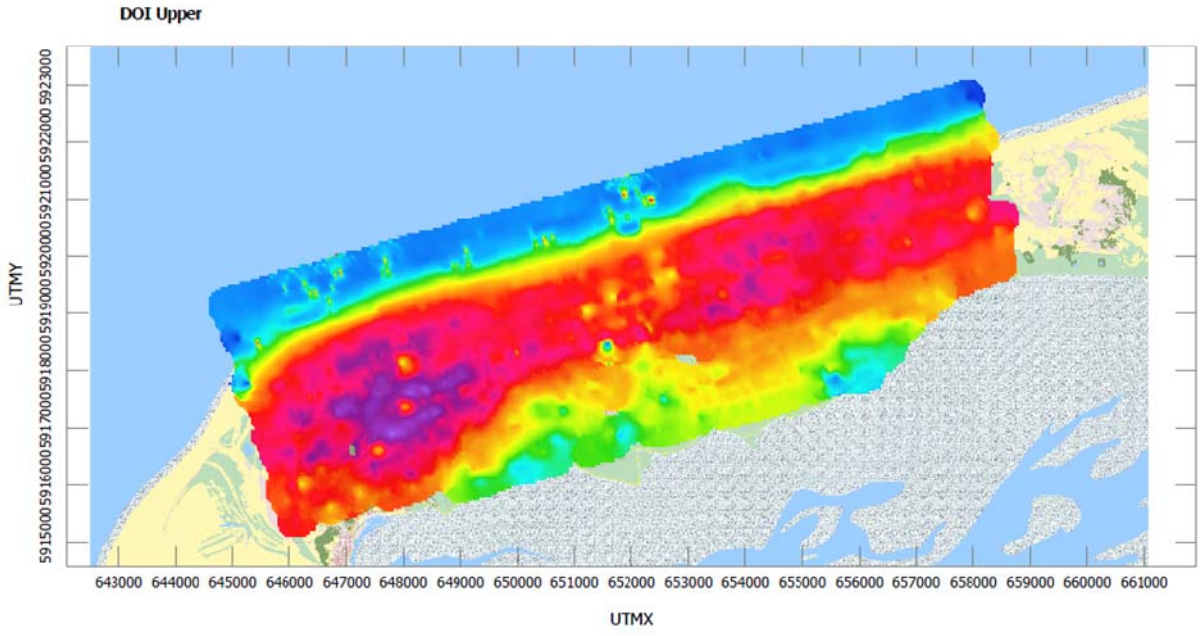
DOI Upper
UTMY
5915000 5916000 5917000 5918000 5919000 5920000 5921000 5922000 5923000
643000 644000 645000 646000 647000 648000 649000 650000 651000 652000 653000 654000 655000 656000 657000 658000 659000 660000 661000
UTMX

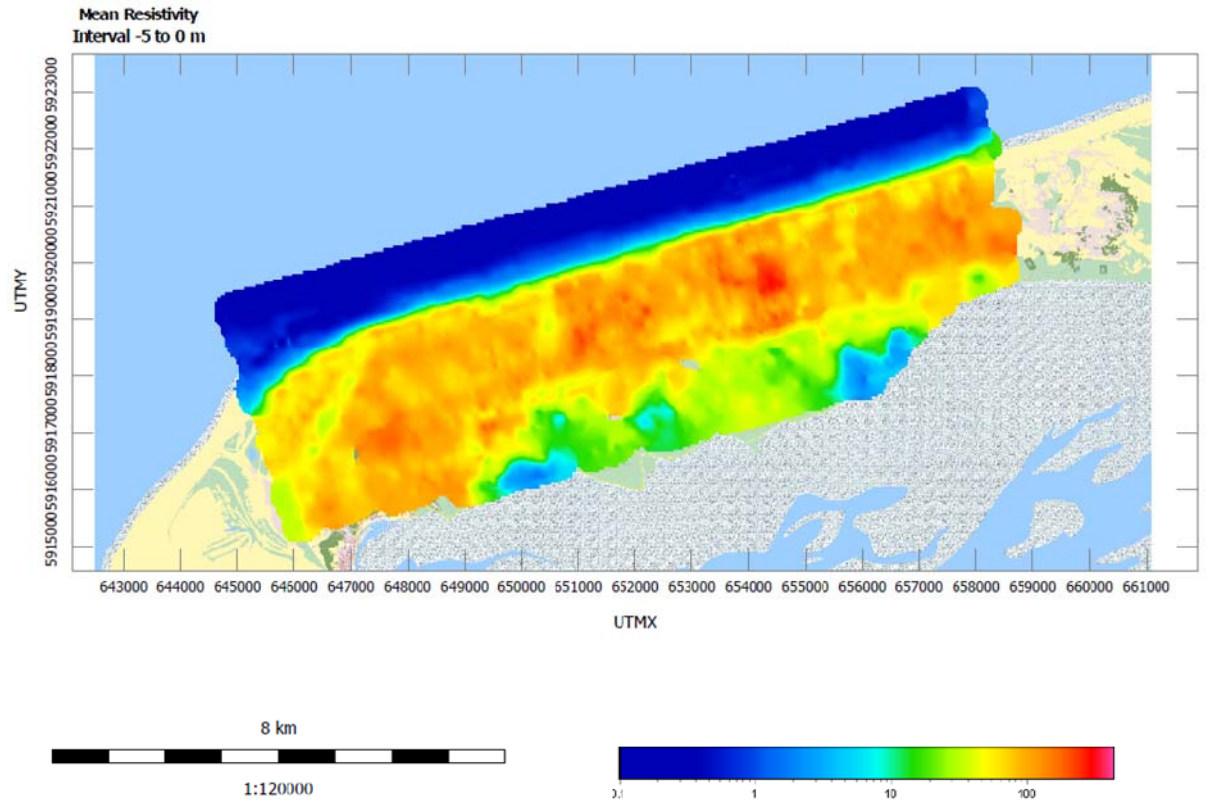
Mean Resistivity
Interval -5 to 0 m
UTMY
UTMX
643000 644000 645000 645000 647000 648000 649000 650000 551000 652000 653000 654000 655000 656000 657000 658000 659000 660000 661000
8 km
1:120000
1
10
100

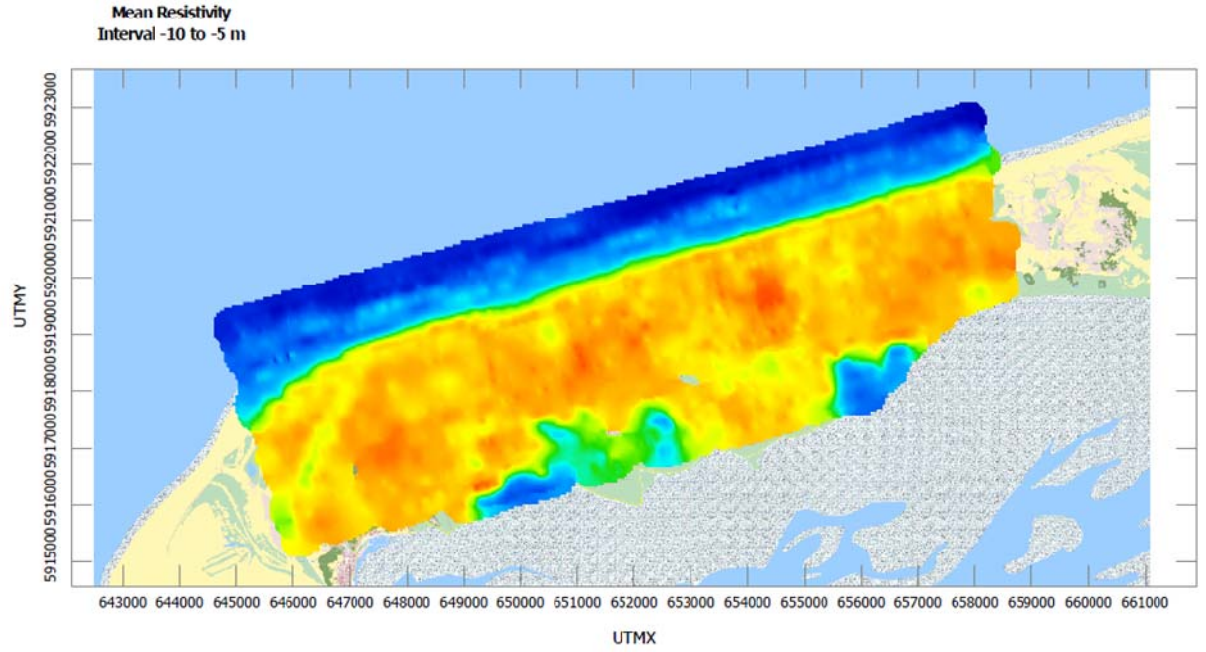
Mean Resistivity
Interval -10 to -5 m
UTMY
UTMX
643000 644000 645000 646000 647000 648000 649000 650000 651000 652000 653000 654000 655000 656000 657000 658000 659000 660000 661000

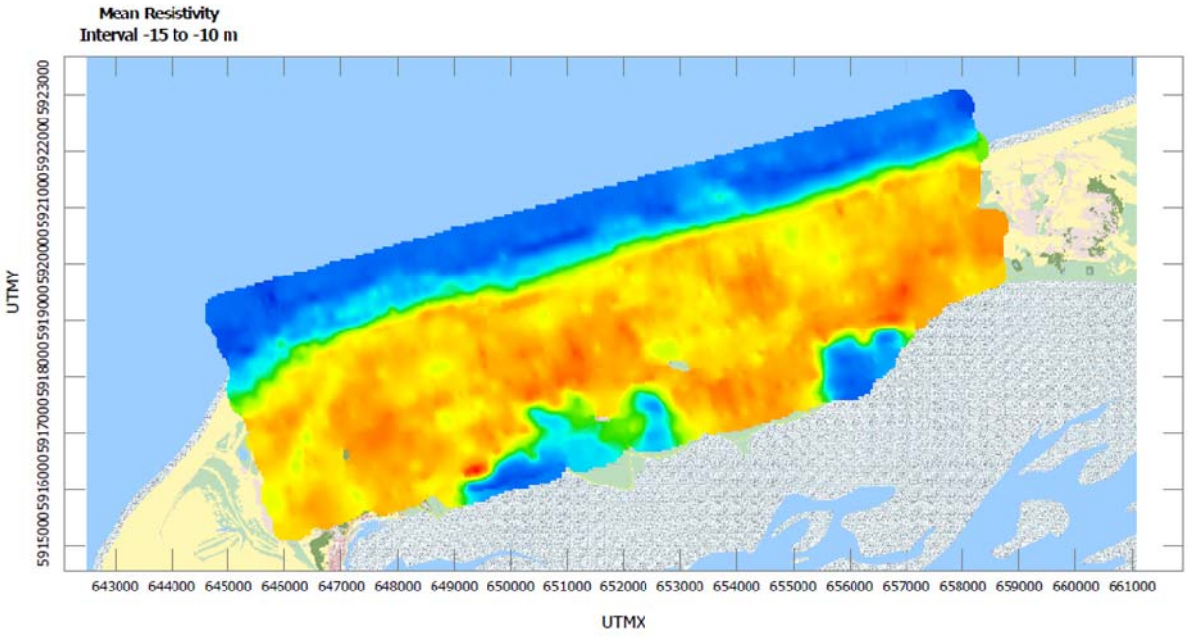
Mean Resistivity
Interval -15 to -10 m
UTMY
5915000 5916000 5917000 5918000 5919000 5920000 5921000 5922000 5923000
643000 644000 645000 645000 647000 648000 649000 650000 651000 652000 653000 654000 655000 656000 657000 658000 659000 660000 661000
UTMX

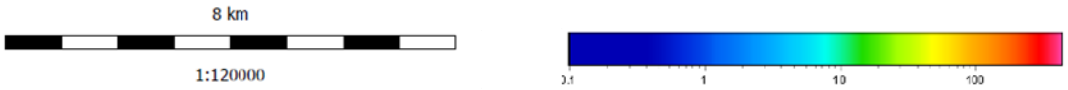
8 km
1:120000
0.1
1
10
100

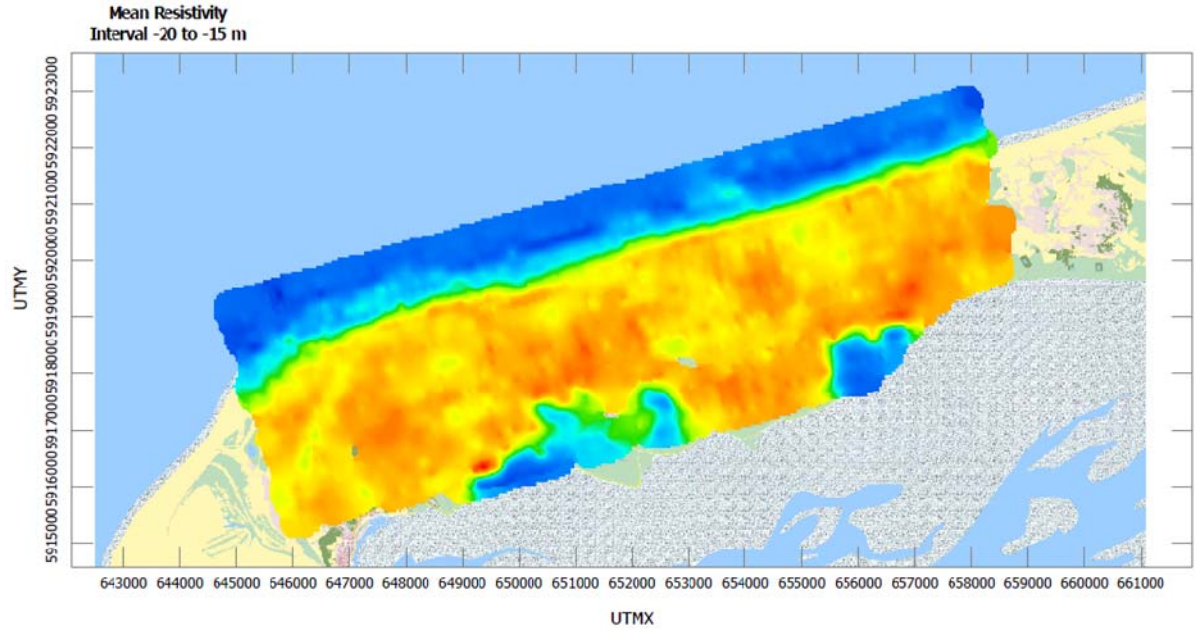
Mean Resistivity
Interval -20 to -15 m
UTMY
5915000 5916000 5917000 5918000 5919000 5920000 5921000 5922000 5923000
643000 644000 645000 646000 647000 648000 649000 650000 651000 652000 653000 654000 655000 656000 657000 658000 659000 660000 661000
UTMX

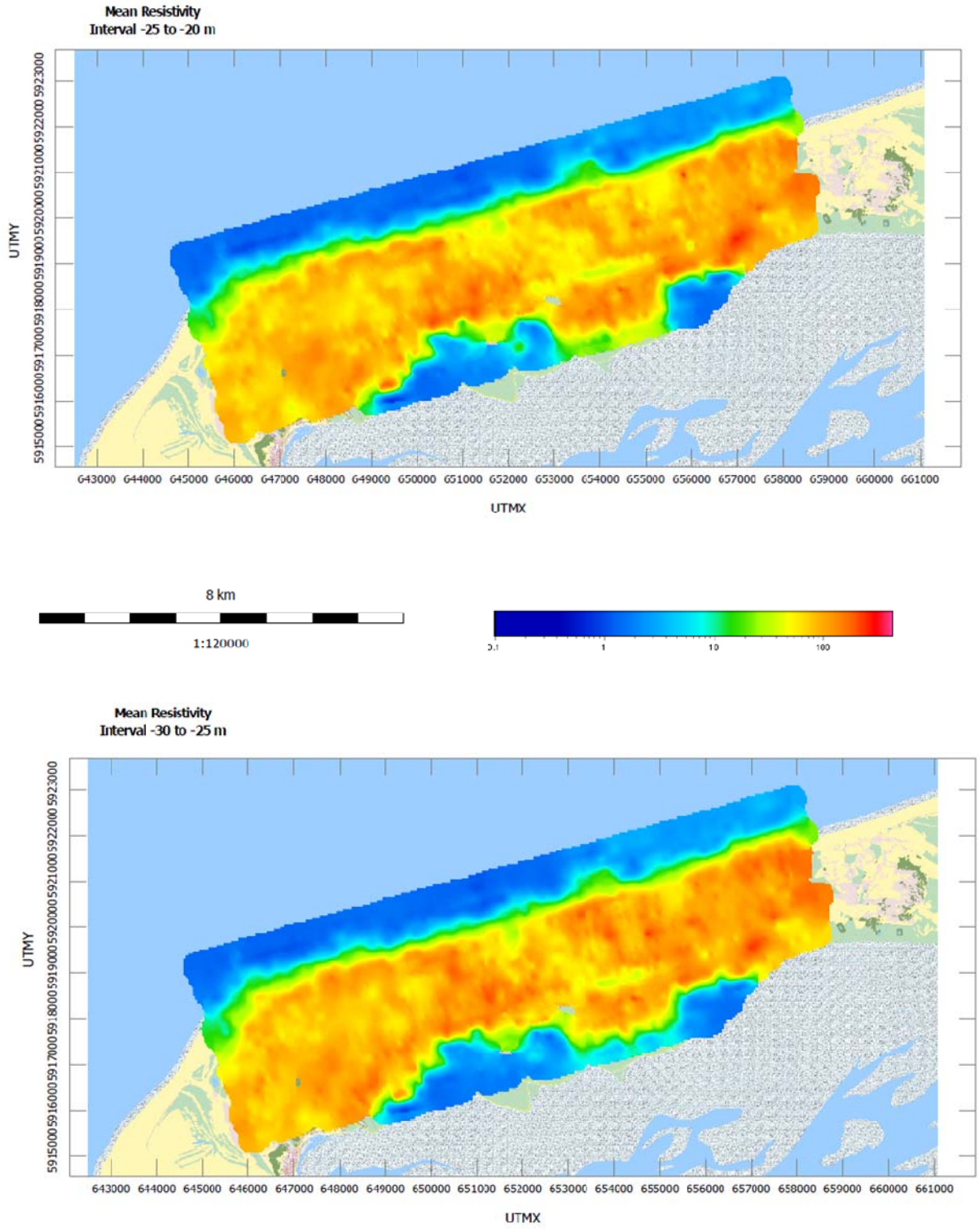
Mean Resistivity
Interval -25 to -20 m
UTMY
UTMX
8 km
1:120000
Mean Resistivity
Interval -30 to -25 m
UTMY
UTMX

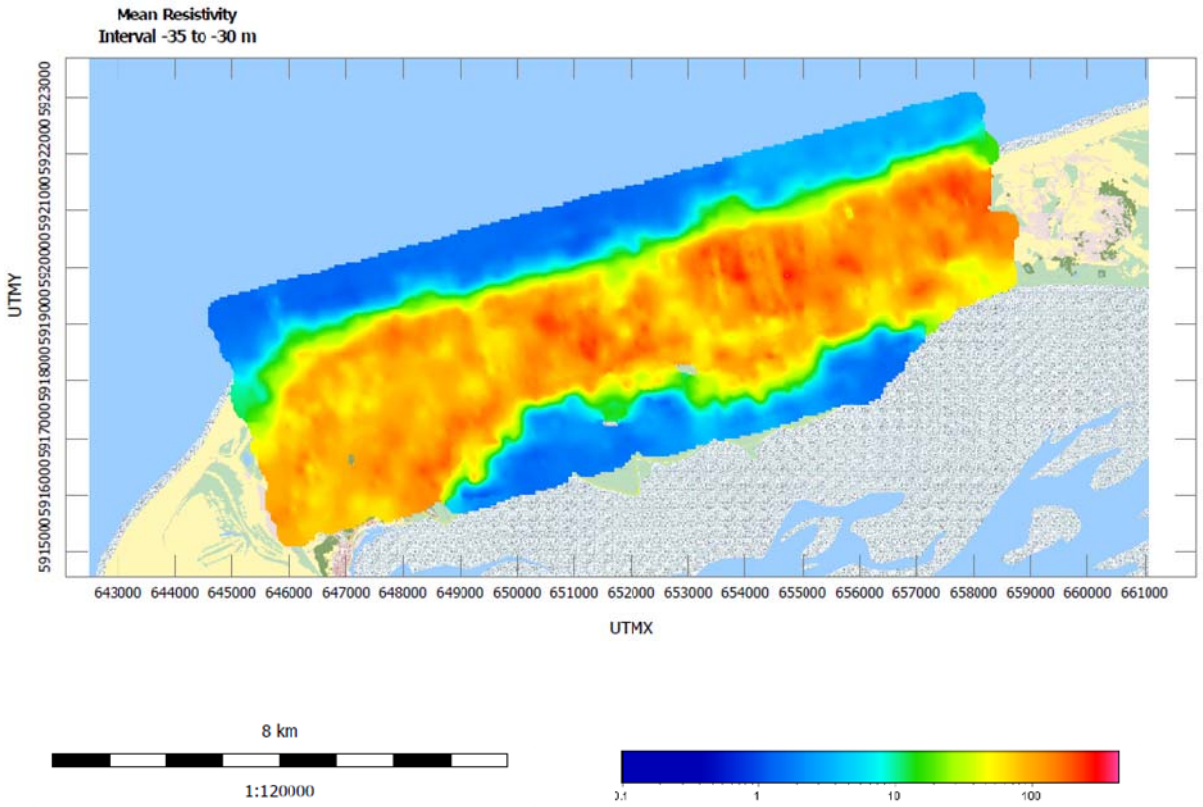
Mean Resistivity
Interval -35 to -30 m
UTMY
5915000 5916000 5917000 5918000 5919000 5920000 5921000 5922000 5923000
643000 644000 645000 646000 647000 648000 649000 650000 651000 652000 653000 654000 655000 656000 657000 658000 659000 660000 661000
UTMX
8 km
1:120000
0.1
1
10
100

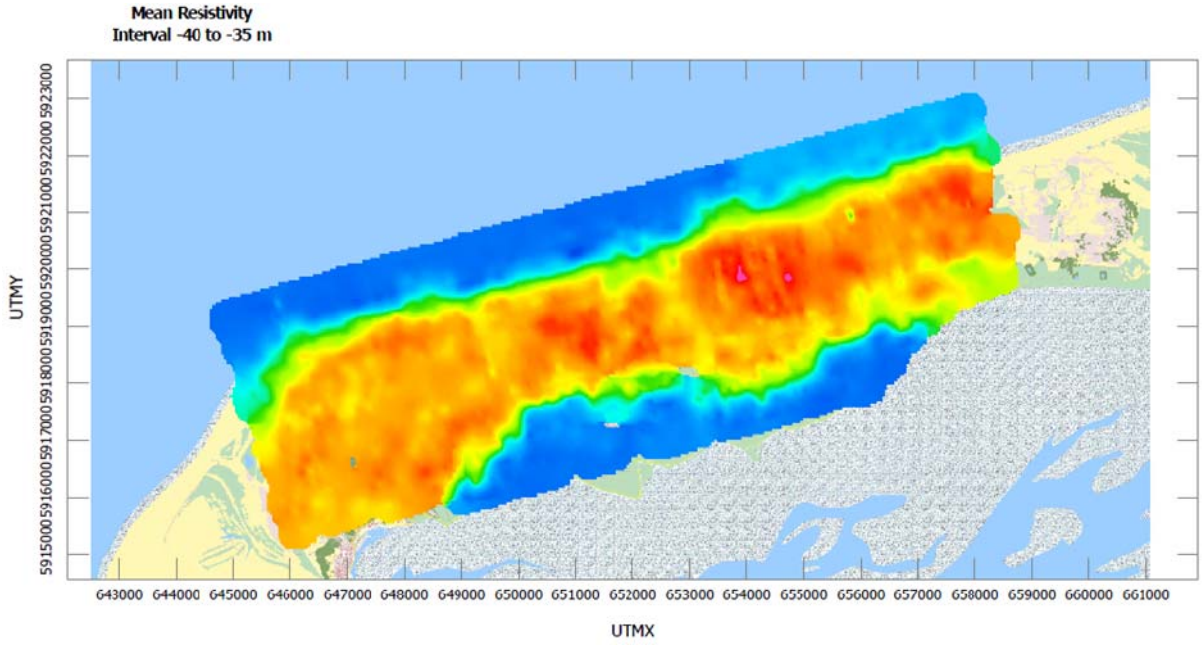
Mean Resistivity
Interval -40 to -35 m
UTMY
5915000 5916000 5917000 5918000 5919000 5920000 5921000 5922000 5923000
643000 644000 645000 646000 647000 648000 649000 650000 651000 652000 653000 654000 655000 656000 657000 658000 659000 660000 661000
UTMX

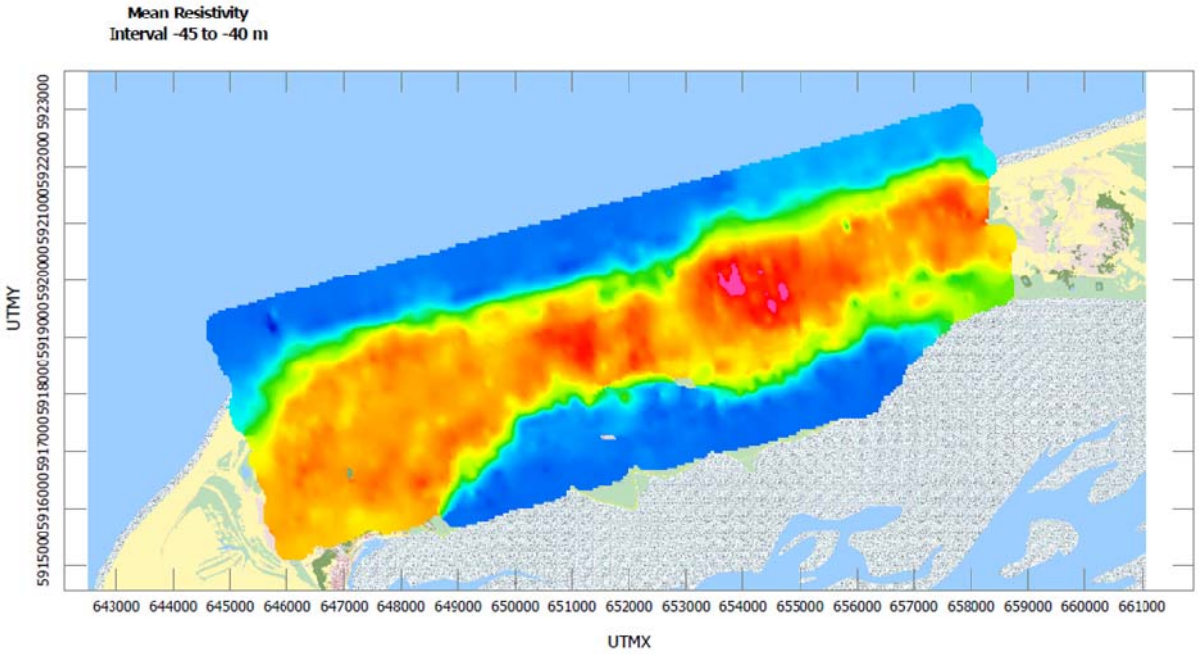
Mean Resistivity
Interval -45 to -40 m
UTMY
5915000 5916000 5917000 5918000 5919000 5920000 5921000 5922000 5923000
643000 644000 645000 646000 647000 648000 649000 650000 651000 652000 653000 654000 655000 656000 657000 658000 659000 660000 661000
UTMX
8 km
1:120000
0.1
1
10
100

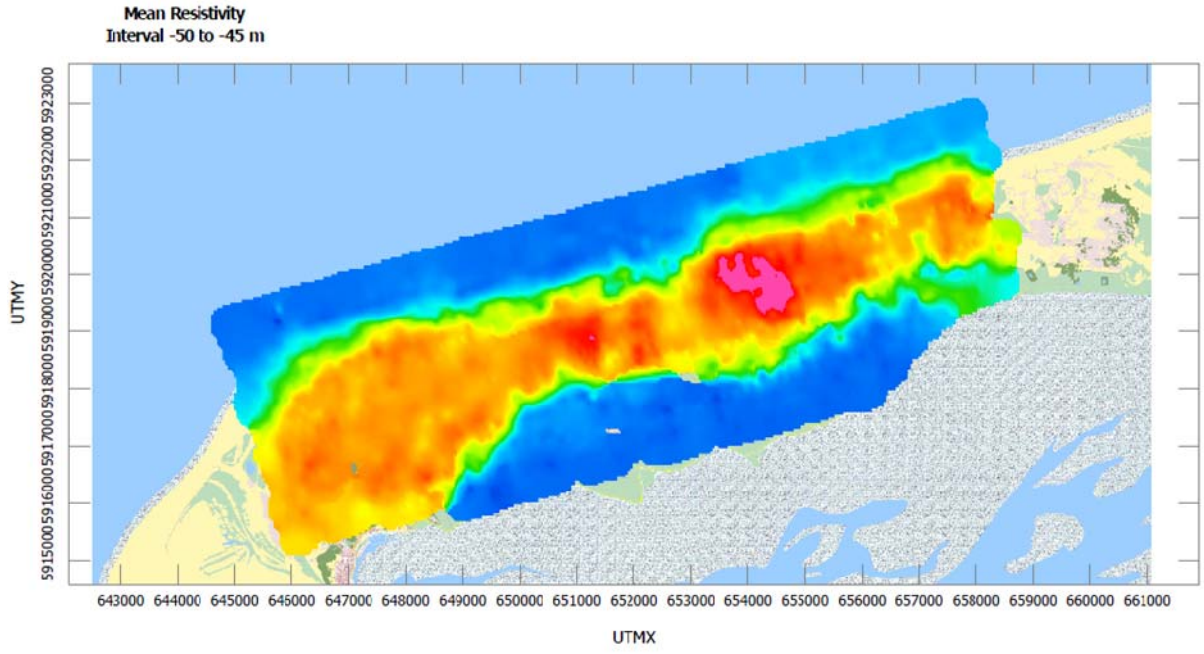
Mean Resistivity
Interval -50 to -45 m
UTMY
5915000 5916000 5917000 5918000 5919000 5920000 5921000 5922000 5923000
643000 644000 645000 646000 647000 648000 649000 650000 651000 652000 653000 654000 655000 656000 657000 658000 659000 660000 661000
UTMX

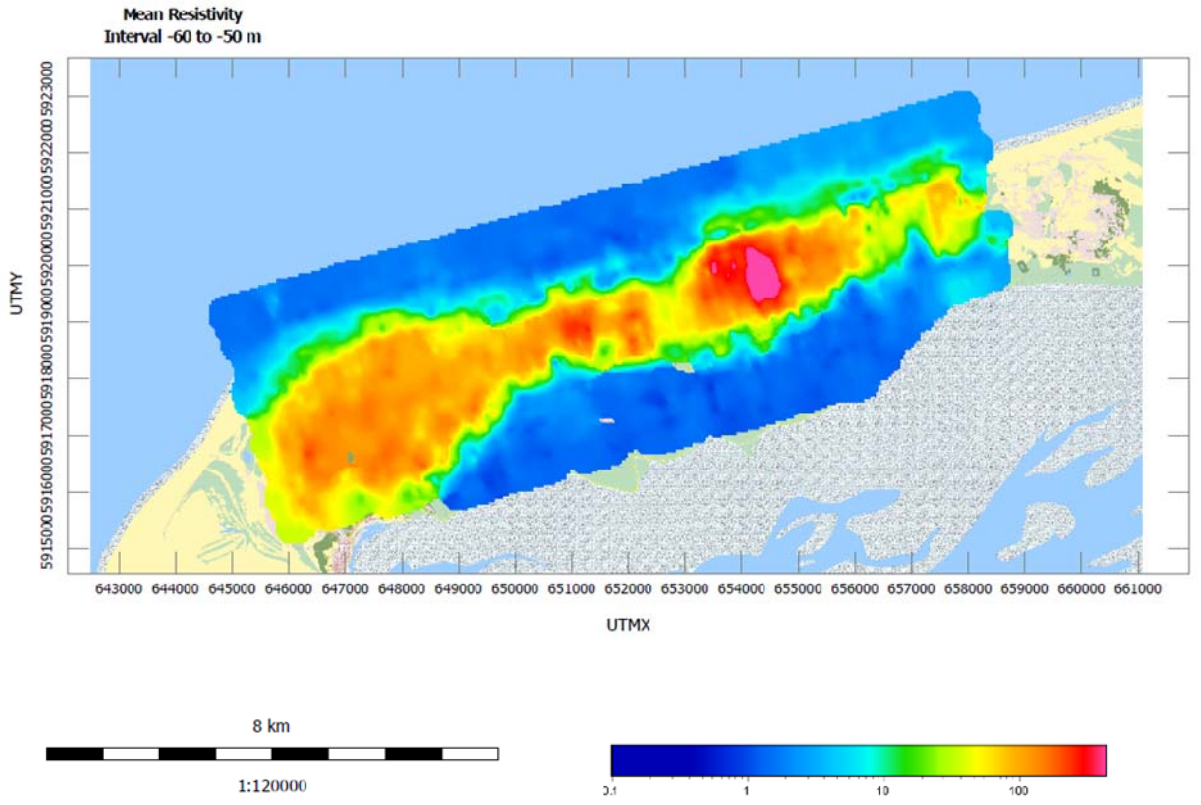
Mean Resistivity
Interval -60 to -50 m
UTMY
5915000 5916000 5917000 5918000 5919000 5920000 5921000 5922000 5923000
643000 644000 645000 646000 647000 648000 649000 650000 651000 652000 653000 654000 655000 656000 657000 658000 659000 660000 661000
UTMX
8 km
1:120000
0.1
1
10
100

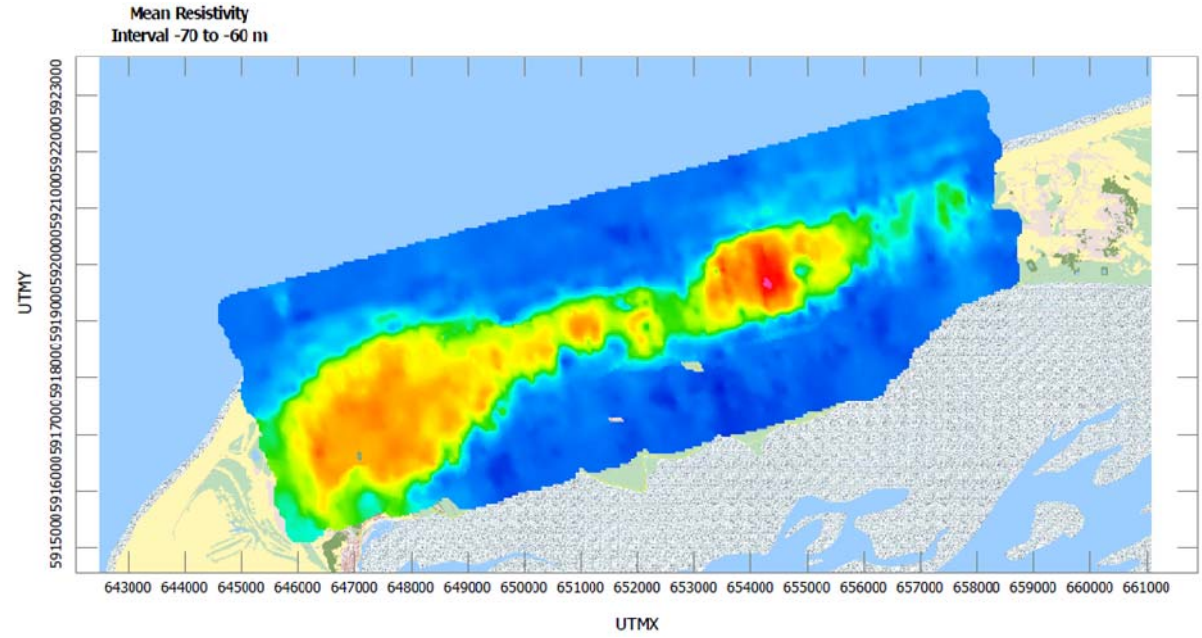
Mean Resistivity
Interval -70 to -60 m
UTMY
5915000 5916000 5917000 5918000 5919000 5920000 5921000 5922000 5923000
643000 644000 645000 646000 647000 648000 649000 650000 651000 652000 653000 654000 655000 656000 657000 658000 659000 660000 661000
UTMX

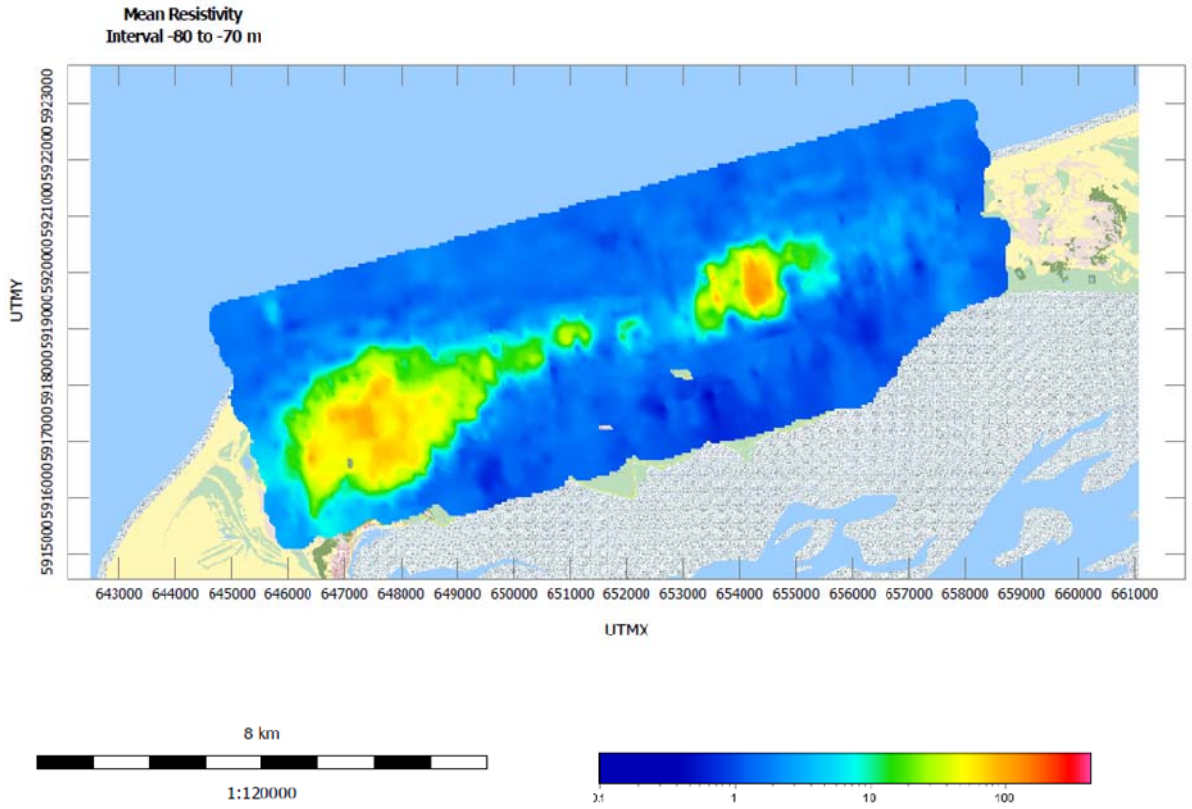
Mean Resistivity
Interval -80 to -70 m
UTMY
5915000 5916000 5917000 5918000 5919000 5920000 5921000 5922000 5923000
643000 644000 645000 646000 647000 648000 649000 650000 651000 652000 653000 654000 655000 656000 657000 658000 659000 660000 661000
UTMX
8 km
1:120000
1
10
100

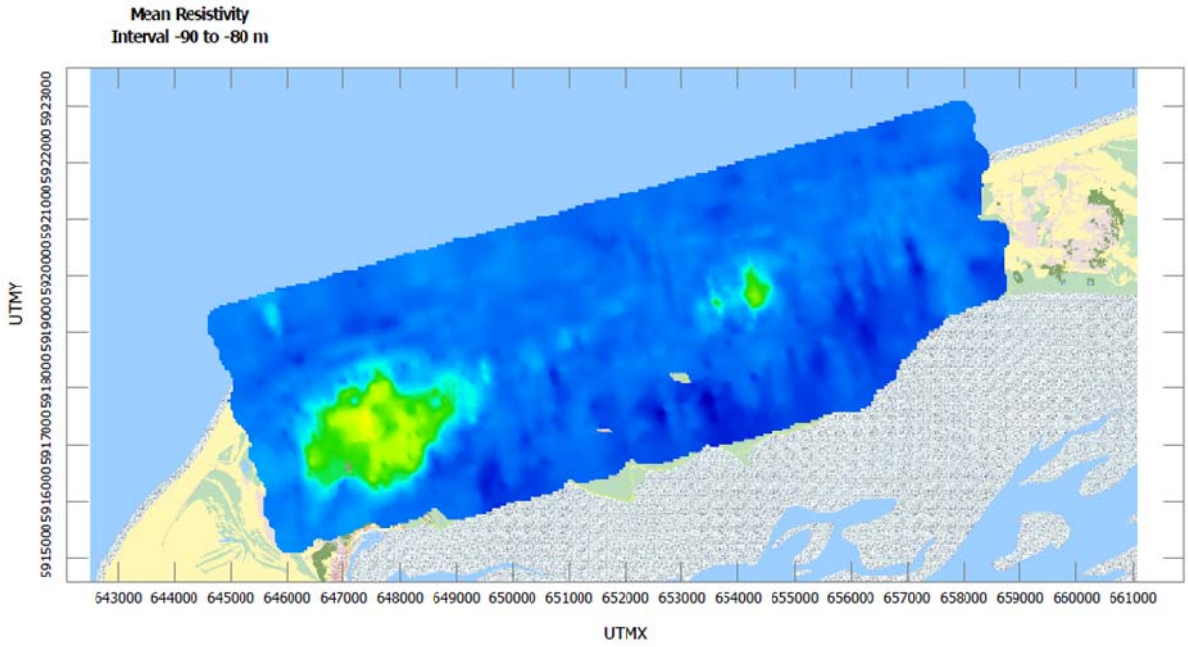
Mean Resistivity
Interval -90 to -80 m
UTMY
5915000 5916000 5917000 5918000 5919000 5920000 5921000 5922000 5923000
643000 644000 645000 646000 647000 648000 649000 650000 651000 652000 653000 654000 655000 656000 657000 658000 659000 660000 661000
UTMX

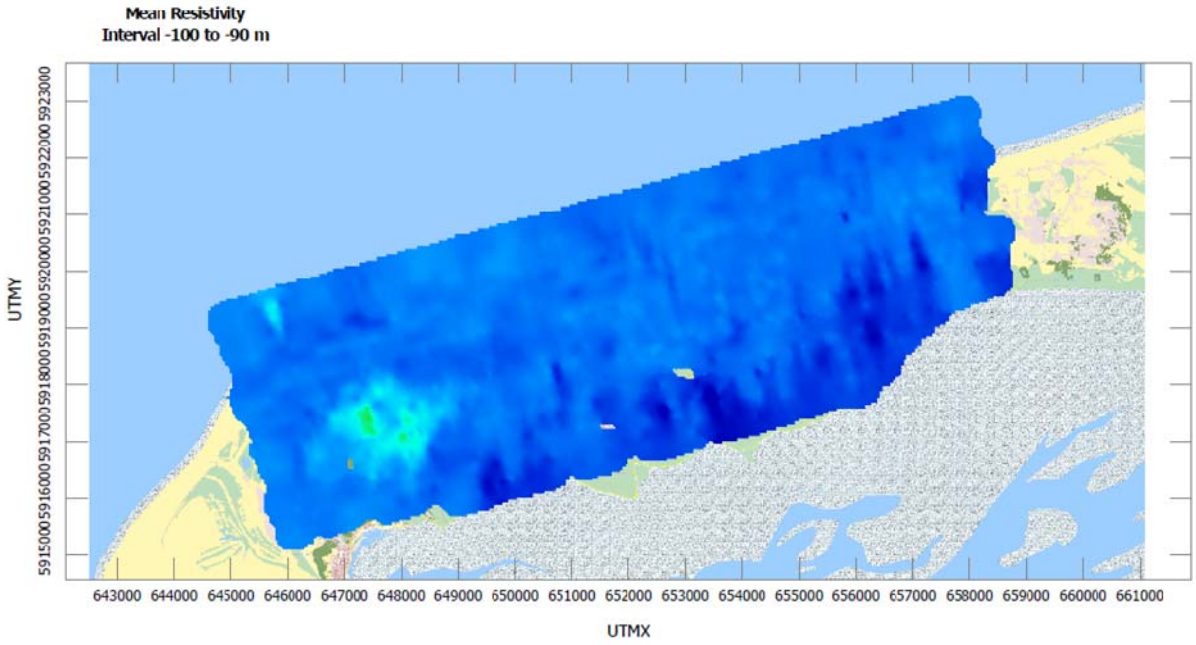
Mean Resistivity
Interval -100 to -90 m
UTMY
5915000 5916000 5917000 5918000 5919000 5920000 5921000 5922000 5923000
643000 644000 645000 646000 647000 648000 649000 650000 651000 652000 653000 654000 655000 656000 657000 658000 659000 660000 661000
UTMX
8 km
1:120000
0.1
1
10
100

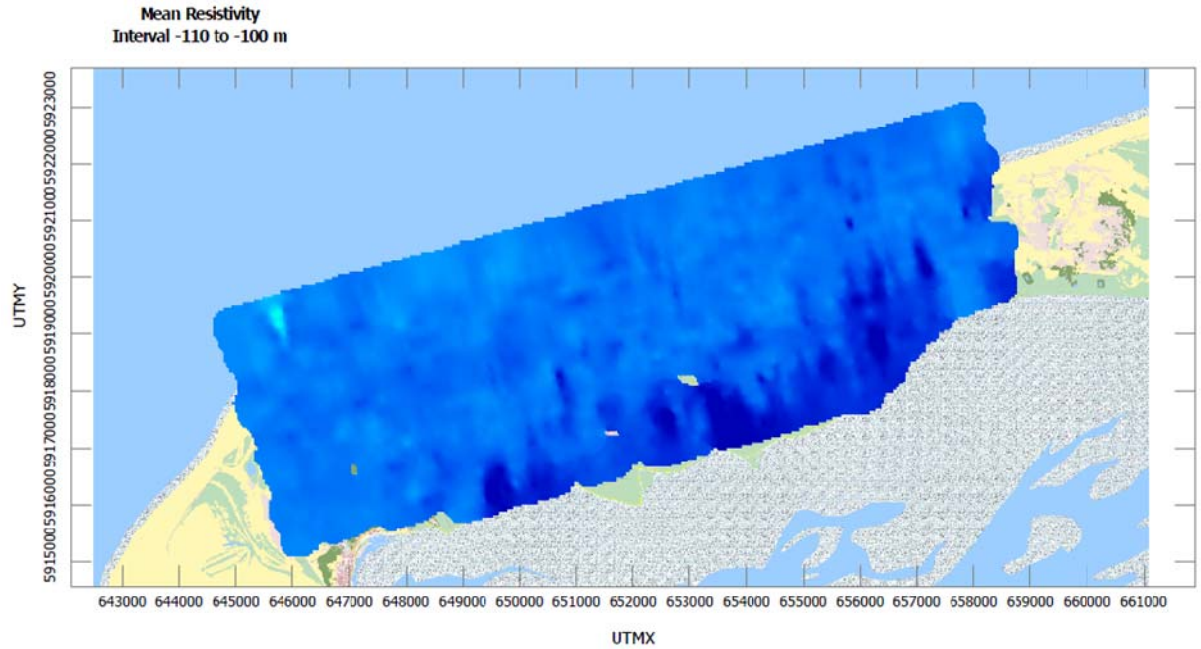
Mean Resistivity
Interval -110 to -100 m
UTMY
5915000 5916000 5917000 5918000 5919000 5920000 5921000 5922000 5923000
643000 644000 645000 646000 647000 648000 649000 650000 651000 652000 653000 654000 655000 656000 657000 658000 659000 660000 661000
UTMX

Appendix 3 – Cross sections of Terschelling Island

The following profiles of the Island of Terschelling show a cross section of resistivity to have an overview of it distribution and then it focus on the location of the thin clay layers.

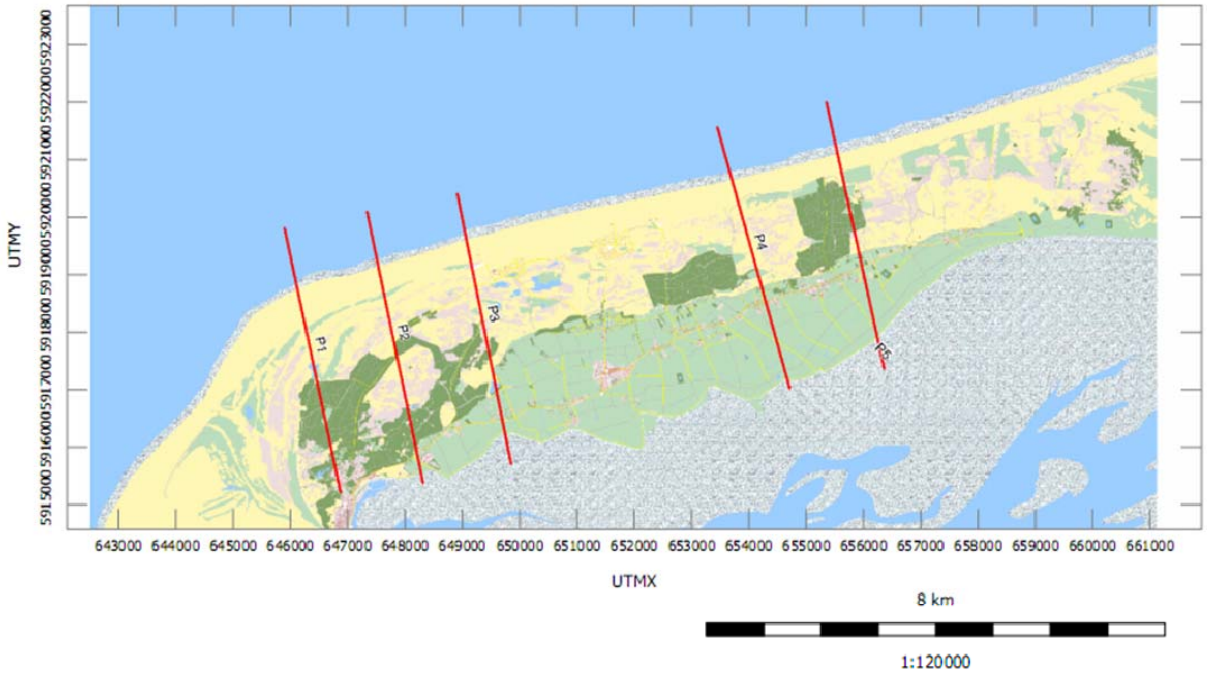

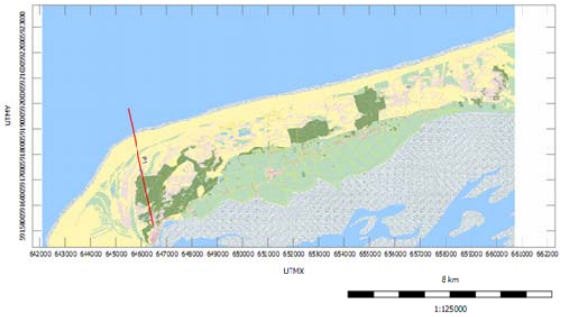
UTMX
8 km
1:125000

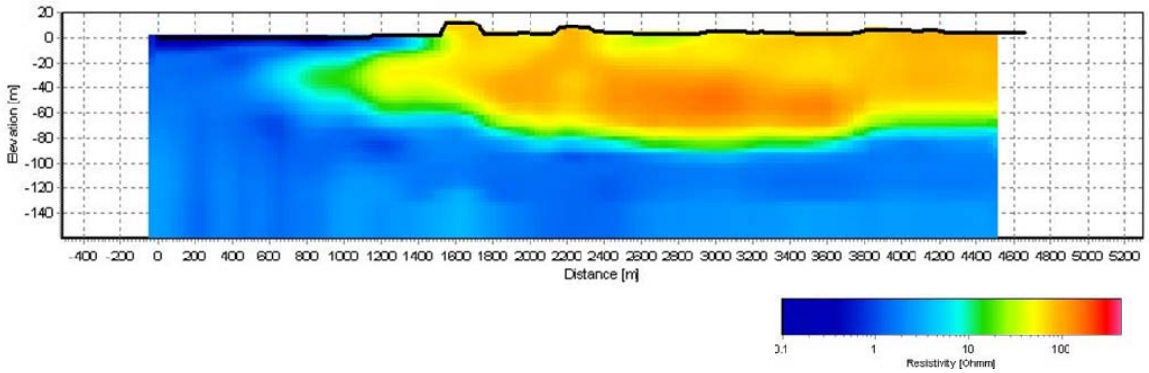
Elevation [m]
Distance [m]
Resistivity [Ohmm]

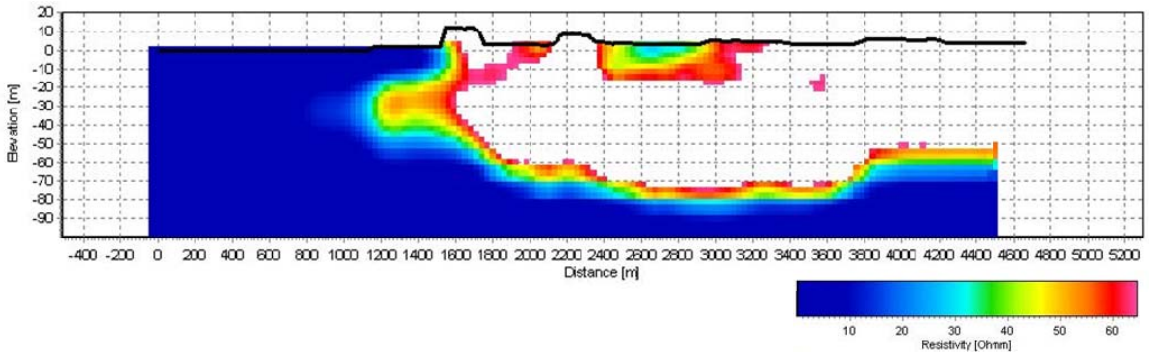
Elevation [m]
Distance [m]
Resistivity [Ohmm]

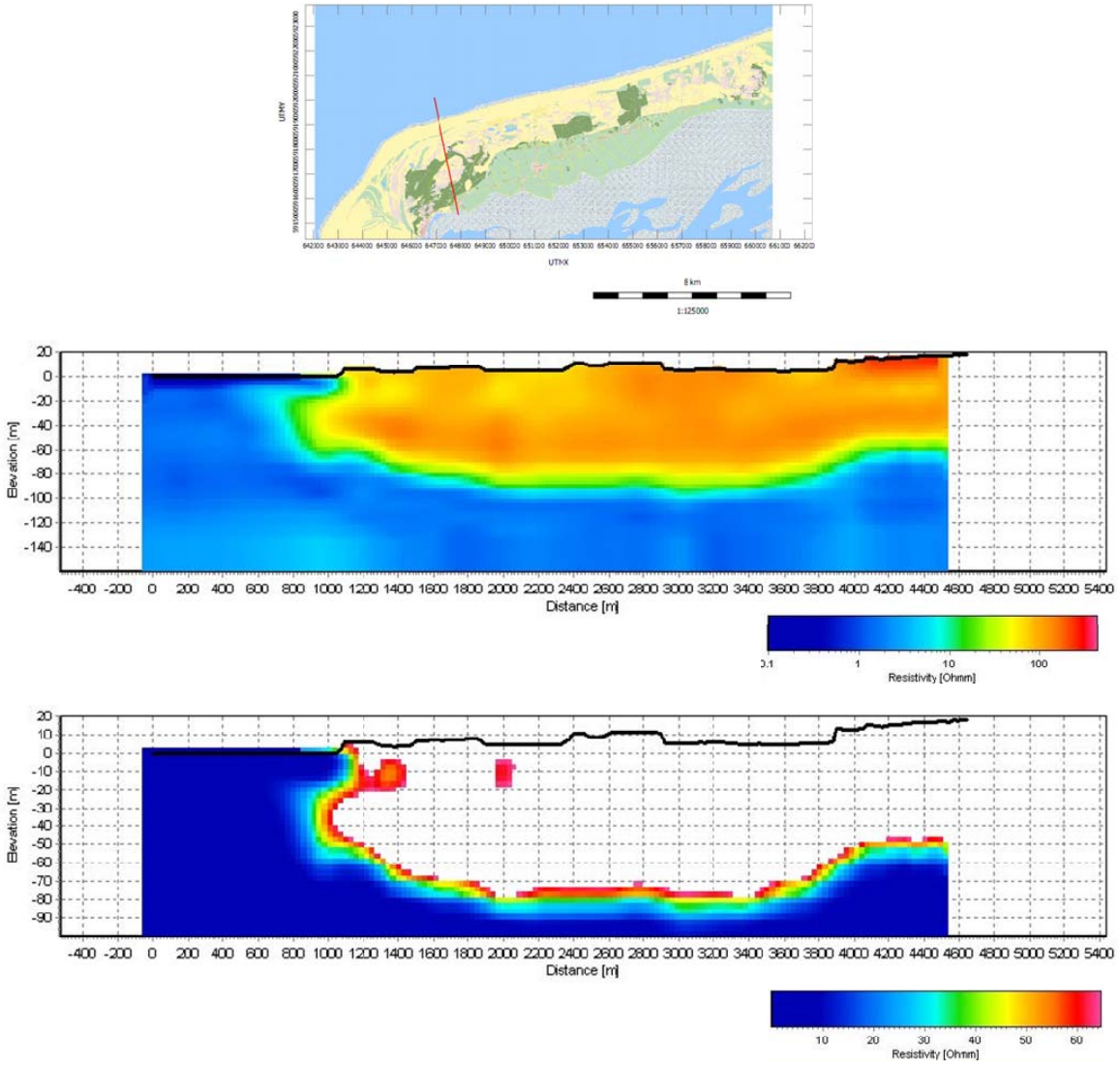
UTMY
UTMX
8 km
1:125000
Elevation [m]
Distance [m]
Resistivity [Ohmm]
Elevation [m]
Distance [m]
Resistivity [Ohmm]

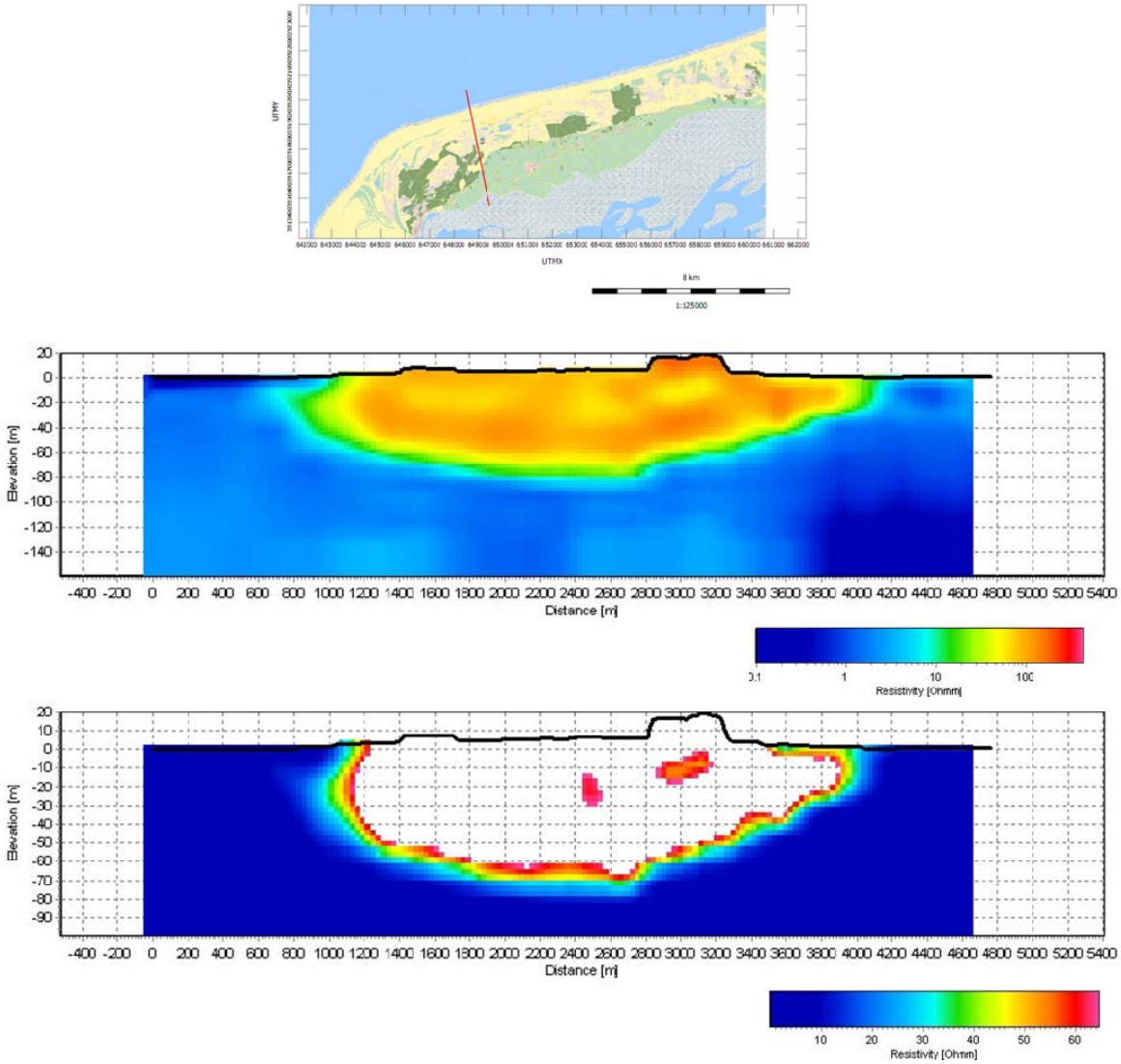
UTMY
UTMX
8 km
1:125000
Elevation [m]
Distance [m]
Resistivity [Ohmm]
Elevation [m]
Distance [m]
Resistivity [Ohm]

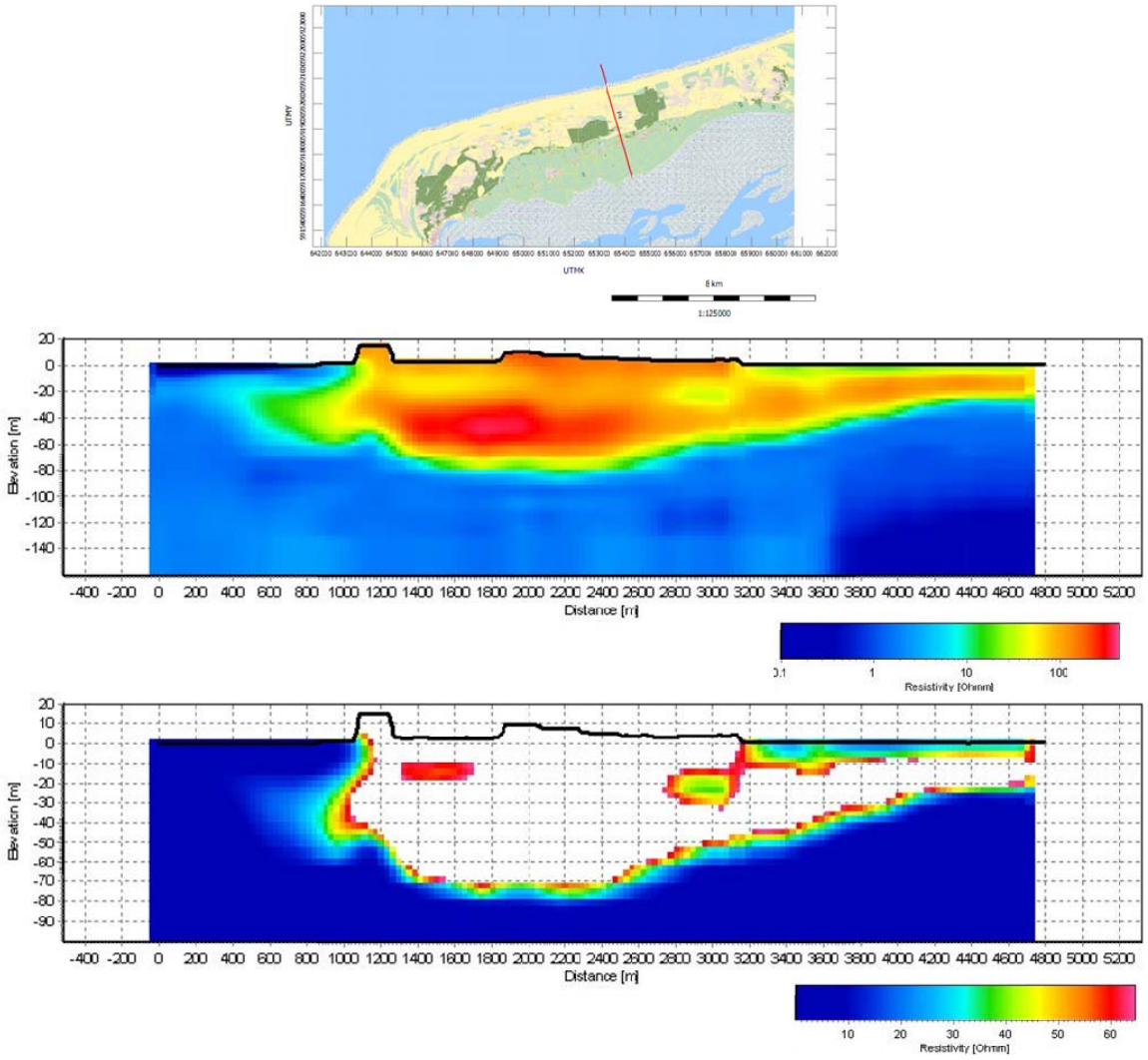
UTMY
UTMX
8 km
1:125000
Elevation [m]
Distance [m]
Resistivity [Ohmm]
Elevation [m]
Distance [m]
Resistivity [Ohmm]

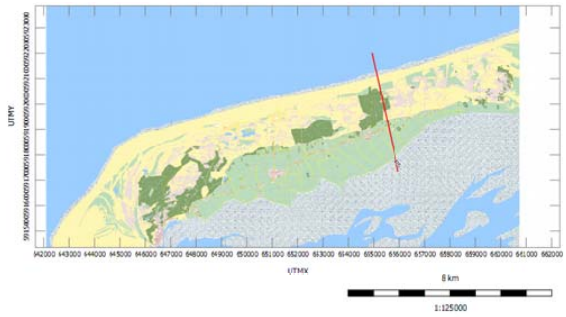
UTMY
UTMX
8 km
1:125000

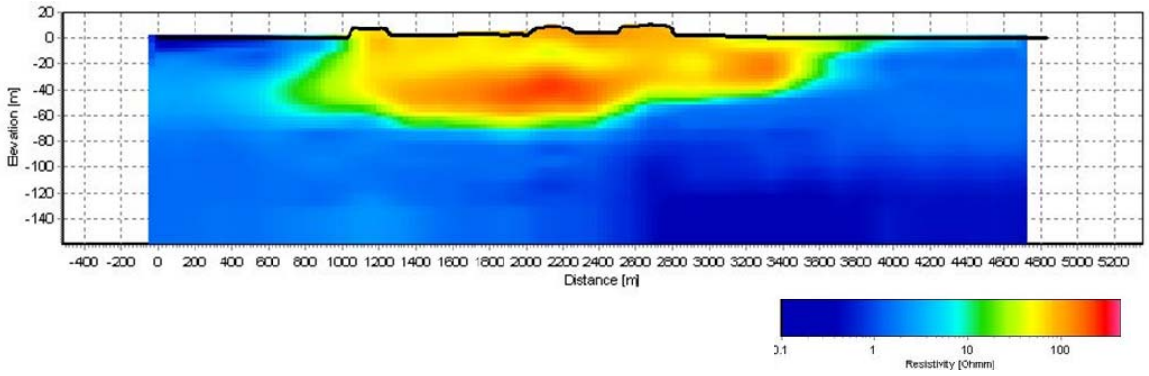
Elevation [m]
Distance [m]
Resistivity [Ohmm]

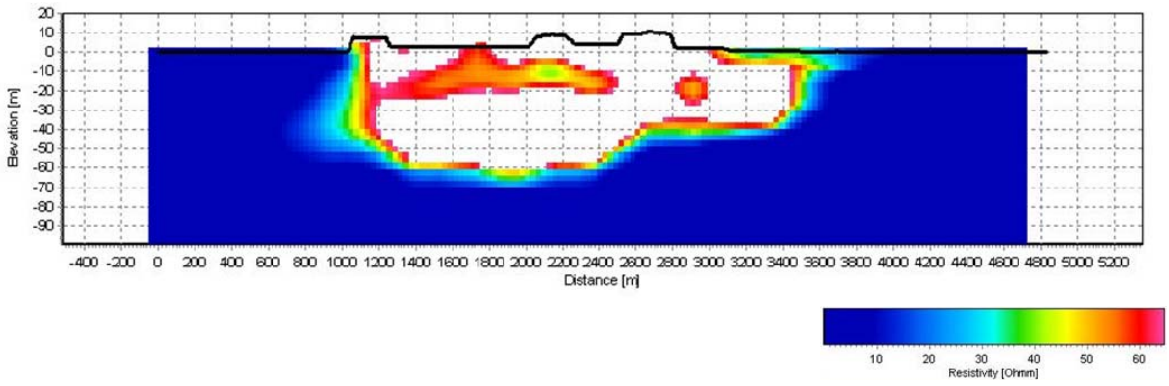
Elevation [m]
Distance [m]
Resistivity [Ohmm]